(2)

AFOSR-TR- 88-0061

AD-A191 310

Grant No: AFOSR-85-0218

BEHAVIOUR OF FIBRE-REINFORCED COMPOSITES UNDER DYNAMIC LOADING

K. Saka, R. K. Y. Li and J. Harding
Department of Engineering Science
University of Oxford
Parks Road
OXFORD OX1-3PJ
UNITED KINGDOM

30 October 1987

Final Report, 1st. May 1986 - 14th. November 1986

Approved for public release; distribution unlimited

Prepared for:

AFOSR/NA
Building 410
Bolling AFB
D. C. 20332

and

European Office of Aerospace
Research and Development
London
ENGLAND

UNCLASSIFIED
SECURITY CLASSIFICATION OF THIS PAGE

JAN 1988 1 2

REPORT DOCUMENTATION PAGE

1a. REPORT SECURITY CLASSIFICATION	1b. RESTRICTIVE MARKINGS
2a. SECURITY CLASSIFICATION AUTHORITY	3. DISTRIBUTION/AVAILABILITY OF REPORT Approval for public release: distribution unlimited.
2b. DECLASSIFICATION/DOWNGRADING SCHEDULE	
4. PERFORMING ORGANIZATION REPORT NUMBER(S)	5. MONITORING ORGANIZATION REPORT NUMBER(S) AFOSR-TR- 88-0061
6a. NAME OF PERFORMING ORGANIZATION Department of Engineering Science, University of Oxford	6b. OFFICE SYMBOL (If applicable) MIC
7a. NAME OF MONITORING ORGANIZATION European Office of Aerospace Research and Development/LTS	
6c. ADDRESS (City, State and ZIP Code) Parks Road Oxford OX1-3PJ U.K.	7b. ADDRESS (City, State and ZIP Code) Box 14, FPO New York 09510
8a. NAME OF FUNDING/SPONSORING ORGANIZATION AFOSR/NA	8b. OFFICE SYMBOL (If applicable) NA
9. PROCUREMENT INSTRUMENT IDENTIFICATION NUMBER AFOSR-85-0218	
8c. ADDRESS (City, State and ZIP Code) Bolling AFB Washington DC 20332	10. SOURCE OF FUNDING NOS.

PROGRAM ELEMENT NO.	PROJECT NO.	TASK NO.	WORK UNIT NO.
61102F	2302	B1	

B1

11. TITLE (Include Security Classification) Behaviour of Fibre-Reinforced Composites under Dynamic Tension

12. PERSONAL AUTHOR(S) K. Saka, R.K.Y. Li and J. Harding

13a. TYPE OF REPORT	13b. TIME COVERED	14. DATE OF REPORT (Yr., Mo., Day)	15. PAGE COUNT
Final	FROM 1.5.86 TO 14.11.86	1987 October 30	77

16. SUPPLEMENTARY NOTATION

17. COSATI CODES			18. SUBJECT TERMS (Continue on reverse if necessary and identify by block number)
FIELD	GROUP	SUB. GR.	Fibre-reinforced composites Tensile impact testing Hopkinson-bar

19. ABSTRACT (Continue on reverse if necessary and identify by block number)

Stress-strain curves are presented for tensile impact tests on plain-weave glass/epoxy and plain-weave carbon/epoxy laminates loaded in a direction at 45° to both the warp and weft directions. From the initial linear-elastic response the in-plane shear moduli for the two types of reinforcement at impact rates of strain are derived. In conjunction with results previously obtained from tensile impact tests on the same laminates loaded in the warp and the weft directions, two-dimensional stiffness matrices for both the glass-fabric and the carbon-fabric reinforced plies are determined. When compared with similar stiffness matrices previously obtained under quasi-static loading a marked effect of strain rate is apparent, particularly for the glass-reinforced ply. (Keywords)

Using the stiffness matrices determined experimentally for the all-glass and the all-carbon plies under impact loading, predictions have been obtained for the tensile moduli of hybrid lay-ups of the two types of ply in terms of the modified laminate theory developed in an

20. DISTRIBUTION/AVAILABILITY OF ABSTRACT UNCLASSIFIED/UNLIMITED ☐ SAME AS RPT. ☐ DTIC USERS ☐	21. ABSTRACT SECURITY CLASSIFICATION

22a. NAME OF RESPONSIBLE INDIVIDUAL	22b. TELEPHONE NUMBER (Include Area Code)	22c. OFFICE SYMBOL
Dr. Dachman	(202)767-4937	NA

DD FORM 1473, 83 APR — EDITION OF 1 JAN 73 IS OBSOLETE.

SECURITY CLASSIFICATION OF THIS PAGE
UNCLASSIFIED

19. Abstract (Continued)

earlier report. The values so derived are found to agree well with both the experimentally measured hybrid moduli and the 'rule-of-mixtures' predictions. This is in accord with the behaviour previously found at a quasi-static loading rate.

In parallel with these studies of the tensile impact response of hybrid composites a new transverse impact testing machine has been developed, based on the principle of the Hopkinson-bar, for studying the initiation of impact damage in hybrid laminates. Using this apparatus tests have been performed on all-glass and all-carbon reinforced laminates and on five different hybrid lay-ups of carbon and glass. These tests show the load measurement technique, using an instrumented input bar, to be unsatisfactory and modifications to the loading system are required. However, examination of impacted specimens using a C-scan, followed either by deplying, to assess fibre fracture, or by sectioning and observation under the optical microscope, to observe micro-mechanisms of damage, reveals a change in the damage accommodation mechanism when glass-reinforced plies are added to an all-carbon laminate and differences in the response of the two types of ply with increasing impact velocity.

PREFACE

This present report is the fourth in a series with the same general title, 'Behaviour of Fibre-Reinforced Composites under Dynamic Tension', describing a continuing programme of research under Grant Nos. AFOSR-82-0436, AFOSR-84-0092 and AFOSR-85-0218. The previous (third progress) report, issued October 1986, related to the first 12 months of the 18 month period, from 1st. May 1985 to 14th. November 1986, covered by the third of these Grants, No. AFOSR-85-0218, for which it was, therefore, an Interim Report. The present report describes work performed during the final 6 months of this grant period and so constitutes the Final Report on Grant No. AFOSR-85-0218. It should, however, be read in conjunction with the previous (third) report since only the additional work undertaken during the final 6 month period is reported on here.

CONTENTS

1. INTRODUCTION

A major problem in the development of fibre-reinforced composite materials for structural applications is their low resistance to impact damage. This is of particular significance when considering their use in the aircraft industry where design tolerances are very tight and where impact loading from, for example, bird-strike or runway debris, is not unexpected. A need is clearly apparent, therefore, both to characterise the impact mechanical response of fibre-reinforced composites and to study ways of improving their impact resistance. In general two approaches are possible in seeking to tackle this problem, either to attempt to determine the effect of loading rate on the fundamental material mechanical response and the specific micromechanisms of composite failure or to seek to reproduce in experimental form the impact loading configuration experienced in practice.

So far in the present investigation it is the first of these two approaches which has been followed. Room temperature tensile stress-strain curves have been obtained for various hybrid composites of carbon and glass and of their constituent plies over a range of strain rates from quasi-static ($\sim 10^{-3}$/s) to impact (~ 1000/s) and the operative micromechanisms of deformation and fracture have been investigated by optical and scanning electron microscopy to assess how far hybridisation allows an optimisation of the mechanical properties under impact loading. Analytical expressions have been developed relating the strength and stiffness of the hybrid specimens to the properties of the constituent plies and the lamination parameters.

The quasi-static two-dimensional stiffness matrix has been determined for each type of reinforcing ply and predicted moduli have been obtained for the hybrid specimens. Good agreement is found between these predicted values and those derived from the rule of mixtures and both closely follow the experimentally measured values of tensile modulus. In the present report the equivalent two-dimensional stiffness matrix for each type of reinforcing ply under impact loading conditions is determined and the corresponding predicted tensile moduli for the various hybrid specimens are obtained and again compared with both the rule of mixtures and the experimentally measured values. The results of this study were presented at the recent International Conference at Bremen, IMPACT 87, and a preprint of the conference paper is attached to this report (1).

In the second progress report (2) it was concluded that the low failure strains in the hybrid specimens under tensile impact loading were related to a restriction of the damage zone in the glass-reinforced plies due to the presence of neighbouring carbon reinforced plies. This is primarily a geometrical effect associated with the tensile loading configuration. Under transverse impact loading a greater hybrid effect might well be ex-

(1) Harding, J., Saka, K. and Taylor, M. E. C., "The Effect of Strain Rate on the Tensile Failure of Woven-Reinforced Carbon/Glass Hybrid Composites", Proc. IMPACT 87, Bremen, May 1987 (in press)

(2) Saka, K. and Harding, J., "Behaviour of Fibre-Reinforced Composites under Dynamic Tension", Final Report on Grant No. AFOSR-84-0092, September 1985 (Oxford University Engineering Laboratory Report No. OUEL No. 1602/85)

pected if the glass-fibre reinforced plies are situated in those regions of the specimen experiencing the largest deformations. A few exploratory tests were proposed (3), therefore, in which the same laminates as have been used in the preparation of the tensile test specimens would also be subjected to controlled transverse impact loading. Such a loading configuration corresponds much more closely to that often obtained in practice and so follows the second approach described in the first paragraph above.

Previous attempts to simulate the transverse impact loading often encountered in practical engineering structures, and from which data on the structural, rather than material, response might be obtained, have been made by several investigators. In early work Beaumont et al. (4) observed the damage resulting in fuselage skin materials after impact at different velocities. The results obtained were qualitative and no attempt was made to measure the loads applied during the impact process. In many subsequent investigations, however, instrumented drop-weight impact tests were developed. Broutman and Rotem (5), for example, impacted beam specimens at centre span, the ends being supported on load cells, while a high-speed camera was used to observe the deformation. For GFRP specimens they found increased strength and energy absorbtion at high rates of loading and observed that the mechanism of energy absorbtion was by delamination between layers and between fibres and could, therefore, be affected by the surface treatment of the fibres and the surface characteristics of the laminae.

More commonly the load cell, often a piezo-electric force transducer, was attached directly directly to the falling weight (6, 7, 8, 9) and the resulting force-time curve used to obtain energy, velocity and displacement as functions of time and force as a function of displacement. This requires the assumption of quasi-static equilibrium within the specimen.

---

(3) Harding, J., Saka, K. and Taylor, M. E. C., "Behaviour of Fibre Reinforced Composites under Dynamic Tension", Interim Report on Grant No. AFOSR-85-0218, October 1986 (Oxford University Engineering Laboratory Report No. OUEL No. 1654/86)

(4) Beaumont, P. W. R., Riewald, P. G. and Zweben, C., "Methods for Improving the Impact Resistance of Composite Materials", Foreign Object Impact Damage to Composites, ASTM STP 568, Amer. Soc. for Testing and Materials, (1974) 134.

(5) Broutman, L. J. and Rotem, A., "Impact Strength and Toughness of Fiber Composite Materials", ibid, 114.

(6) Caprino, G., Crivelli Visconti, I. and Di Ilio, A., "Elastic Behaviour of Composite Structures under Low-Velocity Impact", Composites, Vol. 15, No. 3, (1984) 231.

(7) Teti, R., Langella, F., Crivelli Visconti, I. and Caprino, G., "Impact Response of Carbon Cloth Reinforced Composites", Proc. ICCM V, TMS-AIME, (1985) 373.

(8) Winkel, J. D. and Adams, D. F., "Instrumented Drop-Weight Impact Testing of Cross-Ply and Fabric Composites", Composites, Vol. 16, No. 4, (1985) 268.

In many cases oscillations were observed on the force-time signals obtained from the load cells even though filtering techniques were used to smooth the data (6, 8), an indication of stress wave reflections within the load cell as well as the specimen. Despite these oscillations, however, Elber (10) has shown that for impact velocities up to 7m/s the assumption of quasi-static equilibrium in the specimen may not be unreasonable, although a detailed examination of the resulting damage showed differences between that caused by impact loading, where fibre failure was greater in plies close to the back surface, and that caused by quasi-static loading where fibre failure was greatest nearer the centre plies.

Residual damage in CFRP panels was also studied by Dorey and Sidey (11) after impact at a wide range of velocities. Below 60m/s simple bending theory, and the assumption of quasi-static conditions in the specimen, could be used to predict the critical incident energy to produce failure. Above 80m/s a relatively clean hole was punched in the specimen, which could be treated as effectively rigid during the period of loading. It was in the intermediate range of velocity, from 60 to 80m/s, where stress wave reflections within the specimen clearly affected the mechanical response, that the most marked drop in residual strength was observed.

In the light of these earlier investigations an attempt has been made to develop an improved transverse impact test for composite laminates in which the instrumentation provided will allow an unambiguous determination of force, velocity and displacement without the need to assume conditions of quasi-static equilibrium, and in which the importance of stress wave reflections within the specimen may be determined for any chosen geometry. A description of the testing machine and its operation is given in section 2 below and its use to study the development of impact damage in woven hybrid carbon/glass and all-carbon laminates is described in section 3. A summary of this work, as presented to the Sixth International Conference on Composite Materials (ICCM VI) at Imperial College, London, in July 1987, is given in the attached preprint (12).

---

(9) Davis, C. K. L., Turner, S. and Williamson, K. H., "Flexed Plate Impact Testing of Carbon Fibre-Reinforced Polymer Composites", Composites, Vol. 16, No. 4, (1985) 279.

(10) Elber, W., "Failure Mechanisms in Low-Velocity Impacts on Thin Composite Plates", NASA Technical Paper 2152, May 1983.

(11) Dorey, G. and Sidey, G. R., "Residual Strength of CFRP Laminates after Ballistic Impact", Proc. Conf. on Mech. Props. at High Rates of Strain, Inst. of Physics Conf. Ser. No. 21, (1974) 344.

(12) Li, R. K. Y. and Harding, J., "Studies of Transverse Impact Damage in Composite Materials using a Hopkinson Type Pressure-Bar Technique", Proc. ICCM VI, Elsevier Applied Science, London and New York, Vol. 3, (1987) 3.76.

2. EXPERIMENTAL PROCEDURE

The only changes in the experimental procedure since the third progress report was issued relate to the development of the transverse impact test. This is illustrated schematically in fig. 2.1 along with the associated Lagrange (elastic wave propagation) diagram. A small air-gun, not shown, is used to accelerate the projectile to velocities from between 2 and 20m/s. The projectile makes coaxial impact on an instrumented input bar of the same material and cross-section and compressive stress waves, of magnitude $\sigma = \frac{1}{2}\rho cv$, where ρ is the density and c the longitudinal elastic wave speed for the bar material and v is the impact velocity, propagate in both directions from the point of impact, giving strain-time signals at the two gauge stations which have the idealised form shown. The projectile and input bar, which have lengths of 0.33 and 0.99m respectively and are machined from 12.5 mm diameter steel bars, separate at time T, the input bar continuing to oscillate and to apply a st[illegible]d loading and displacement to the centre of the circular plate spec[illegible]. The end of the input bar in contact with the specimen is hemispherical and the specimen is fully clamped at the edges with an exposed diameter of 60mm. In principle, by varying the impact velocity and the length of the projectile, it should be possible to control the magnitude and duration of the force applied to the specimen. In practice, oscillations in the input bar lead to complications in the calculation of the load. A better arrangement, which has been introduced more recently, is to have the projectile and input bars of the same length, giving the most rapid decay of these oscillations.

Typical input bar signals from gauge stations I and II, as stored in a Datalabs type 912 dual channel transient recorder and subsequently transferred to an IBM.PC microcomputer, are shown in fig. 2.2. The signals, which in this case relate to a test on an all-carbon laminate at an air-gun firing pressure of ∿30psi, corresponding to a projectile velocity of ∿2m/s, have been superimposed in time and processed in the computer to give stress levels in MPa. From these stress-time traces, using the standard Hopkinson bar analysis, the velocity, displacement and load at the interface between the input bar and the centre of the specimen may be determined and are shown in figs. 2.3, 2.4 and 2.5 respectively. The effect of wave reflections in the input bar is to give a series of velocity pulses of decreasing magnitude to the specimen, see fig. 2.3, leading to a corresponding series of steps on the displacement-time curve of fig. 2.4. The Hopkinson-bar analysis for stress depends on the difference between the computed incident and reflected waves in the input bar. At the low impact velocities required to study the initiation of damage, and hence for the low applied loads, the calculation will be extremely sensitive to small variations in the signals from the input bar gauges shown in fig. 2.2. This leads to the high frequency noise on the computed load-time curve of fig. 2.5. Clearly, for the present type of specimen, this is not a very satisfactory method for measuring the applied loads.

It is possible, however, to deduce from fig. 2.5 that the duration of loading of the specimen is of the order of 1.5ms. This is very much longer than the time, of the order of 10 to 20μs, for stress waves to reflect within the specimen and suggests that the specimen can be considered to be in quasi-static equilibrium for most of the duration of loading. As an alternative method of determining the load applied to the specimen, therefore, strain

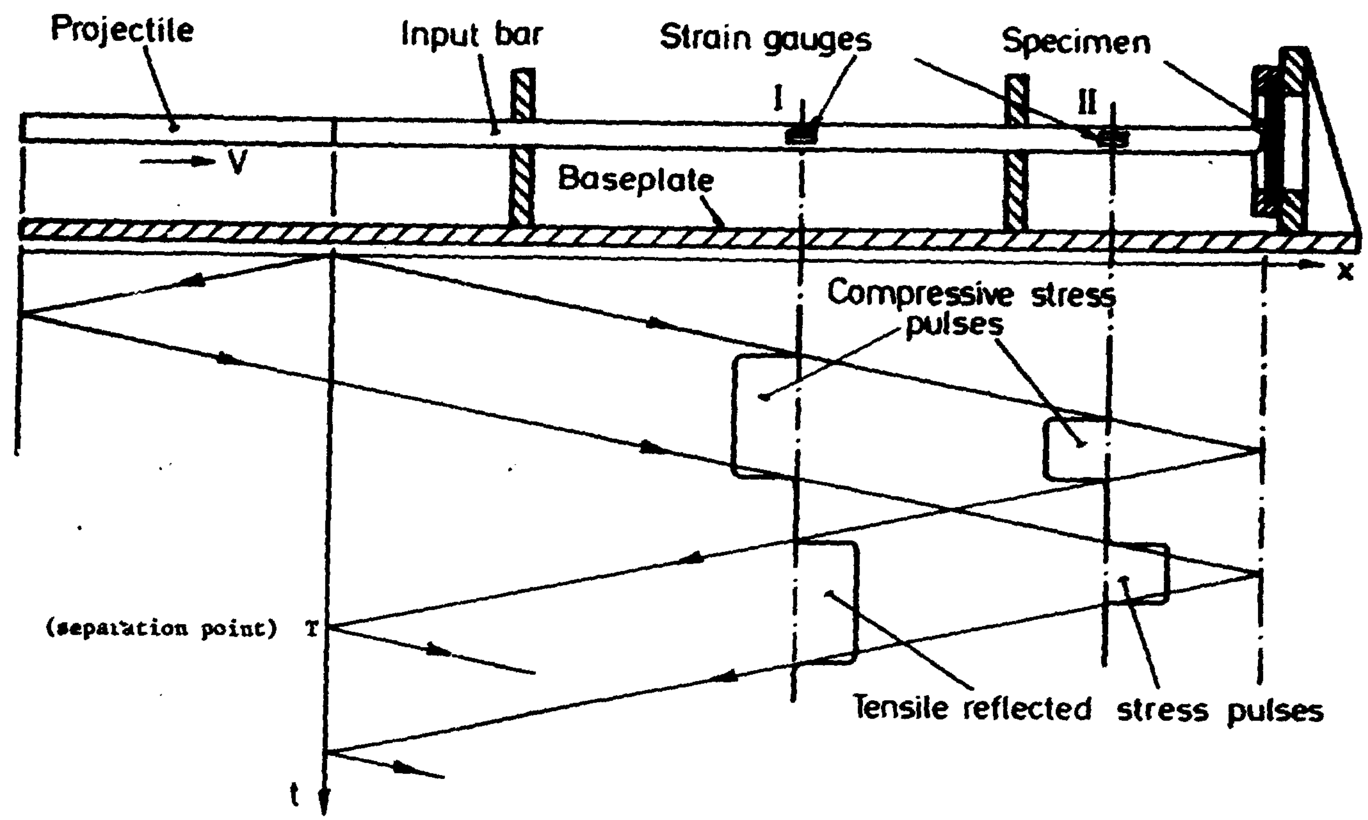

Fig. 2.1 SCHEMATIC VIEW OF TRANSVERSE IMPACT APPARATUS AND RELATED LAGRANGE (ELASTIC WAVE PROPAGATION) DIAGRAM

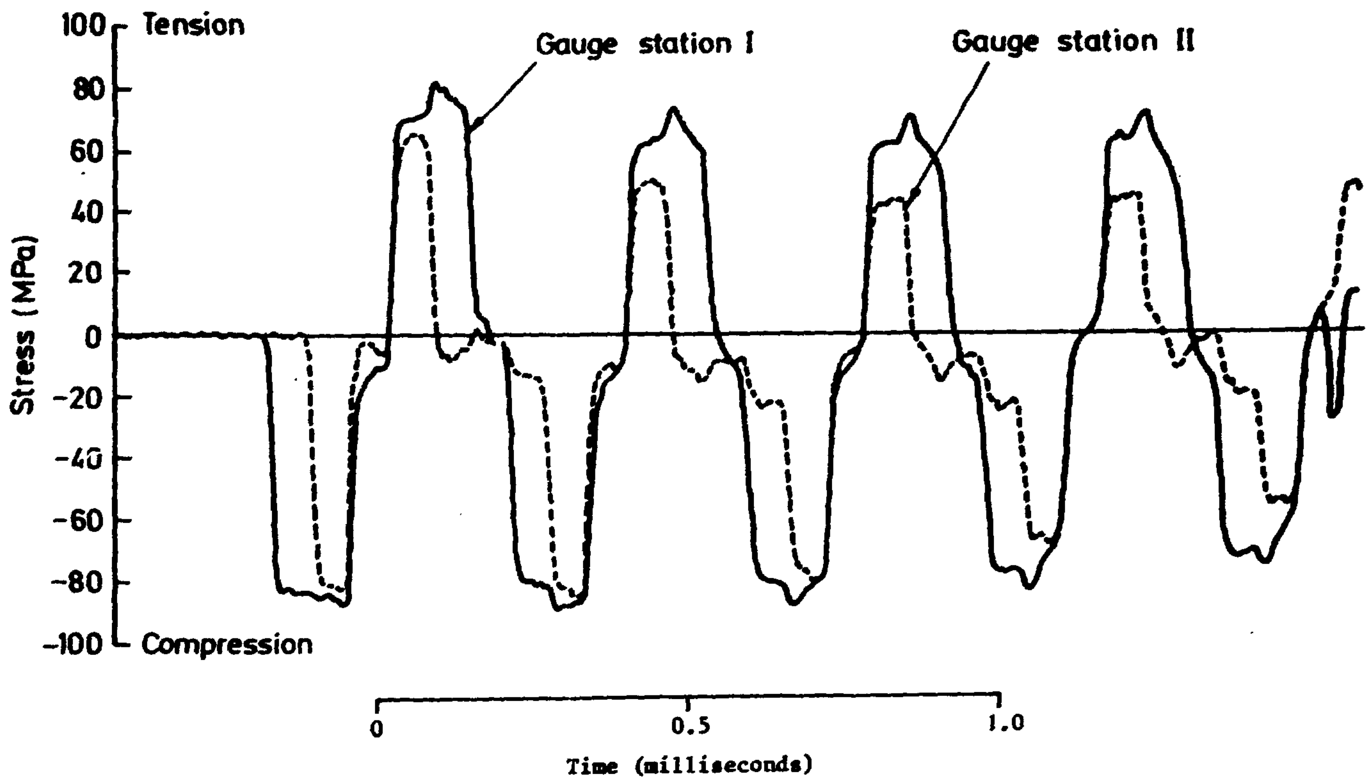

Fig. 2.2 INPUT BAR STRAIN GAUGE RECORDS FOR TEST ON ALL-CARBON LAMINATE
(Air-gun firing pressure: 30psi)

Fig. 2.3 COMPUTED VELOCITY-TIME CURVE FOR TEST OF FIG. 2.2

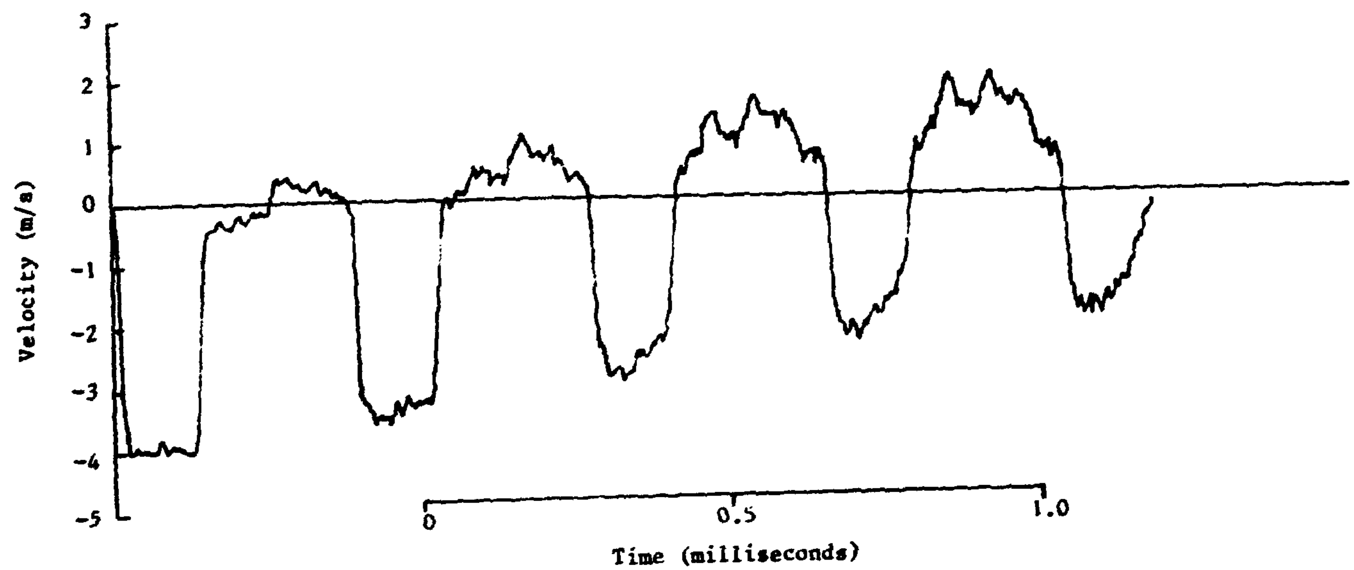

Fig. 2.4 COMPUTED DISPLACEMENT-TIME CURVE FOR TEST OF FIG. 2.2

Fig. 2.5 FORCE-TIME CURVE DERIVED FROM HOPKINSON BAR ANALYSIS FOR TEST OF FIG. 2.2

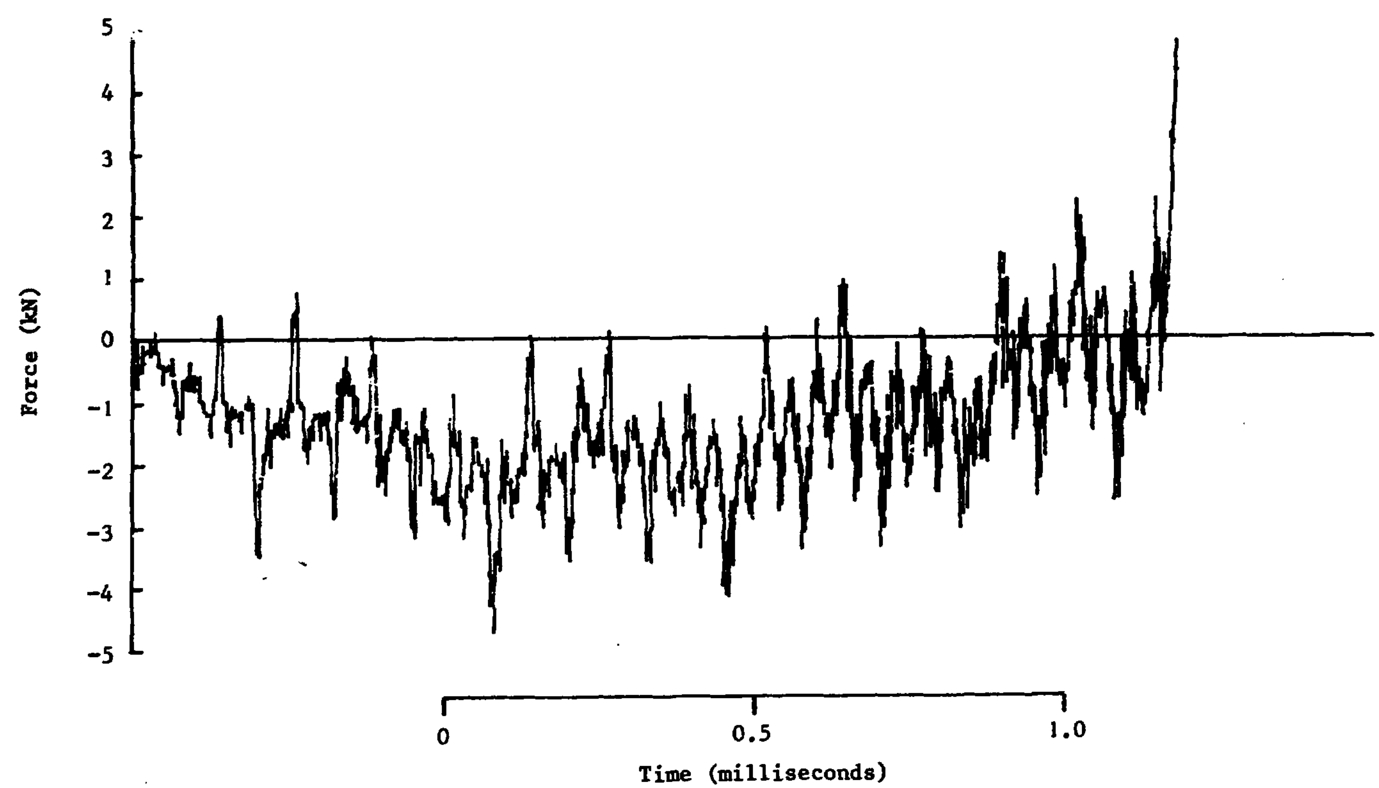

gauges were attached directly to the back surface of the specimen, see fig. 2.6. Initially gauges were fixed at the centre point behind the input bar contact point and aligned with the warp and weft directions, positions A and B respectively, not shown in fig. 2.6. Signals stored in the transient recorder from these two gauges for the same impact as in fig. 2.2 are shown in figs.2.7a and b. Almost identical tensile strain signals are obtained, confirming the balanced plain weave lay-up of the all-carbon laminate. Both showed a stepped response closely similar to that of the displacement-time trace of fig. 2.4, as would be expected if the specimen were in a state of quasi-static equilibrium, although the small superimposed oscillations may indicate the presence of stress waves within the specimen induced by each successive velocity pulse.

Unfortunately, in tests at higher impact velocities, required to induce more damage in the specimen, gauges in positions A and B often failed early in the test so alternative positions, C and D and E and F, see fig. 2.6, were chosen. For gauge stations E and F the output signals, again for the test of fig. 2.2, are shown in fig. 2.8. Note that here, because the plate specimen is fully clamped at the edges, the radially aligned gauge F experiences a compressive strain. Otherwise the same general features as before, a stepped profile overall with small superimposed oscillation, are observed. To determine the specimen loading a quasi-static calibration was performed in which the strain gauge signals were recorded for known transverse loads applied statically to the centre of the specimen. Calibrations lines for the four gauge stations, C, D, E and F, are shown in fig. 2.9. Taking gauge station F, for which the calibration of fig. 2.9 is the most nearly linear, the gauge signal of fig. 2.8b can be used to derive the variation of load with time at the centre of the specimen during impact. The load-time trace so obtained is compared in fig. 2.10 with that derived from the Hopkinson-bar analysis and shown in fig. 2.5. The general shape of the two curves is seen to be closely similar, the noise on the Hopkinson bar curve falling more or less symmetrically about the curve derived from strain gauge F.

Finally, using the load-time curve from strain gauge F and the displacement-time curve of fig. 2.4, a load-displacement record, as shown in fig. 2.11, may be obtained for the impact. Although, largely due to the stepped nature of the applied loading but possibly also to stress waves within the specimen, this load-displacement trace shows large variations from a smooth loading curve its general form is clear and, in particular, a peak load of ∿2.6kN and a peak displacment of ∿1.2mm in a time of about 1ms can be deduced for this impact.

There are several limitations, however, to this technique for load determination. In the test of fig. 2.2 subsequent examination of the impacted specimen failed to detect any signs of damage. However, at the higher loads required to initiate damage an extrapolation of the calibration curves of fig. 2.9 will be required. Also, as significant damage is introduced the calibration is likely to become increasingly non-linear. Under such conditions only an approximate estimate of the peak load can be obtained. In addition the calibration will be different for different specimen hybrid lay-ups, although, as shown in fig. 2.12, gauge F will still exhibit the most nearly linear response. For these reasons two modified versions of the transverse impact test are being developed. The first, and simplest, replaces the projectile and input bar by two equal

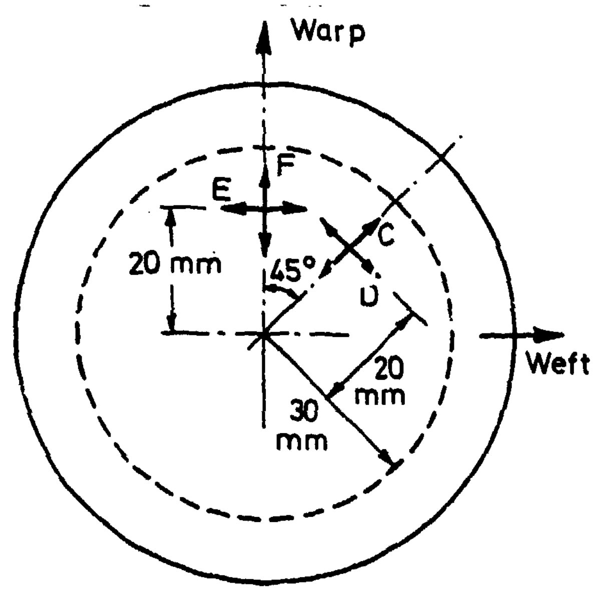

Fig. 2.6 STRAIN GAUGE STATIONS ON SPECIMEN BACK SURFACE

Fig. 2.7 SIGNALS FROM STRAIN GAUGES AT CENTRE OF SPECIMEN BACK SURFACE FOR TEST OF FIG. 2.2

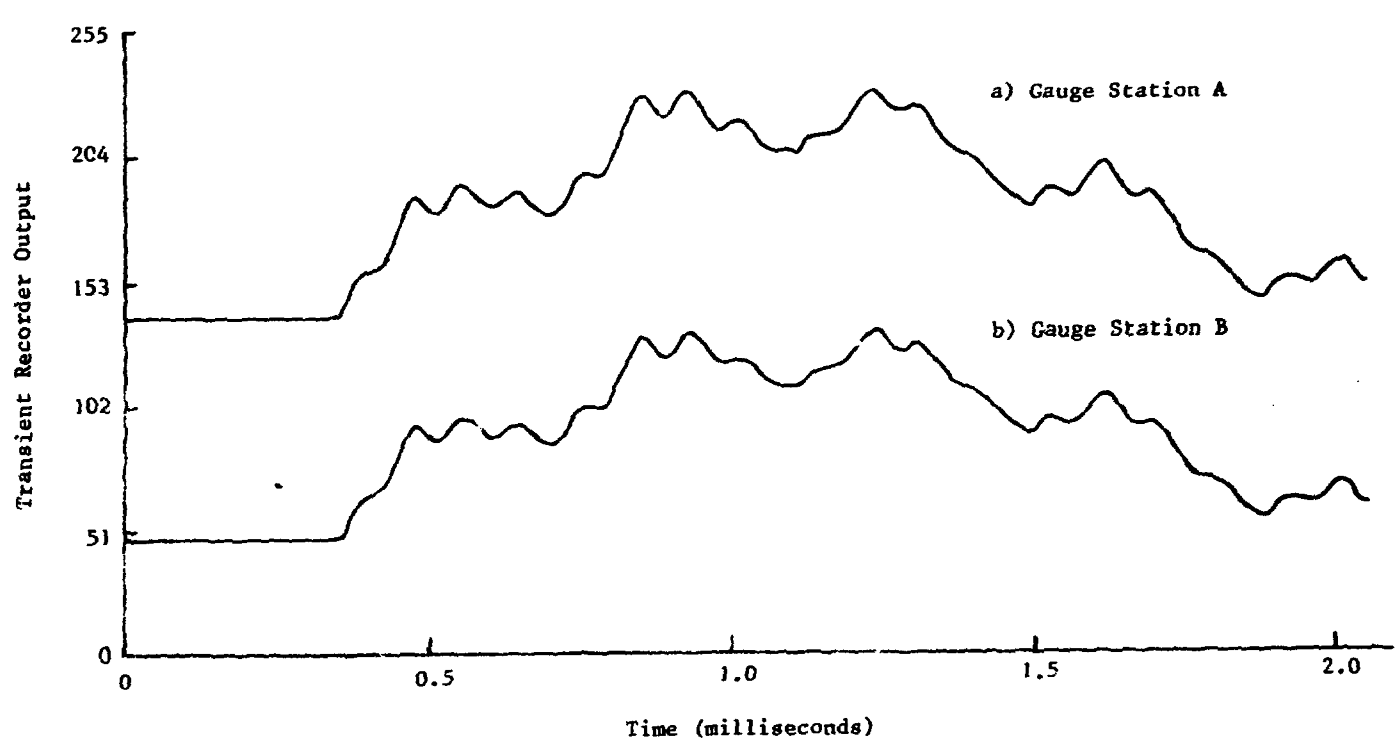

Fig. 2.8 SIGNALS FROM BACK SURFACE STRAIN GAUGES IN POSITIONS E and F FOR TEST OF Fig. 2.2

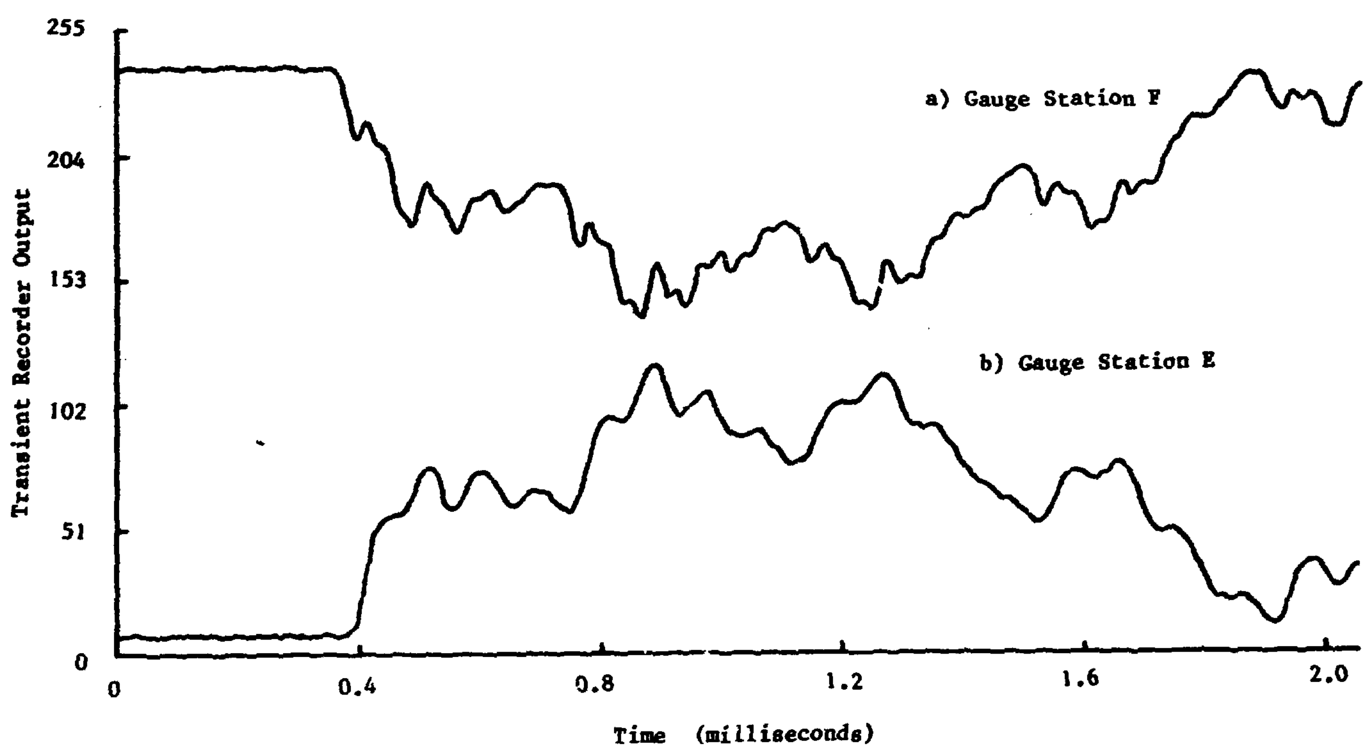

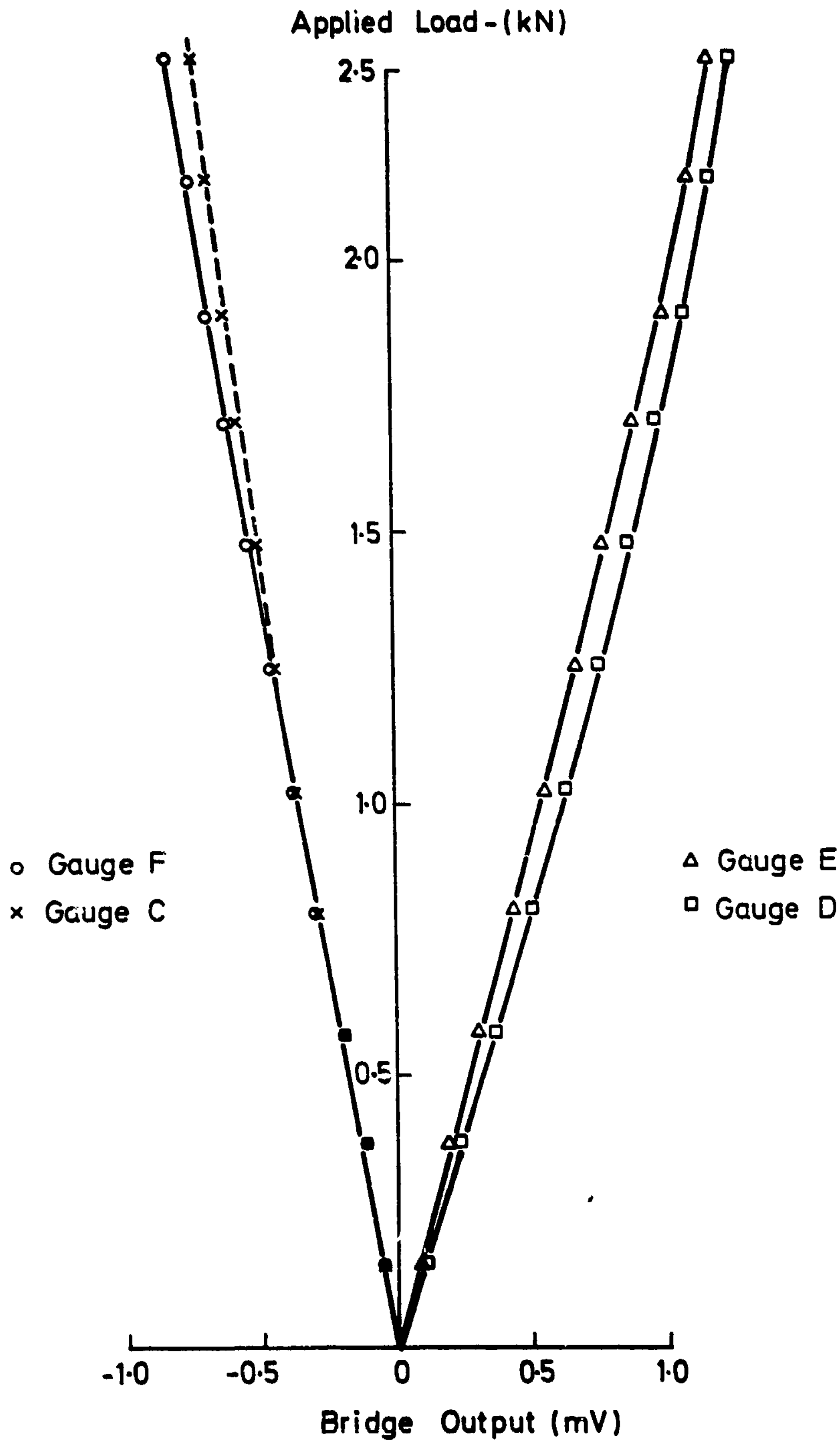

Fig. 2.9 QUASI-STATIC CALIBRATIONS OF BACK SURFACE STRAIN GAUGES FOR WOVEN CARBON/EPOXY SPECIMEN

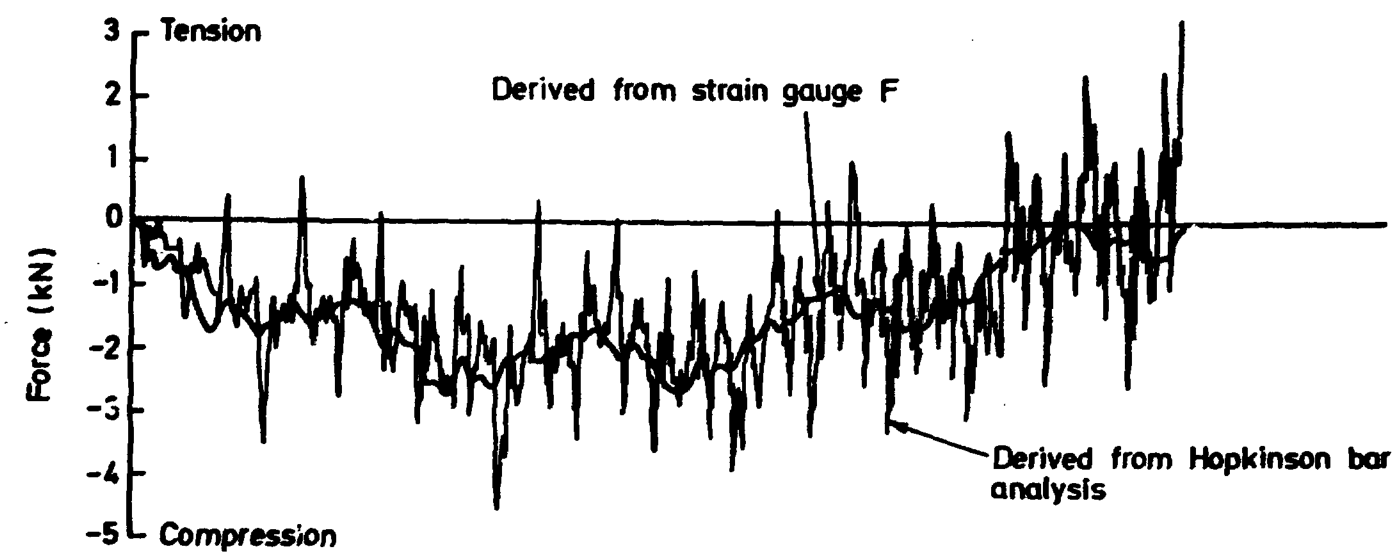

Fig. 2.10 COMPARISON OF LOAD-TIME CURVES DERIVED FROM STRAIN GAUGE STATION F AND FROM HOPKINSON-BAR ANALYSIS

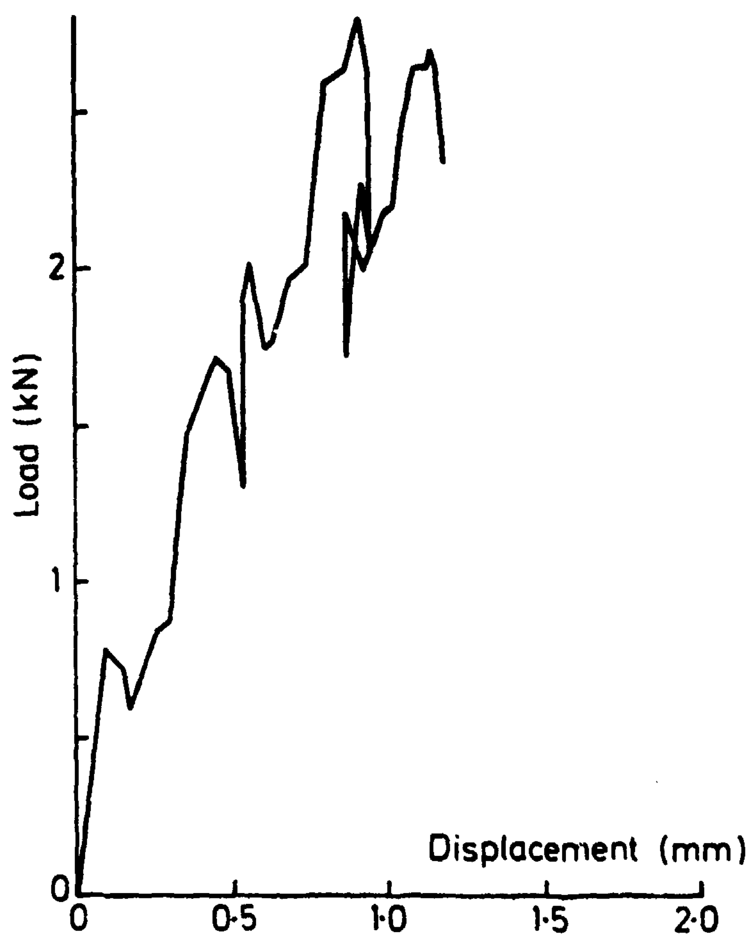

Fig. 2.11 LOAD-DISPLACEMENT CURVE FOR TEST OF Fig. 2.2

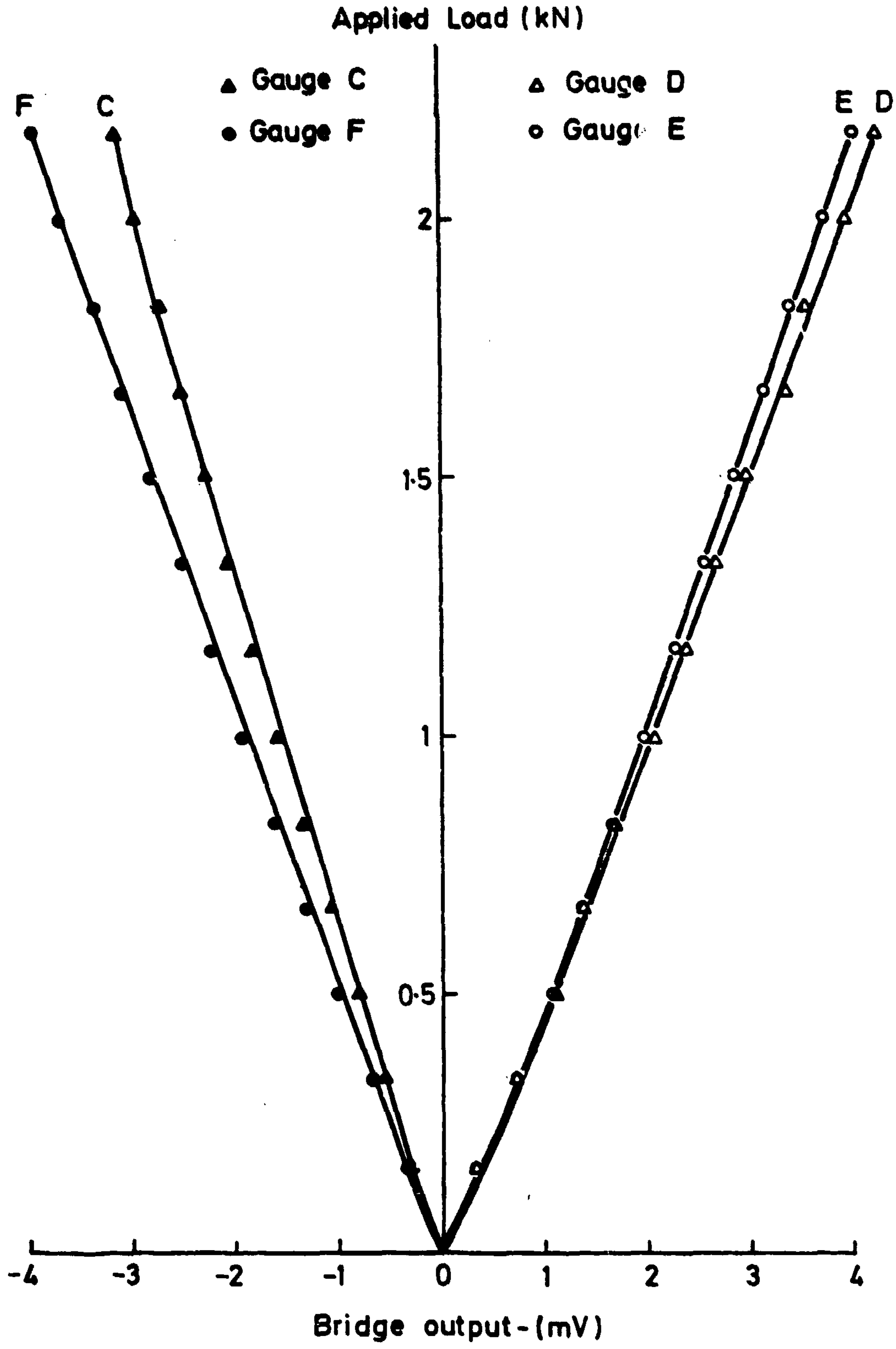

Fig. 2.12 QUASI-STATIC CALIBRATIONS OF BACK SURFACE STRAIN GAUGES FOR TYPE V HYBRID SPECIMEN

length titanium alloy loading bars in an attempt to minimise the effect of oscillations in the input bar. The second seeks to use the projectile to accelerate the input bar to a constant velocity in an unstressed state before it impacts the specimen. The input bar gauges will then give a direct measure of the load applied to the specimen. The success or otherwise of these proposals will be considered in the next report.

3. EXPERIMENTAL RESULTS

In the six month period following the work described in the third report progress has been made on two fronts. As described in section 3.1 below data has been obtained from which the dynamic elastic properties of the all-carbon and the all-glass reinforcing plies may be determined. Using this data the corresponding dynamic stiffness matrices are determined, see section 4.1, and predictions are made of the tensile elastic moduli for the three hybrid lay-ups, see section 4.2. In parallel with this work, the transverse impact testing machine described in section 2 has been used to study the effect of hybrid lay-up on the development of damage under this type of loading. A separate report (13) which fully describes this work is attached. An outline of the main results is given in section 3.2 below.

3.1 Determination of Dynamic Elastic Properties

3.1.1 Waisted Specimens

As described in the third progress report (3) impact tests have been performed on the standard design of tensile specimen, i.e. waisted in the thickness direction, for both the all-glass and the all-carbon laminates loaded in both the warp (A) and the weft (B) directions. The data obtained in these tests are summarised in Table 3.1 below.

TABLE 3.1 Mechanical Properties in Warp and Weft Directions for All-Glass and All-Carbon Specimens under Impact Loading

Material	Direction of loading	E GPa	σ_{max} MPa	ε_f %	σ_y MPa	ε_y %
All-carbon	Warp (A)	48.7 ±14%	562 ±7%	1.32 ±6%	501 ±6%	1.04 ±14%
	Weft (B)	49.0 ±8%	508 ±2%	1.10 ±9%	482 ±5%	1.00 ±14%
All-Glass	Warp (A)	24.0 ±4%	494 ±1%	4.21 ±5%	151 ±5%	0.62 ±6%
	Weft (B)	17.1 ±13%	427 ±4%	4.45 ±9%	165 ±14%	0.96 ±18%

3.1.2 Tests on Parallel-Sided Coupons

Although the results of Table 3.1 do give an estimate of the dynamic values of Youngs moduli for the two materials in the two directions of reinforcement it is still required to determine the corresponding values of Poisson's ratio, ν_{AB} and ν_{BA}, and the in-plane shear modulus G_{AB}. In the

(13) Li, R. K. Y. and Harding, J., "Studies of Transverse Impact Damage in Composite Materials using a Hopkinson-Type Pressure Bar Technique", Oxford University Engineering Laboratory Report No. OUEL 1706/87

quasi-static tests reported earlier (3) these were determined using parallel sided coupons cut from the two laminates with the loading axis in either the warp or the weft directions or at 45° to these directions, i.e. the C direction, as shown schematically in fig. 3.1. These coupons were reloaded several times within the elastic range and the longitudinal and transverse strains measured each time using strain gauge rosettes attached to the two surfaces of the coupon. Under impact loading, however, it is not possible to interrupt the test and unload the specimen before the elastic limit is exceeded. Nevertheless, it is still advantageous to use parallel-sided coupons instead of waisted specimens since the limiting elastic load is higher and the accuracy with which the elastic constants may be determined is greater. Further tests, therefore, were performed on parallel-sided coupons loaded in both the warp and the weft directions, as in figs. 3.1a and b, the longitudinal and the transverse strain being measured in each case.

A typical set of strain gauge records for such a test on an all-carbon specimen loaded in the warp direction is shown in fig. 3.2. The stress in the specimen is determined from the output bar gauge signal, fig. 3.2d, the strain in the loading direction from the axial strain gauge, fig. 3.2c, and the strain in the 90° direction from the transverse strain gauge, fig. 3.2e, the latter showing a negative signal corresponding to a compressive strain. The other signals come from the input bar gauges and are normally used in determining the dynamic stress-strain curve when a standard specimen is tested. For the present purpose the signals of figs. 3.2d and 3.2c are adjusted to the same time zero and then plotted against each other to give the elastic stress-strain response up to the point at which the coupon pulls out of the loading bars. The results of three such tests are compared in fig. 3.3. The linear slopes obtained correspond to moduli in the warp direction ranging from 54.1 to 59.4GPa. In the same way Poisson's ratio may be obtained by cross-plotting the signals of figs. 3.2e and 3.2c, as shown in fig. 3.4 for the same three tests, the initial linear region giving values of ν_{AB} ranging from 0.058 to 0.065. Similar results for tests on the all-glass reinforced material loaded in the weft direction are shown in figs. 3.5 and 3.6, respectively. A complete set of data obtained in this way is given in Table 3.2 below.

TABLE 3.2 Youngs Moduli and Poisson's Ratios for All-Carbon and All-Glass Laminates from Tests on Parallel-Sided Coupons

Material	E_A GPa	E_B GPa	ν_{AB}	ν_{BA}	ν^*_{AB}	Error
All-Carbon	54.1	66.3	0.061	0.094	0.075	-0.019
	54.3	54.0	0.058	0.063	0.063	------
	59.4	62.4	0.065	0.080	0.068	-0.012
	55.9	60.9	0.061	0.079	0.066	-0.013
	±2.6	±6.2	±0.004	±0.015	±0.006	
All-Glass	29.9	23.0	0.169	0.151	0.130	-0.021
	28.6	24.3	0.184	0.160	0.156	-0.004
	27.5	23.5	0.176	0.155	0.150	-0.005
	28.7	23.6	0.176	0.155	0.145	-0.010
	±1.2	±0.6	±0.007	±0.005	±0.013	

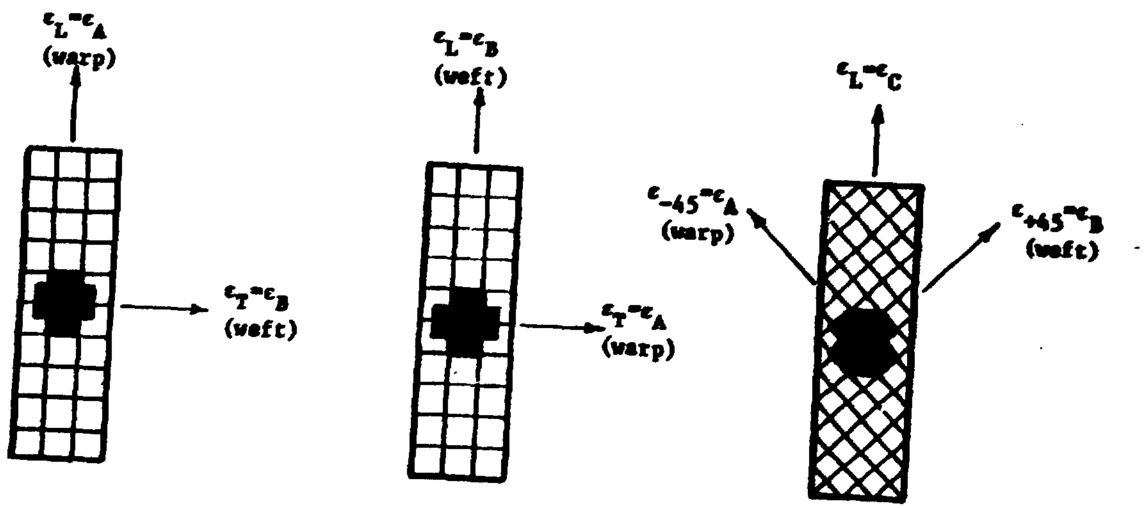

Fig.3.1 <u>TEST SPECIMENS FOR STIFFNESS MATRIX DETERMINATION</u>

Fig. 3.2 STRAIN GAUGE RECORDS FOR AN IMPACT TEST ON AN ALL-CARBON REINFORCED PARALLEL-SIDED COUPON LOADED IN THE WARP ('A') DIRECTION

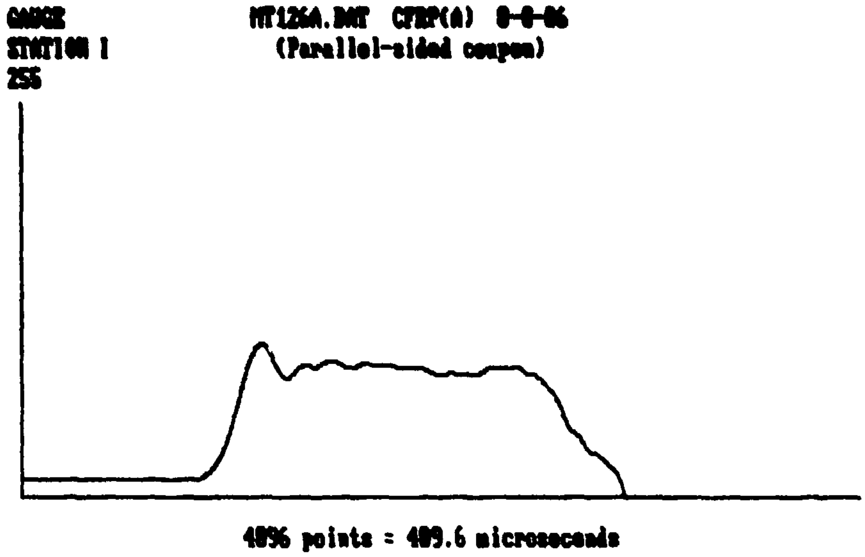

a) Input-bar signal - gauge station I

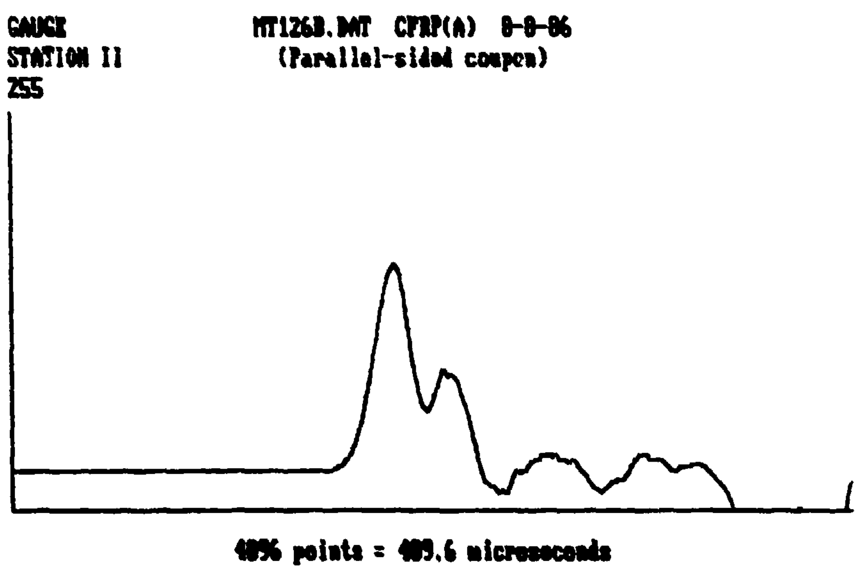

b) Input-bar signal - gauge station II

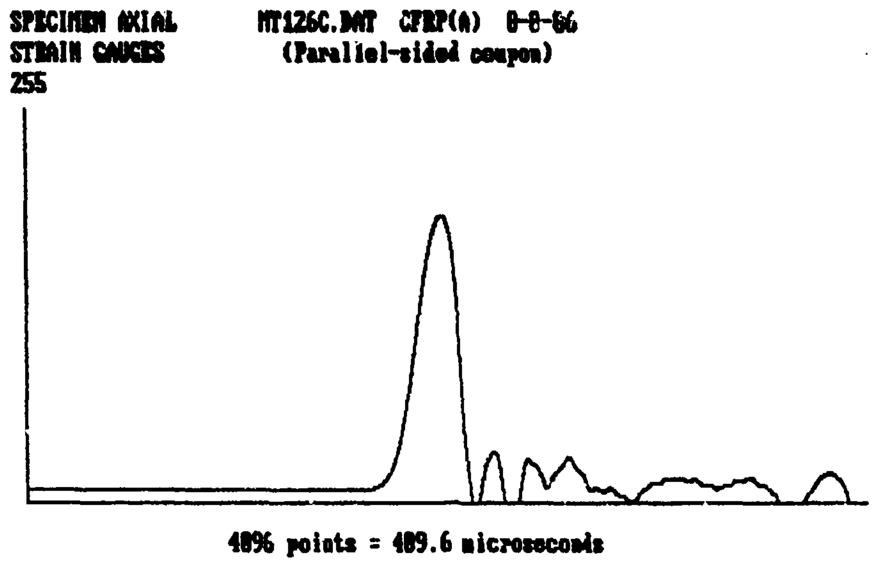

c) Specimen strain - loading direction

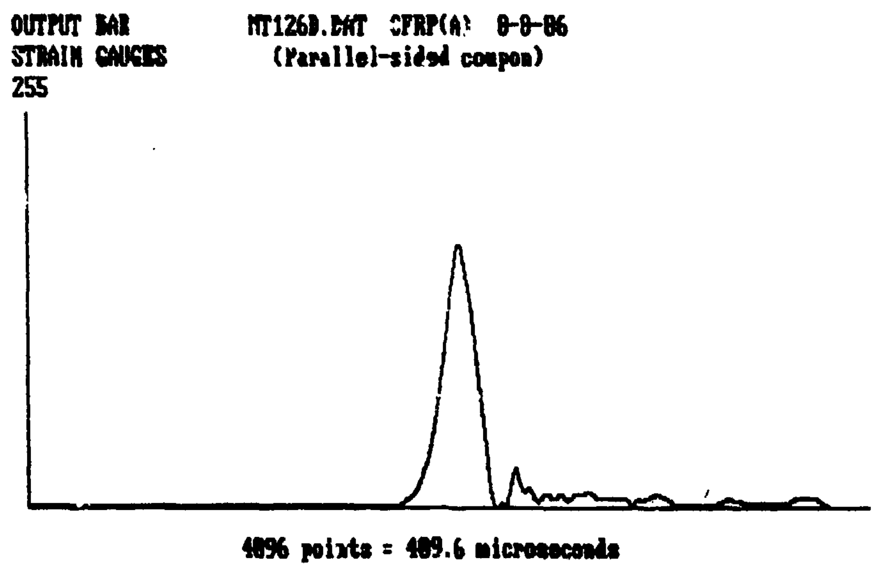

d) Output-bar signal - gauge station III

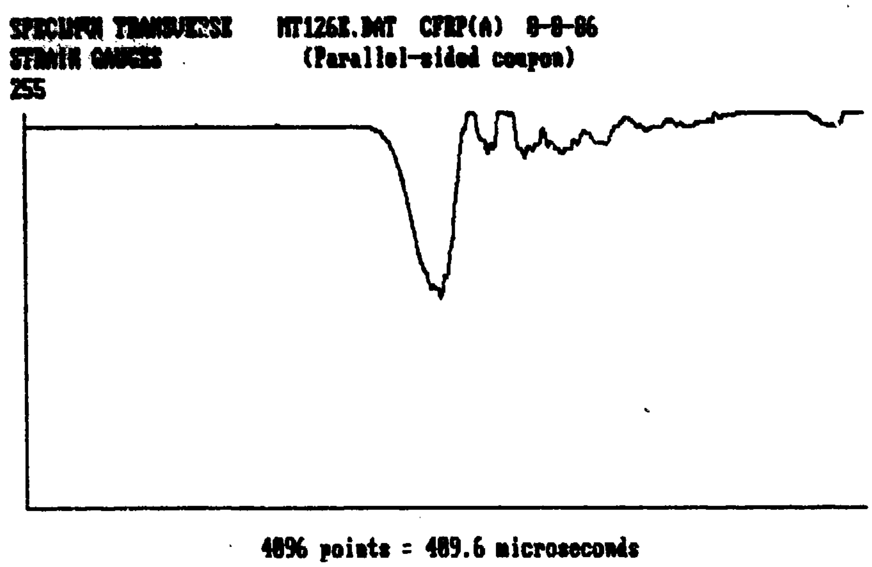

e) Specimen strain - transverse direction

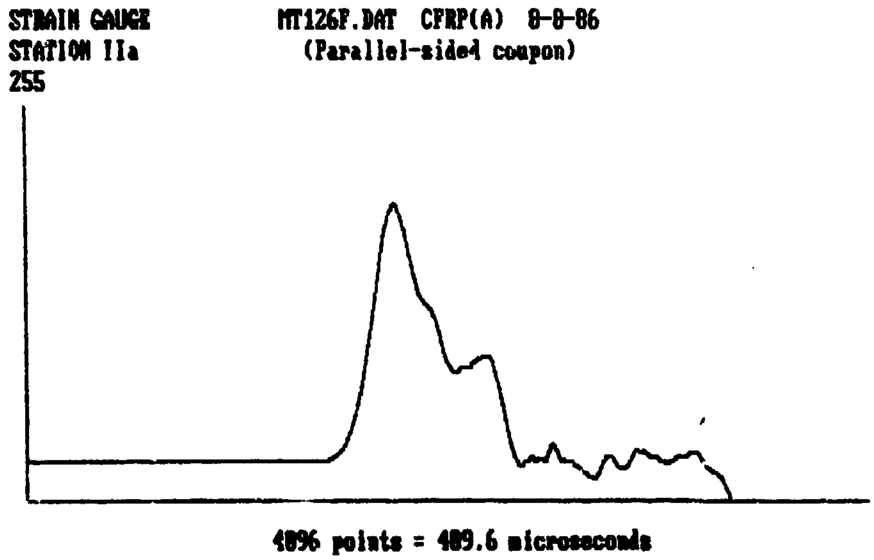

f) Input-bar signal - gauge station IIa

Fig. 3.3 <u>STRESS v. SPECIMEN STRAIN IN LOADING DIRECTION FOR TEST OF Fig. 3.2</u>

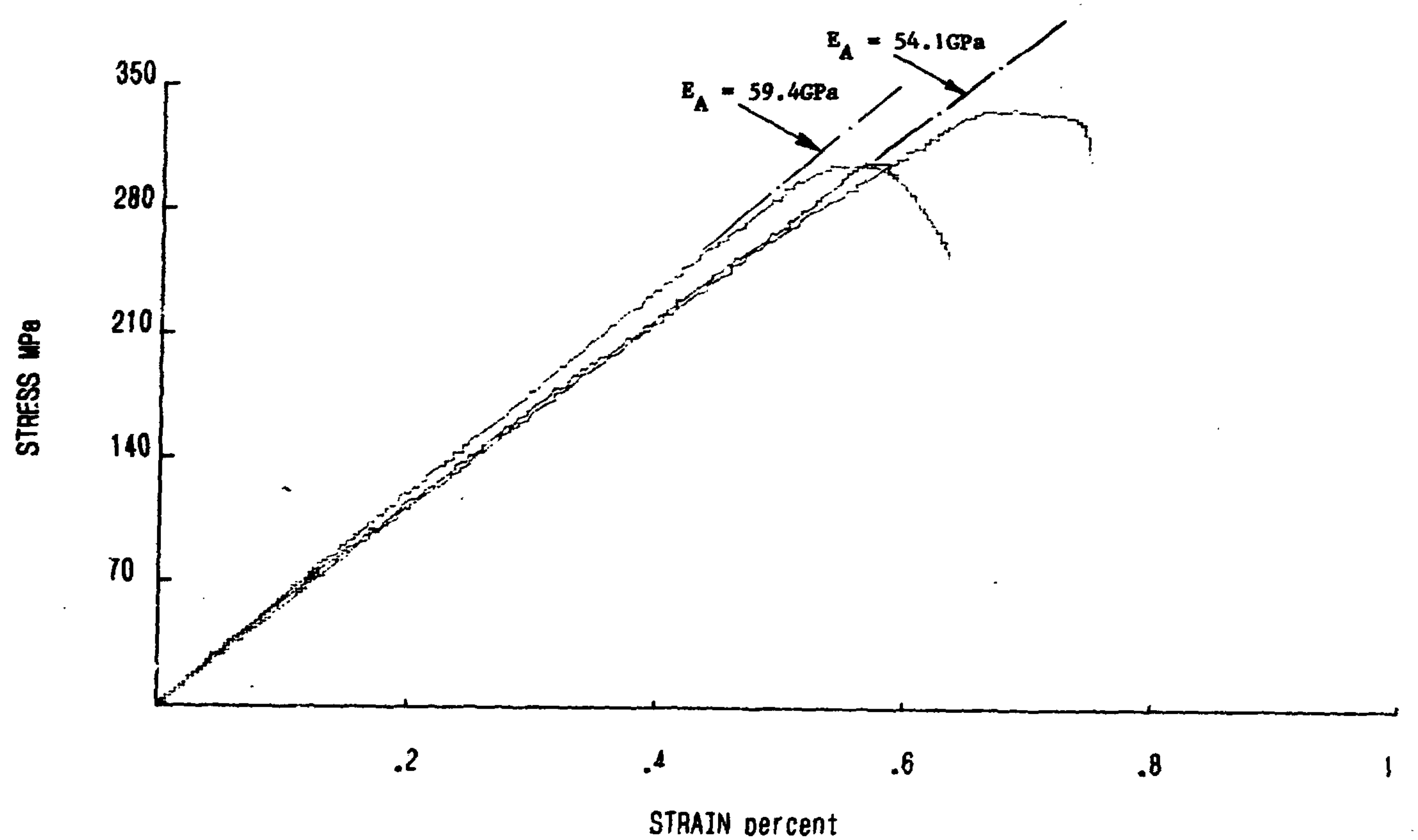

Fig. 3.4 SPECIMEN STRAIN IN TRANSVERSE DIRECTION v. SPECIMEN STRAIN IN LOADING DIRECTION FOR TEST OF Fig. 3.2

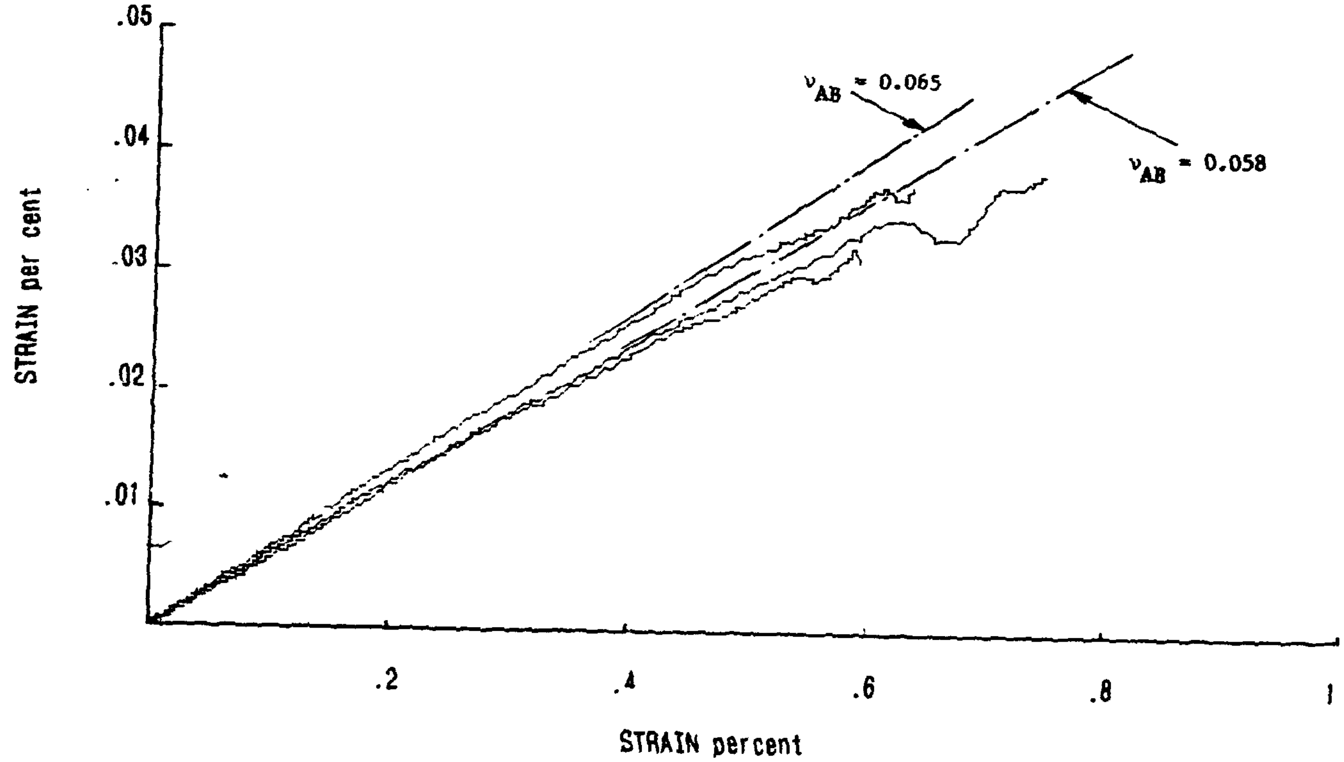

Fig. 3.5 STRESS v. SPECIMEN STRAIN IN LOADING DIRECTION FOR TEST ON ALL-GLASS REINFORCED PARALLEL-SIDED COUPON LOADED IN WEFT ('B') DIRECTION

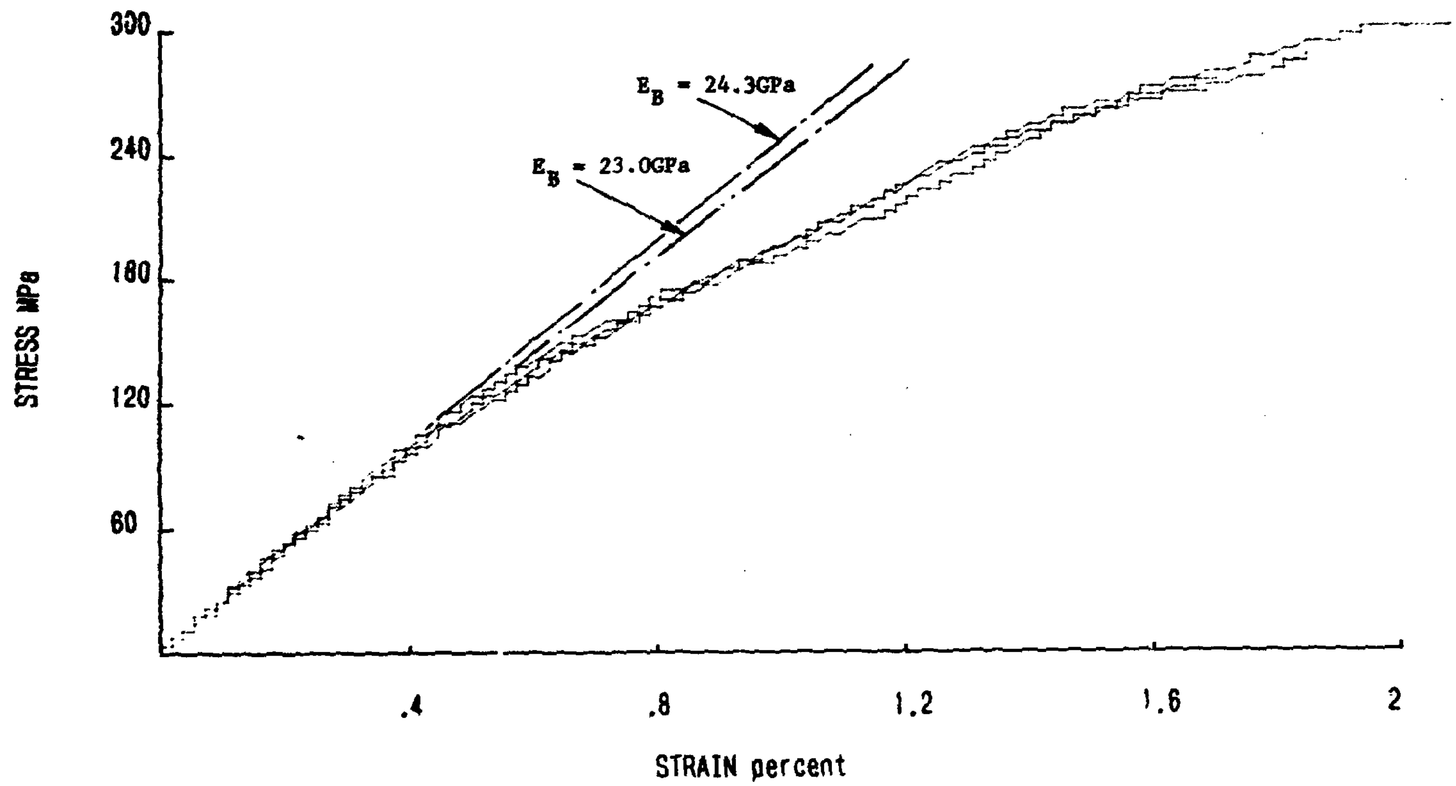

Fig. 3.6 <u>SPECIMEN STRAIN IN TRANSVERSE DIRECTION v. SPECIMEN STRAIN IN LOADING DIRECTION FOR TEST OF Fig. 3.5</u>

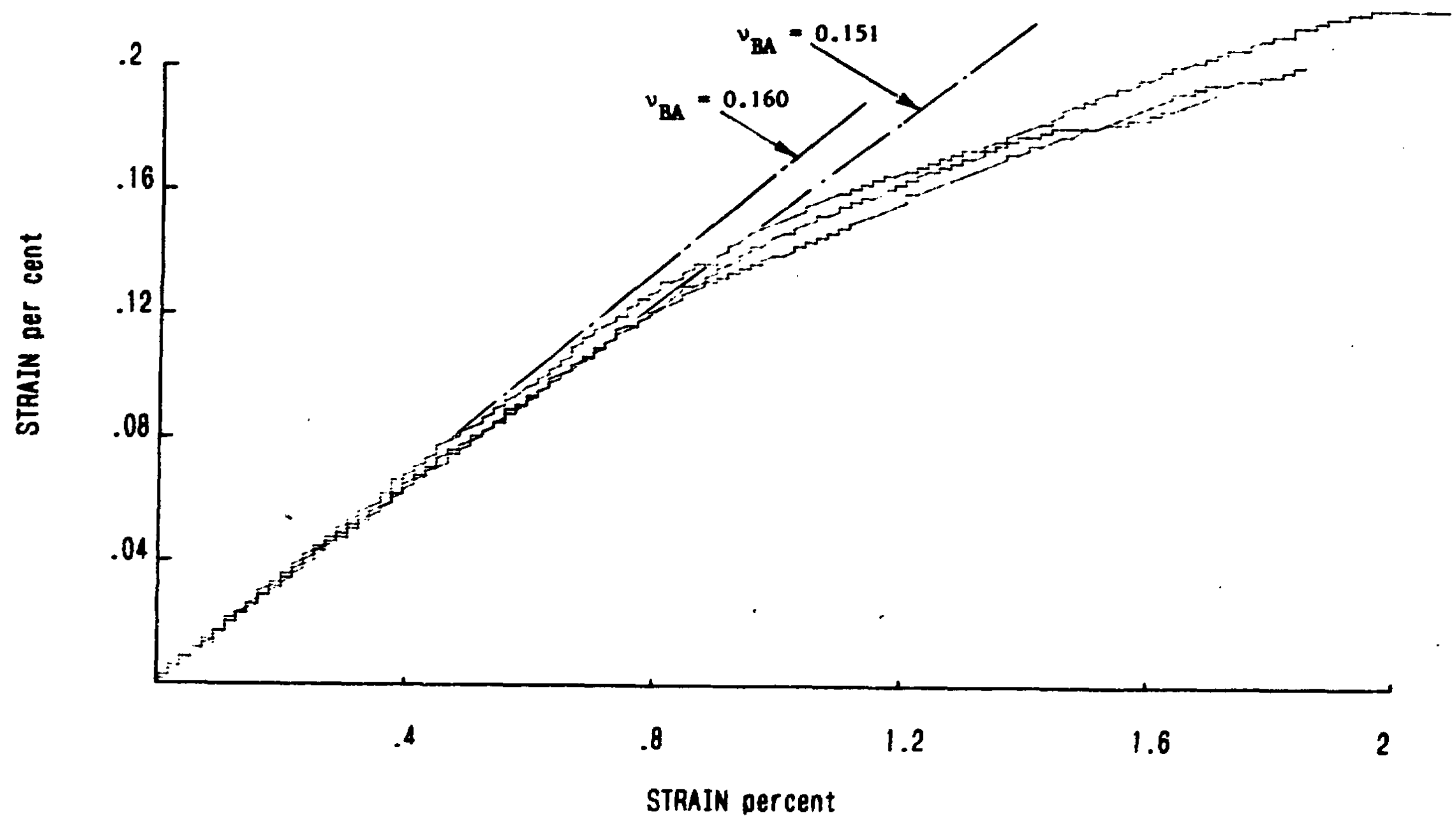

For comparison, ν_{AB} is also determined from the symmetry hypothesis for an orthotropic laminate, i.e. from

$$E_A \nu_{BA} = E_B \nu_{AB},$$

giving an alternative value, ν^*_{BA}. The discrapancy between these two values is indicated in the "error" column in Table 3.2. It is not unusual to find such a discrepancy (13,14) and in such cases it is generally the practice to use the ν_{BA} value in determining the stiffness matrix. A further, and more marked, discrepancy is found, however, when comparing the measurements of Youngs modulus from the waisted specimens, table 3.1, with those from the parallel-sided coupons, table 3.2. The contrast between the two sets of data is seen very clearly in table 3.3 below.

TABLE 3.3 Comparison of Youngs Modulus as Measured from Waisted Specimens and from Parallel-Sided Coupons

Specimen Type	All-Carbon Specimens		All-Glass Specimens	
	E_A (GPa)	E_B (GPa)	E_A (GPa)	E_B (GPa)
Waisted	48.7 ±7.1	49.0 ±4.1	24.0 ±0.9	17.1 ±2.2
Parallel-sided	55.9 ±2.6	60.9 ±2.6	28.7 ±1.2	23.6 ±0.6

In each case the measured modulus for the parallel-sided coupon exceeded that for the waisted specimen by between 15 and 30%, a difference considerably greater than the experimental scatter within any one set of measurements. Although a similar trend may be observed in the earlier quasi-static modulus measurements (3) the effect there was extremely small and was ignored. In the present tests, however, this is not possible and so, in the absence as yet of any explanation, both sets of data have been recorded and will be considered when the results are subsequently analysed.

3.1.3 Tests on Specimens Loaded in the 'C' Direction

For the impact tests in the 'C' direction waisted specimens, rather than parallel-sided coupons, were chosen so that, in addition to the data required for the determination of the dynamic in-plane shear modulus, complete dynamic stress-strain curves could also be obtained. Specimens were strain gauged as shown in fig. 3.1c. A typical set of strain gauge records for such a test on an all-glass specimen is shown in fig. 3.7. Signals from the specimen strain gauges aligned with the warp (-45° or A), the weft ($+45^{\circ}$ or B) and the loading (0° or C) directions are given in figs. 3.7f, e and c respectively while the input and output bar gauge signals, stations I, II and II, respectively, are given in figs. 3.7a, b and d. Using these latter three signals the standard Hopkinson-bar analysis may be used to derive a dynamic stress-strain curve. Such a

(14) Lempriere, B. M., "Uniaxial Loading of Orthotropic Materials", AIAA Journal, 6, (1968), 365-368.

(15) Bert, C. W., Mayberry, B. L. and Ray, J. D., "Behaviour of Fibre-Reinforced Plastic Laminates under Biaxial Loading", ASTM STP 460, (1969), 362-380

Fig. 3.7 STRAIN GAUGE RECORDS FOR AN IMPACT TEST ON AN ALL-GLASS REINFORCED WAISTED SPECIMEN LOADING IN THE 'C' DIRECTION

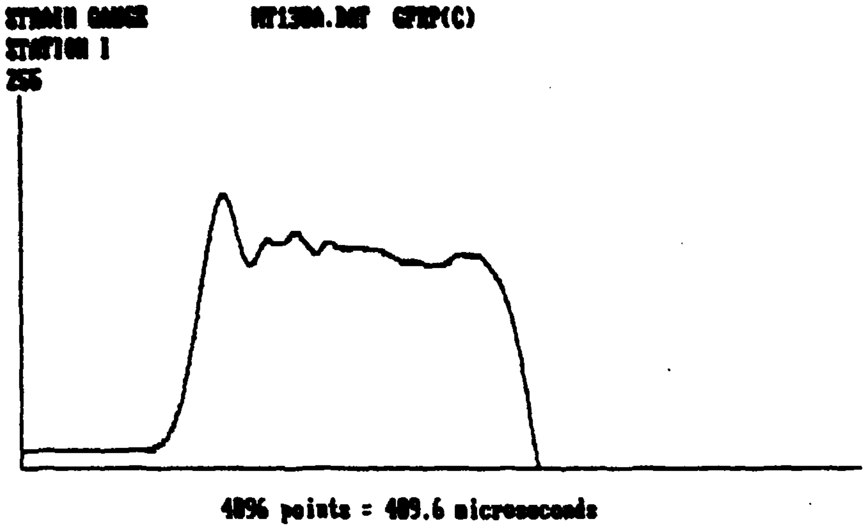

a) Input-bar signal - gauge station I

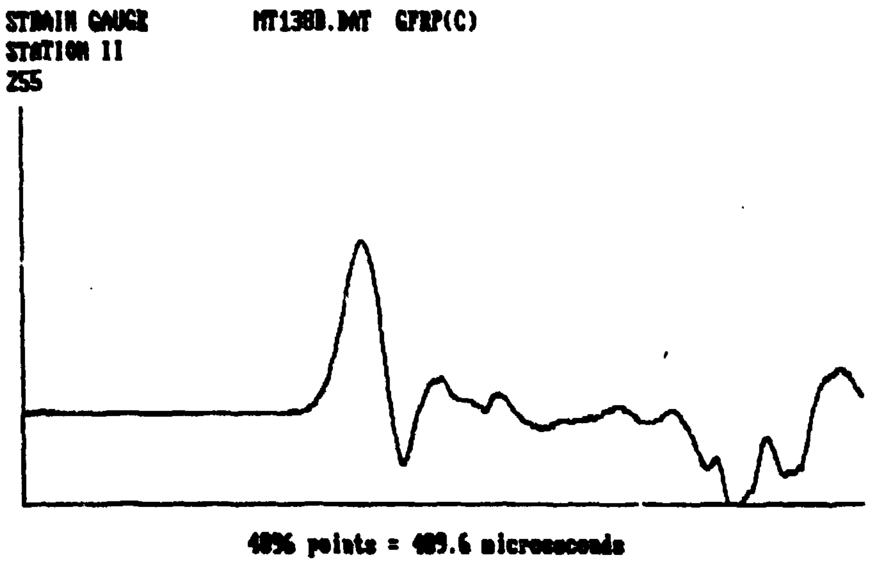

b) Input-bar signal - gauge station II

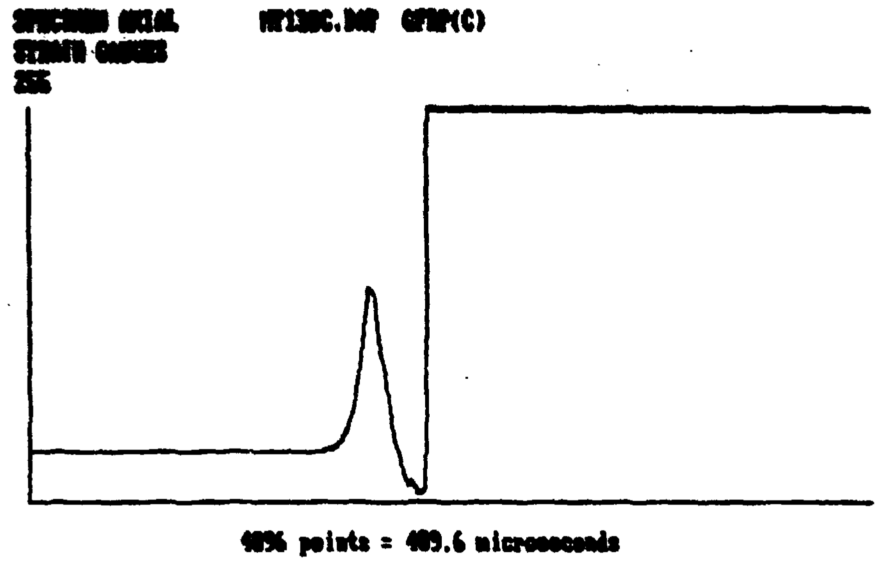

c) Specimen strain - loading direction

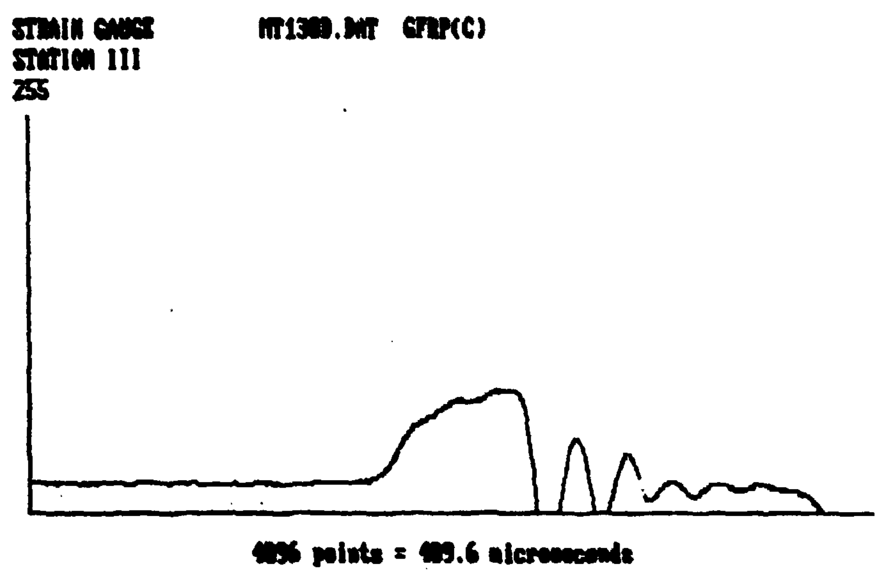

d) Output-bar signal - gauge station III

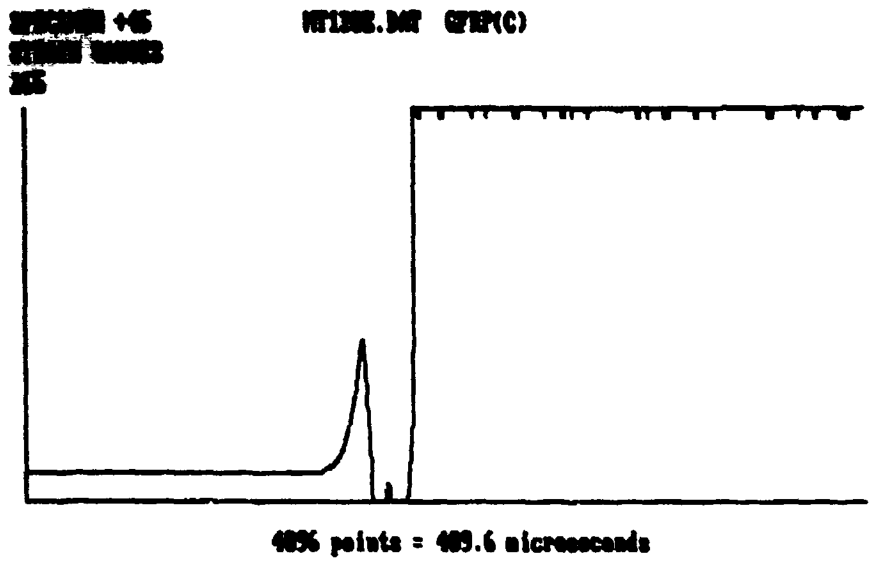

e) Specimen strain - weft (+45°) direction

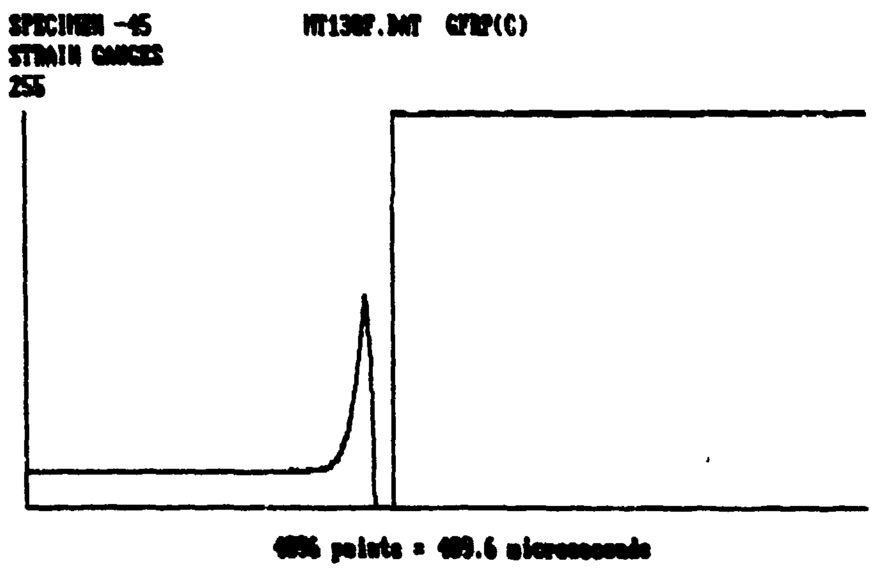

f) Specimen strain - warp (-45°) direction

curve for a test on an all-carbon specimen loaded in the C direction is shown in fig. 3.8. Also in fig. 3.8 is included the stress-strain curve derived directly from the output bar signal, fig. 3.7d, which gives the specimen stress, and the signal from the specimen strain gauges aligned with the loading direction, fig. 3.7c, which gives the specimen strain up to the point at which surface damage on the specimen results in failure of these gauges. While the maximum strain reached in this case is limited, the curve obtained does gives a more accurate measure of the elastic modulus, here designated E_C. The specimen strain gauges are used, therefore, both to determine the elastic moduli of the specimen material and also, as described in the previous report (3) for tests on specimens loaded in the A and B directions, to correct the initial part of the dynamic stress-strain curve. The resulting corrected curve is also shown in fig. 3.8.

In these earlier tests (3) the specimen strain gauges always failed before the specimen elastic limit was reached. In the present tests, however, when all-carbon specimens are loaded in the C direction, the specimen strain gauges aligned in the loading direction (corresponding to $\epsilon_L = \epsilon_C$ in fig. 3.1) continued, in some cases, to give an output signal to strains well beyond the elastic limit, as shown in fig. 3.8. Because of this several anomalies become apparent which were not previously seen. Thus the yield stress for the stress-strain curve derived from the specimen strain gauges lies significantly below that for the corrected Hopkinson-bar curve as do also the subsequent stress levels up to a point at which a crossover is seen between a region at low strains, where, in comparison with the specimen strain gauges, the Hopkinson-bar analysis at any given stress overestimates the specimen strain and a region at high strains where the Hopkinson-bar analysis underestimates the specimen strain. A possible explanation for this crossover in response follows from the different effective gauge lengths used in calculating the two curves of fig. 3.8. For the curve derived from the specimen strain gauges the gauge length is the active length of the strain gauge itself, about 2mm, lying entirely within the central parallel region of the specimen. For the curve derived from the Hopkinson-bar analysis, however, the effective gauge length is the gap between the loading bars, about 25mm for the all-carbon specimens, which includes the tapered as well as the parallel region of the specimen. Although this estimate of gauge length should not be too greatly in error while the deformation is elastic, once damage begins to develop in the central parallel region of the specimen the effective gauge length is likely to be reduced, and hence the measured strain increased, by about a factor of 3. This is apparent from from fig. 3.9 which shows the fracture appearances typical of all-carbon and all-glass specimens following tensile impact in the C direction. A concentration of the impact damage within the central third, i.e. the parallel region of the specimen, is apparent in both materials. To allow for this a second correction has been applied to the Hopkinson-bar curve of fig. 3.8, the inelastic strain in the post-yield region being increased by this factor of 3. The resulting curve shows much closer agreement with the stress-strain curve derived from the specimen strain gauges in the post-yield region, see fig. 3.10, although the discrepancy at the elastic limit remains. The most significant effect of this second correction is to increase the estimated strain at peak load, ϵ_m, from about 2.6% to about 4.5%. Unfortunately in no other test did the specimen strain gauges continue to give a signal

Fig. 3.8 COMPUTED STRESS-STRAIN CURVES FROM THE RAW DATA OF Fig. 3.7

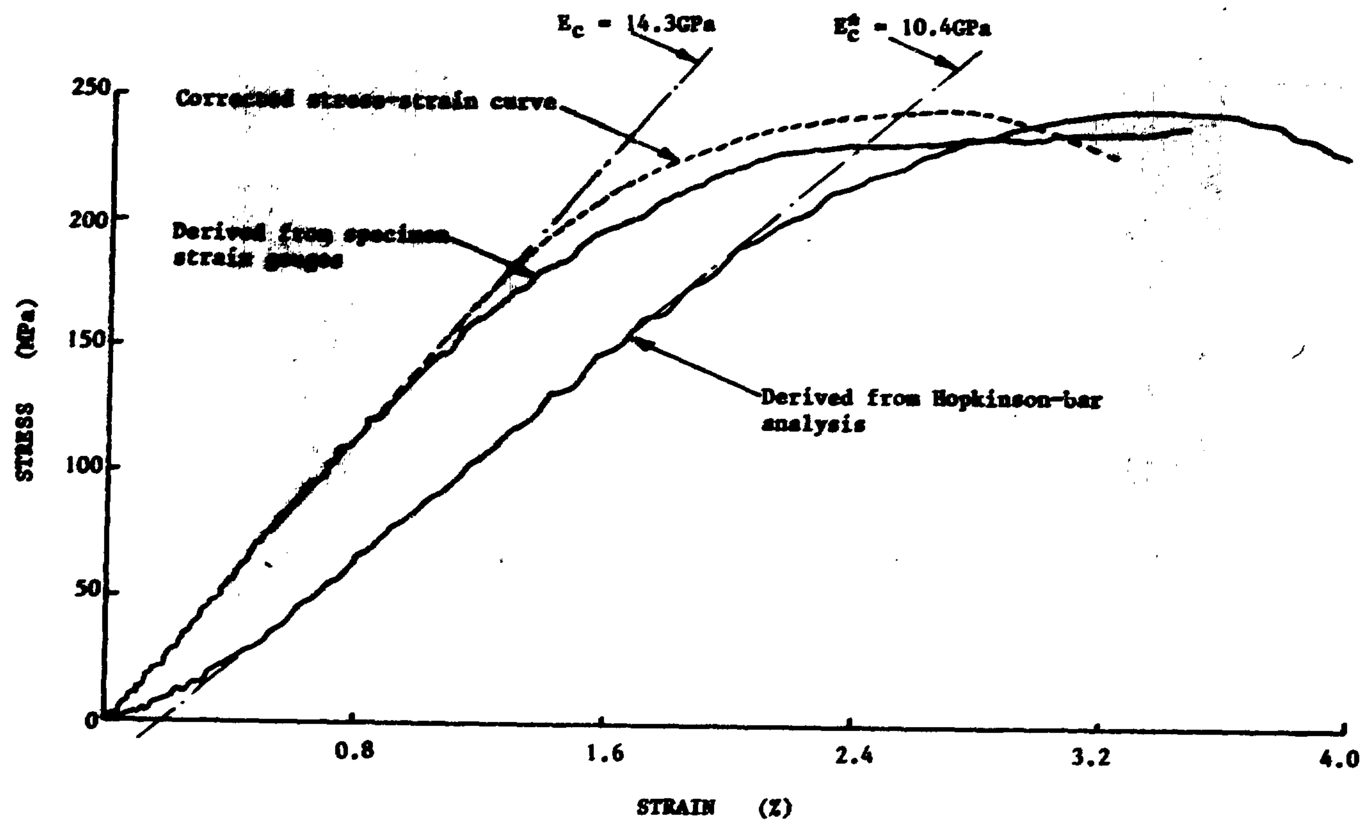

Fig. 3.9 FRACTURE APPEARANCE OF ALL-CARBON AND ALL-GLASS SPECIMENS AFTER IMPACT LOADING IN THE 'C' DIRECTION

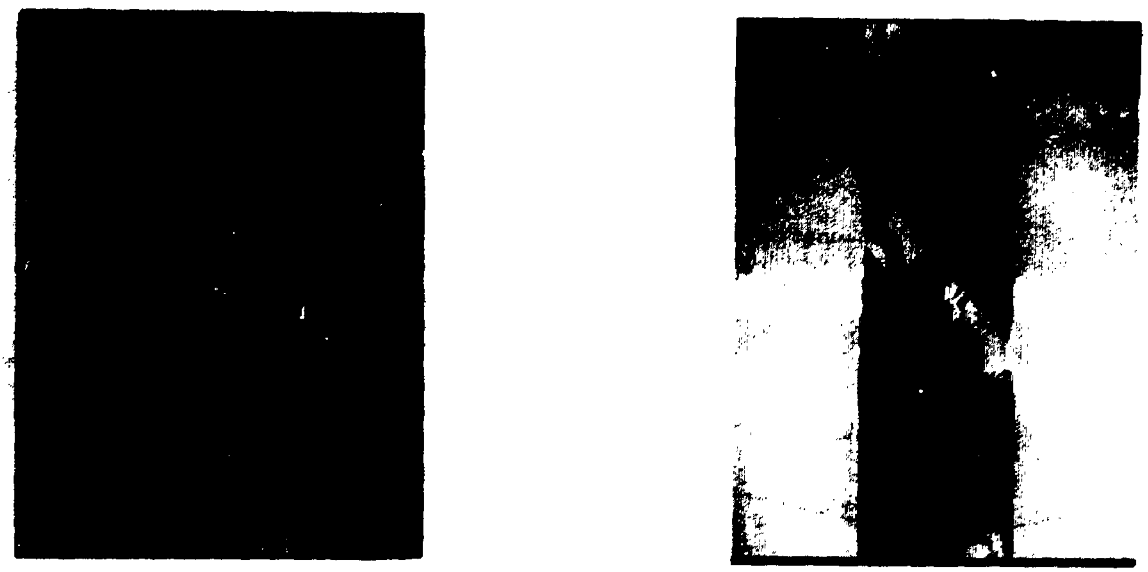

a) All-carbon specimen

b) All-glass specimen

Fig. 3.10 STRESS-STRAIN CURVES OF Fig. 3.8 CORRECTED FOR REDUCED GAUGE LENGTH IN POST-YIELD REGION

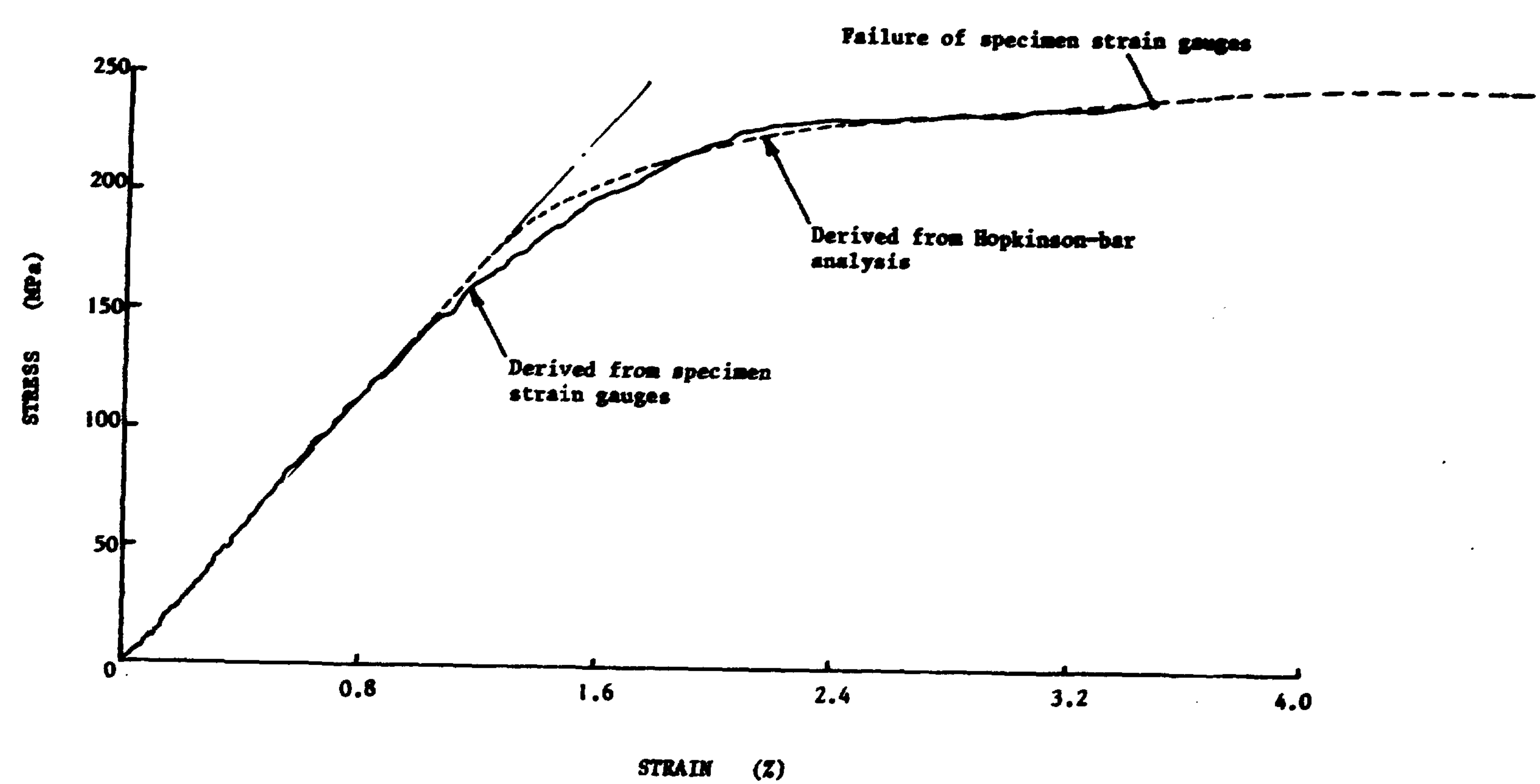

much beyond the elastic limit. Until further evidence is obtained which confirms the behaviour shown in figs. 3.8 and 3.10 the second correction, i.e. the reduction in effective gauge length in the post-yield region, will be ignored.

Three tests were performed on the all-carbon and three on the all-glass specimens. The stress-strain curves obtained, corrected only for the initial elastic slope, are shown in figs. 3.11 and 3.12, for the all-carbon and the all-glass specimens respectively. The data obtained in these tests are summarised in table 3.4, where E_c^* is the modulus in the C direction as derived from the Hopkinson-bar analysis and the quoted ε_m value takes no account of the effective gauge length correction discussed above for the post-yield region. The average strain rate during the test was of the order of 1500/s for the all-carbon specimens and 2000/s for the all-glass specimens

TABLE 3.4 Mechanical Properties of All-Carbon and All-Glass Specimens under Impact Loading in the C Direction

Material	E_c GPa	E_c^* GPa	σ_{max} MPa	ε_f (%)	σ_y MPa	ε_y (%)
All-carbon	14.2	9.84	263.6	2.78	209	2.10
	13.4	10.44	244.6	2.92	172.5	1.65
	14.3	10.43	247.5	2.60	193.5	1.85
	14.0	10.24	251.9	2.77	191.7	1.87
	±0.5	±0.3	±9.5	±0.16	±18.3	±0.23
All-glass	11.7	6.60	-----	----	111.0	1.7
	11.5	7.13	225.1	9.44	100.0	1.4
	11.4	6.57	228.9	12.19	88.0	1.34
	11.5	6.77	227.0	10.82	99.7	1.48
	±0.2	±0.28	±1.9	±1.38	±11.5	±0.18

3.1.4 Determination of In-Plane Shear Modulus

As described in the earlier report (3) the results of tests such as those of section 3.1.3 above may be used to calculate the in-plane shear modulus by either of two methods. The first of these uses the modulus in the C direction, E_c, as listed in Table 3.4, to estimate G_{AB} from equation (3.1)

$$G_{AB} = \{(4/E_c) - (1/E_A) - (1/E_B) + 2(\nu_{AB}/E_A)\}^{-1}. \qquad (3.1)$$

Two different dynamic values for E_A and E_B are available, see Table 3.3. Since, however, E_c was determined from tests on waisted specimens it seems reasonable to use corresponding values for E_A and E_B also taken from tests on waisted specimens. This is not possible where ν_{AB} is concerned since Poisson's ratio was determined only in tests on parallel-sided coupons. The second method of estimating G_{AB} uses equation (3.2)

$$G_{AB} = (1/2)\{(2/E_c) - (1/E_\alpha) - (1/E_\beta)\}^{-1} \qquad (3.2)$$

Fig. 3.11 STRESS-STRAIN CURVES FOR IMPACT TESTS ON ALL-CARBON SPECIMENS LOADED IN THE 'C' DIRECTION

(Corrected for initial elastic slope)

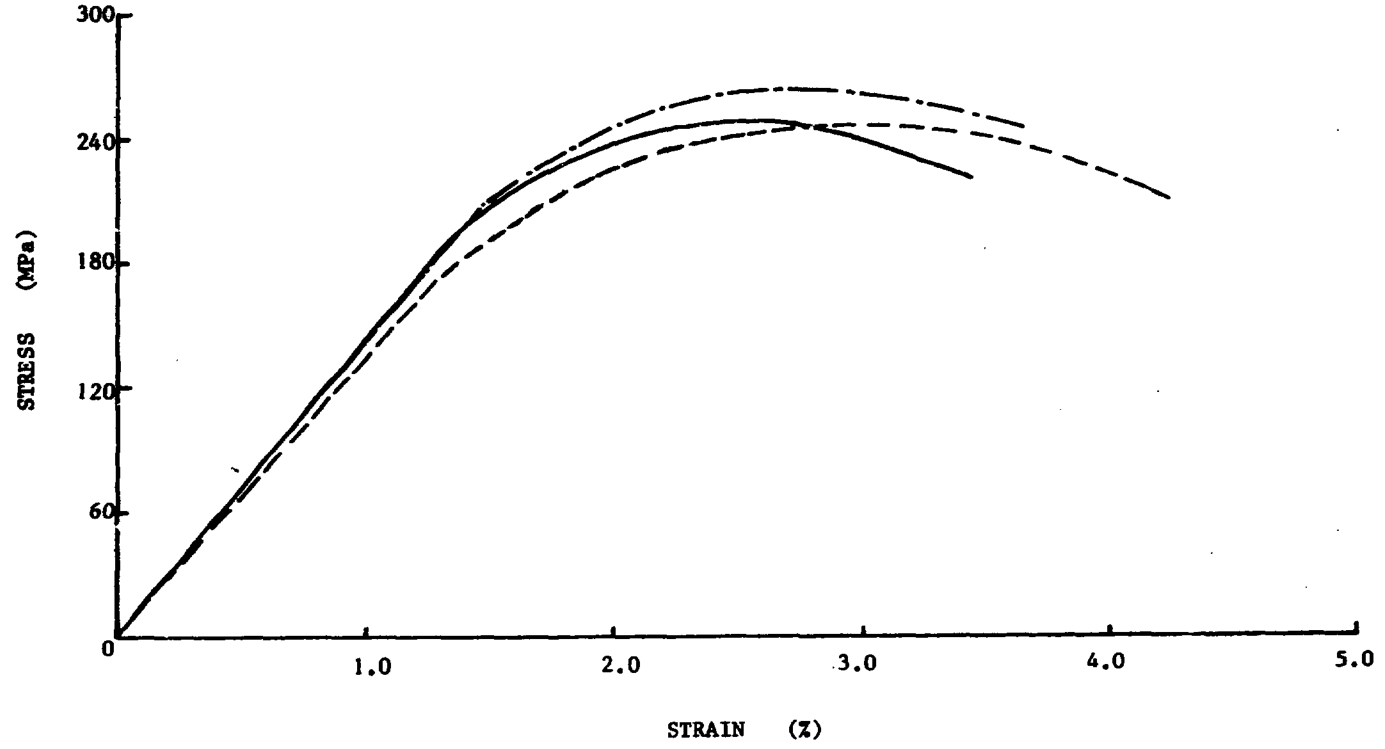

Fig. 3.12 STRESS-STRAIN CURVES FOR IMPACT TESTS ON ALL-GLASS SPECIMENS LOADED IN THE 'C' DIRECTION
(Corrected for initial elastic slope)

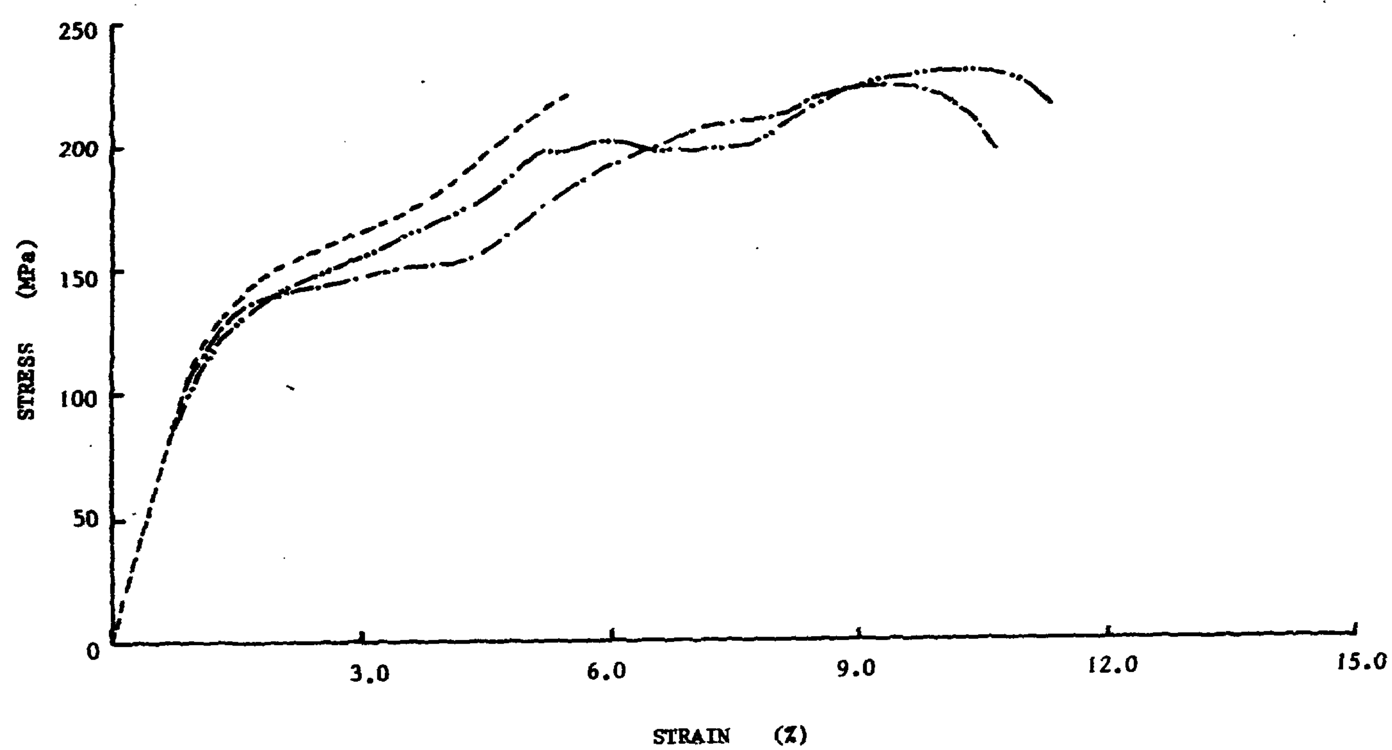

where the "moduli" E_α and E_β are defined as the specimen stress, fig. 3.7d, divided by the strain in either the warp (ε_{-45}) or the weft (ε_{+45}) directions, figs. 3.7e and f respectively. The calculation of equation (3.2) is independent, therefore, of the choice of values for E_A and E_B. Results for the variation of the specimen stress with strain in the warp direction for tests on the all-carbon specimens are shown in fig. 3.13. The corresponding values of moduli for these and similar tests on the all-glass specimens are listed in Table 3.5. Also given in Table 3.5 are the calculated values for G_{AB} as determined from both equation (3.1), giving G^*_{AB}, and equation (3.2), giving G^{**}_{AB}. For the all-carbon specimens there is negligiole difference between the two estimates but for the all-glass specimens equation (3.1) gives a value some 7.5% greater than equation (3.2). By using values for E_A and E_B from Table 3.3 for the parallel-

TABLE 3.5 Elastic Constants from Impact tests on Specimens Orientated in the 'C' Direction

Material	E_c GPa	E_α GPa	E_β GPa	G^*_{AB} GPa	G^{**}_{AB} GPa
All-carbon	14.2	195	85.8	4.11	4.03
	13.4	180	67.5	3.83	3.87
	14.3	131	81.3	4.14	4.17
	14.0	169	78.2	4.03	4.02
	±4%	±19%	±12%	±4%	±4%
All-glass	11.7	64.3	55.3	3.88	3.62
	11.5	63.8	63.0	3.80	3.50
	11.4	63.9	53.0	3.75	3.53
	11.5	64.0	57.1	3.81	3.55
	±1%	±0.5%	±9%	±2%	±2%

sided coupons alternative estimates of G^*_{AB} are obtained givi g 3.55GPa ± 3% for the all-glass specimens and 3.93GPa ± 4% for the all-carbon specimens, i.e. eliminating the previous difference between G^*_{AB} and G^{**}_{AB} for the all-glass specimens but introducing a difference of about 2.5% between those for the all-carbon specimens.

3.2 Transverse Impact tests on Woven-Reinforced Laminates

Tests have been performed on five different hybrid lay-ups, see fig. 3.14, at gas-gun firing pressures of 40 and 60psi. All specimens were C-scanned both before and after testing, to determine the extent of the delaminated region resulting from the impact. All specimens were then either sectioned and examined under the optical microscope or deplied and the residual quasi-static tensile strength of the various plies determined.

3.2.1 Load-Displacement Data

The difficulties which arise when attempting to obtain reliable data for the load in the transverse impact test have already been described in section 2 above. As discussed in (13), however, these difficulties are likely

Fig. 3.13 SPECIMEN STRESS v. WARP STRAIN (ϵ_{-45}) FOR ALL-CARBON SPECIMENS LOADED IN THE 'C' DIRECTION

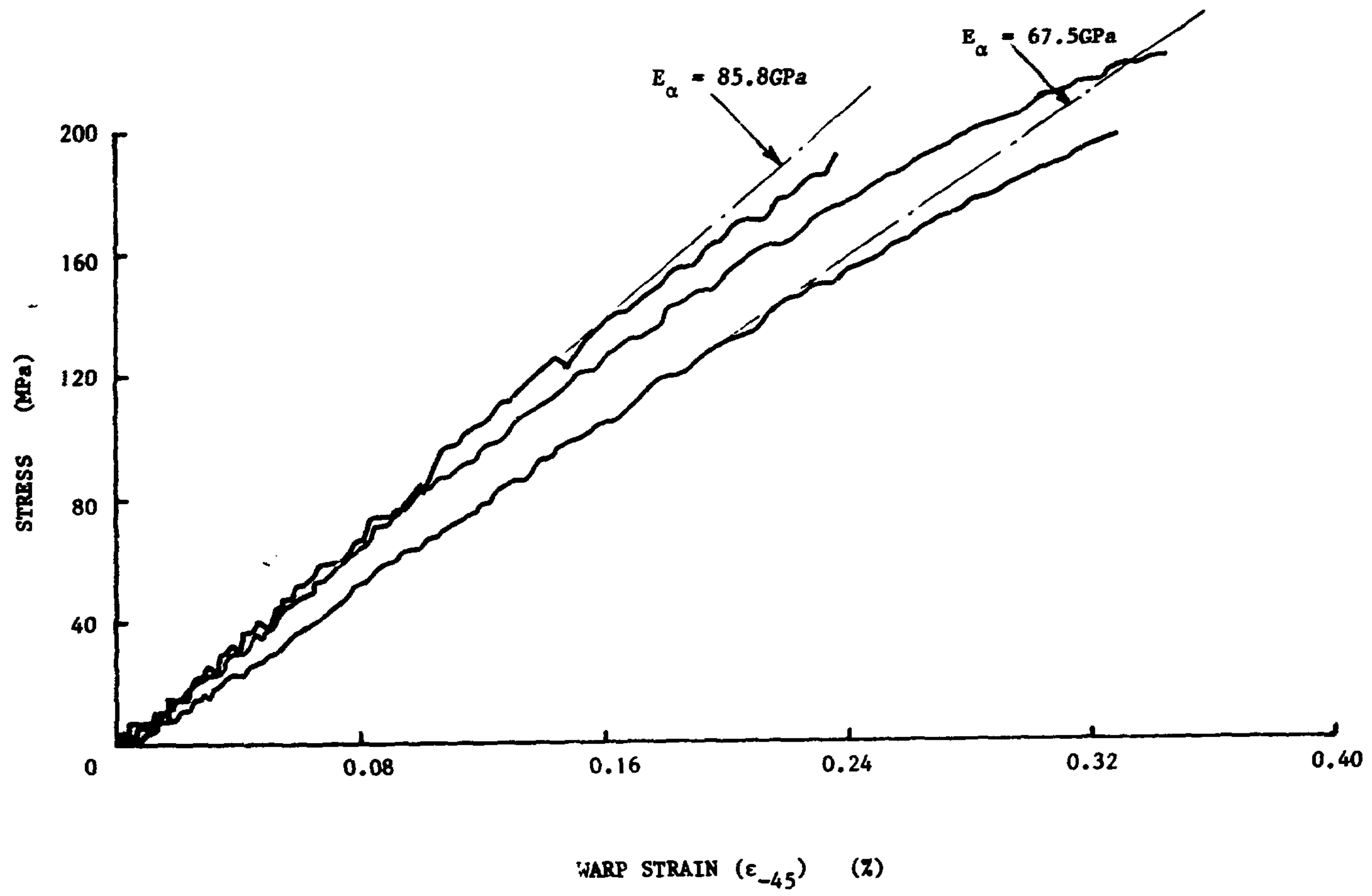

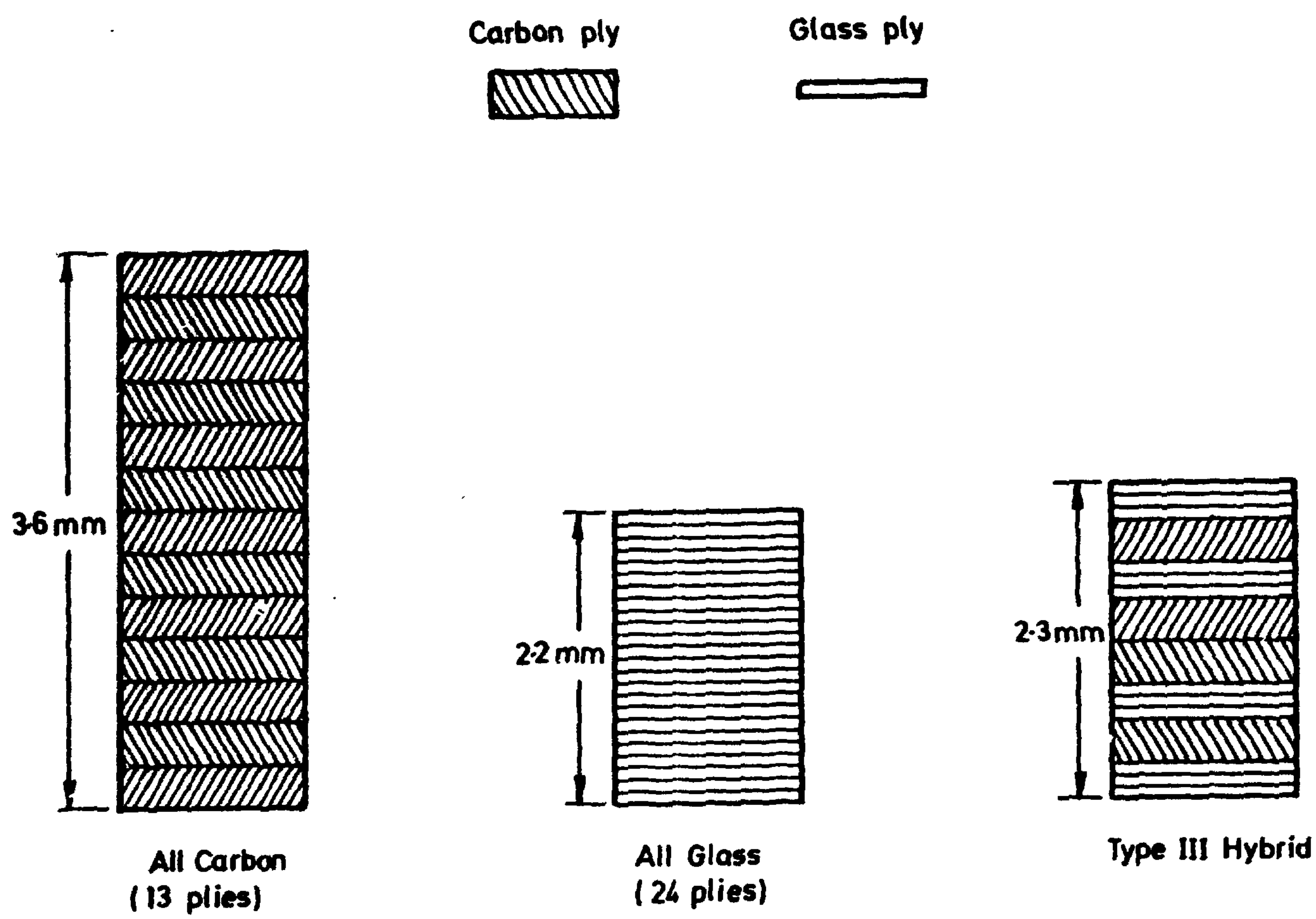

Fig. 3.14 LAY-UP CONFIGURATION FOR VARIOUS SPECIMEN LAMINATES

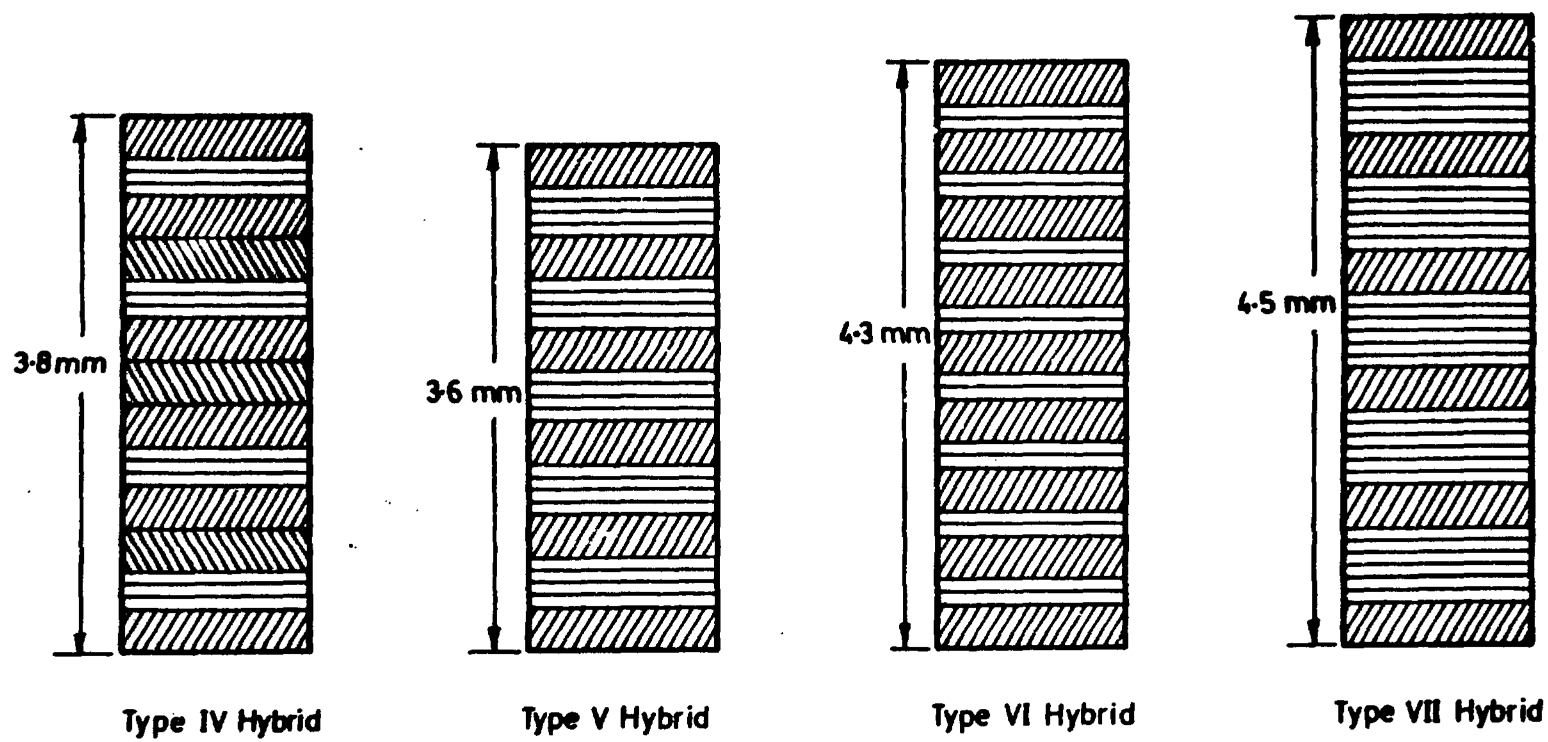

Fig. 3.14 (Continued)

to be at their least severe when stiff laminates are impacted at the lower firing pressures. This was the case for the all-carbon laminate in section 2, where the firing pressure was only 30psi. At this pressure, however, no damage could be detected in the laminate after impact. At the higher pressures required to initiate impact damage and for tests on hybrid laminates, which have a lower stiffness than the all-carbon lay-up, it is likely, therefore, that only by the use of the back surface strain gauges and the related quasi-static calibration will any estimate of load be possible.

Unfortunately, for the hybrid laminates quasi-static calibrations of the back surface strain gauges have only been obtained for the type III and the type V lay-ups. For the type III lay-up the calibration is markedly non-linear for loads above about 0.5kN, see fig. 3.15, whereas for the type V lay-up, see fig. 2.12, a linear calibration is obtained up to about 2kN. The lowest firing pressure for the hybrid laminates was 40psi. Using the test at this pressure on the type V hybrid a further comparison of the two methods of load determination may be made. The load-time and load-displacement curves for this test, calculated from the input-bar signals, are shown in figs. 3.16a and b. Again considerable noise is apparent on the load-time curve and both the load and the displacement fall to around zero after about 1.6 to 1.7ms.

Using the calibrations of fig. 2.12, a load-time curve may also be obtained from the back surface strain gauges. The resulting curve for gauge position F is compared in fig. 3.17 with the earlier curve of fig. 3.16a. As before, the general shape of the two curves is closely similar, the noise on the curve derived from the input-bar signals falling more or less symmetrically about that derived from gauge F. As a further check on the errors involved in the static calibration technique of load determination, since a near linear calibration was also obtained for the back surface gauge at position D, a second estimate of the load-time curve may be obtained from this gauge. The two load-time curves, derived from the two back surface gauges, are compared in fig. 3.18. Bearing in mind that gauge F is measuring a radial strain in the direction of weave and that gauge D is measuring a tangential strain at 45 degrees to the direction of weave, the general agreement between the two curves is surprisingly good. Nevertheless, even if a linear extrapolation of the quasi-static calibration can be assumed up to a load of about 3kN, the absolute accuracy with which the applied load may be determined is limited to no better than about + or - 25%.

Increasing the firing pressure to 60psi results in a load-time curve derived from the input-bar gauges on which there is so much noise that it is now almost impossible to interpret, see fig. 3.19a. The corresponding displacement-time curve, see fig. 3.19b, shows a maximum displacement of about 3mm, compared with 1.2mm for the test at 40psi (fig. 3.16). Also the displacement in the 60psi test only reaches this maximum value after about 1.6ms, i.e. at the end of the calculated part of the test, and no subsequent decay in the displacement is observed. It may still be possible to estimate the load from the back surface strain gauges using the quasi-static calibrations of fig. 2.12. The resulting load-time curves obtained in this way from gauges D and F are compared in fig. 3.20. In contrast with the behaviour found at 40psi, see fig. 3.18, where reasonable

Fig. 3.15 QUASI-STATIC CALIBRATIONS OF BACK SURFACE STRAIN GAUGES FOR TYPE III HYBRID SPECIMEN

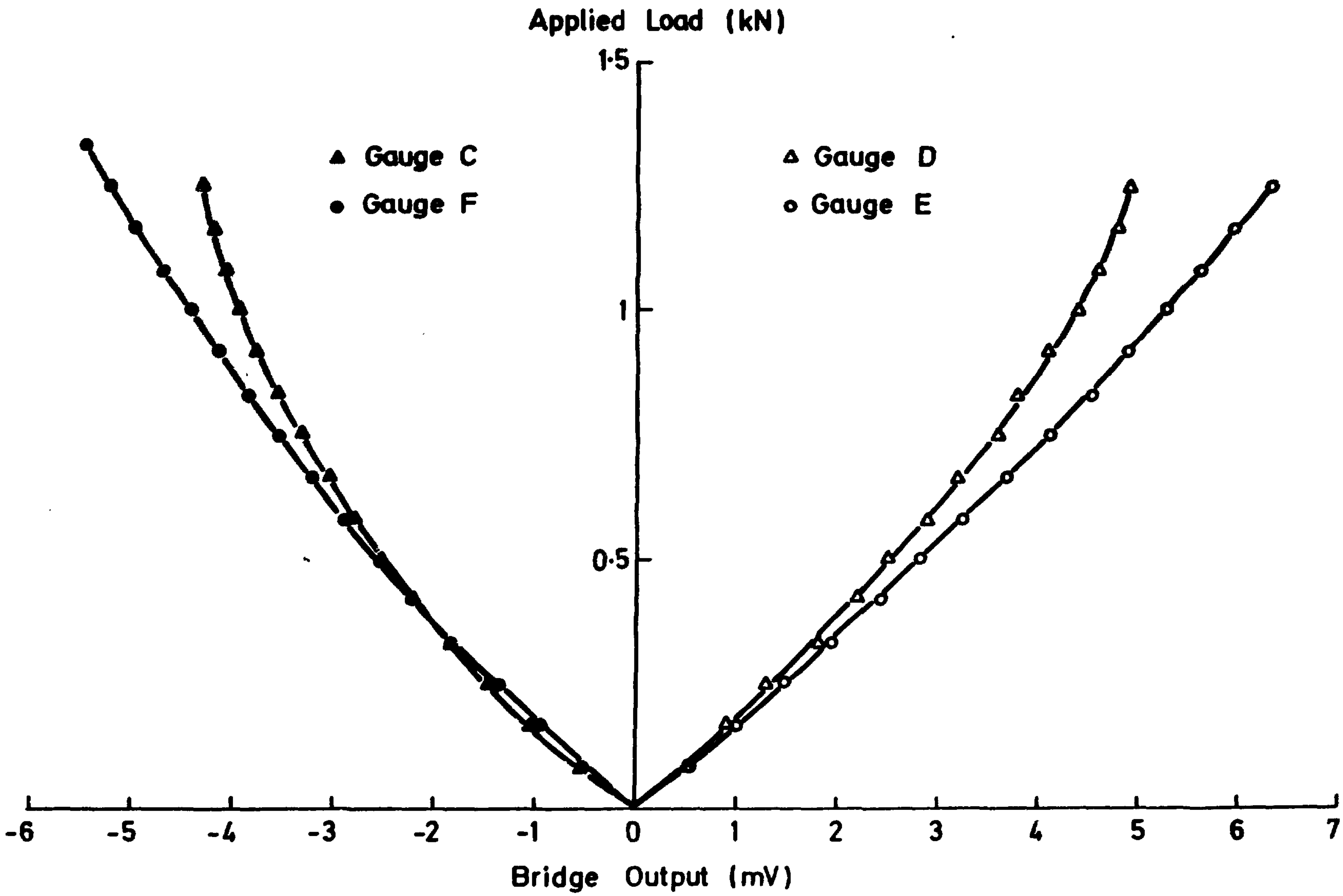

Fig. 3.16 LOAD-TIME AND DISPLACEMENT-TIME CURVES FOR IMPACT AT 40psi ON TYPE V HYBRID SPECIMEN

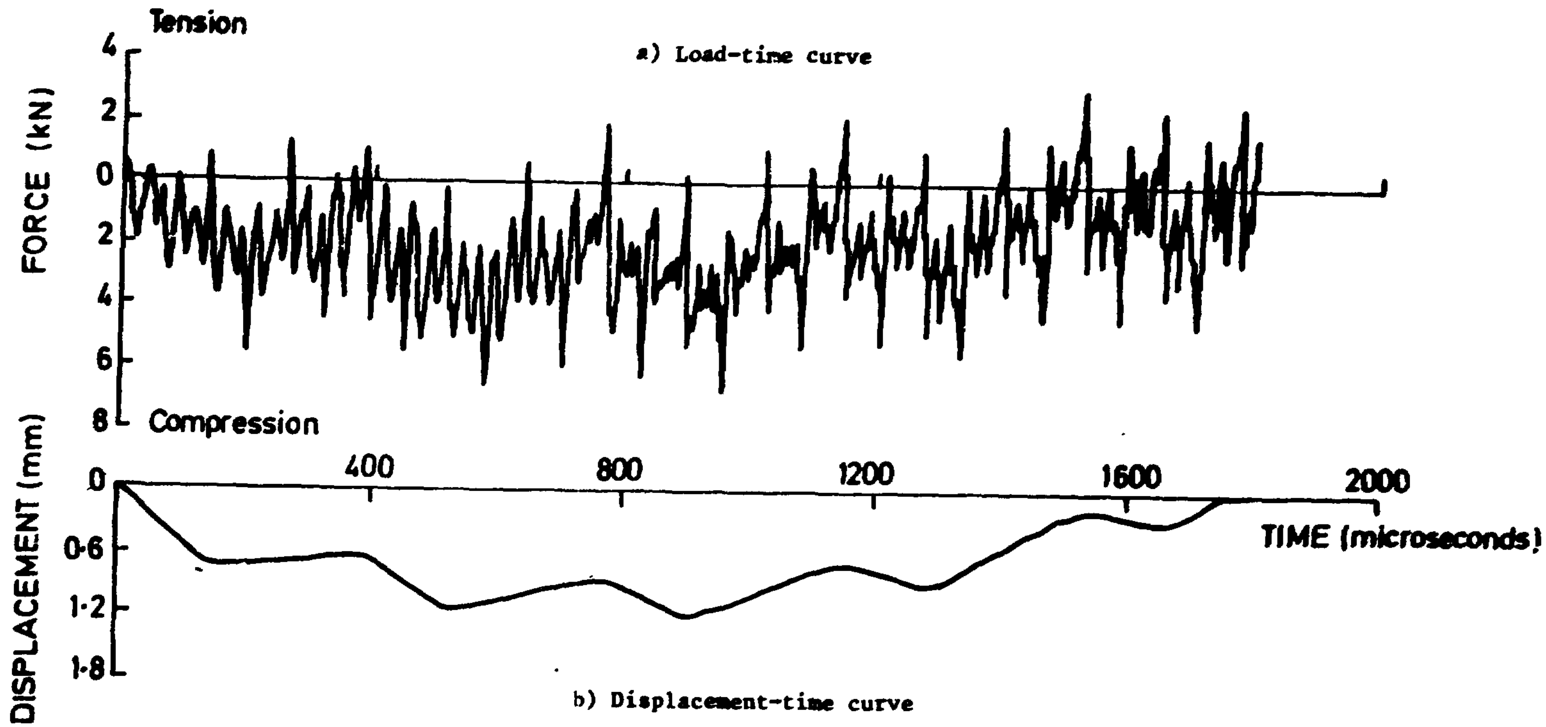

a) Load-time curve

b) Displacement-time curve

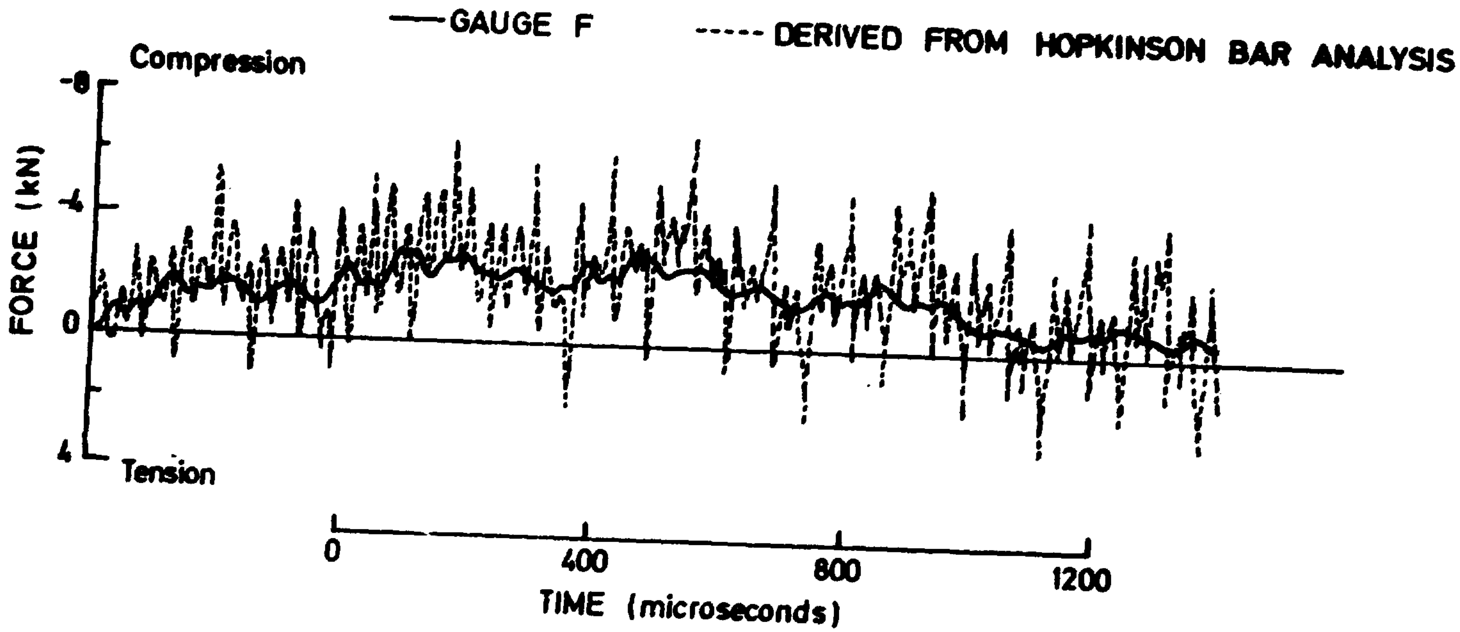

Fig. 3.17 <u>COMPARISON OF LOAD-TIME CURVES DERIVED FROM STRAIN GAUGE F AND FROM HOPKINSON-BAR ANALYSIS FOR TEST OF Fig. 3.16</u>

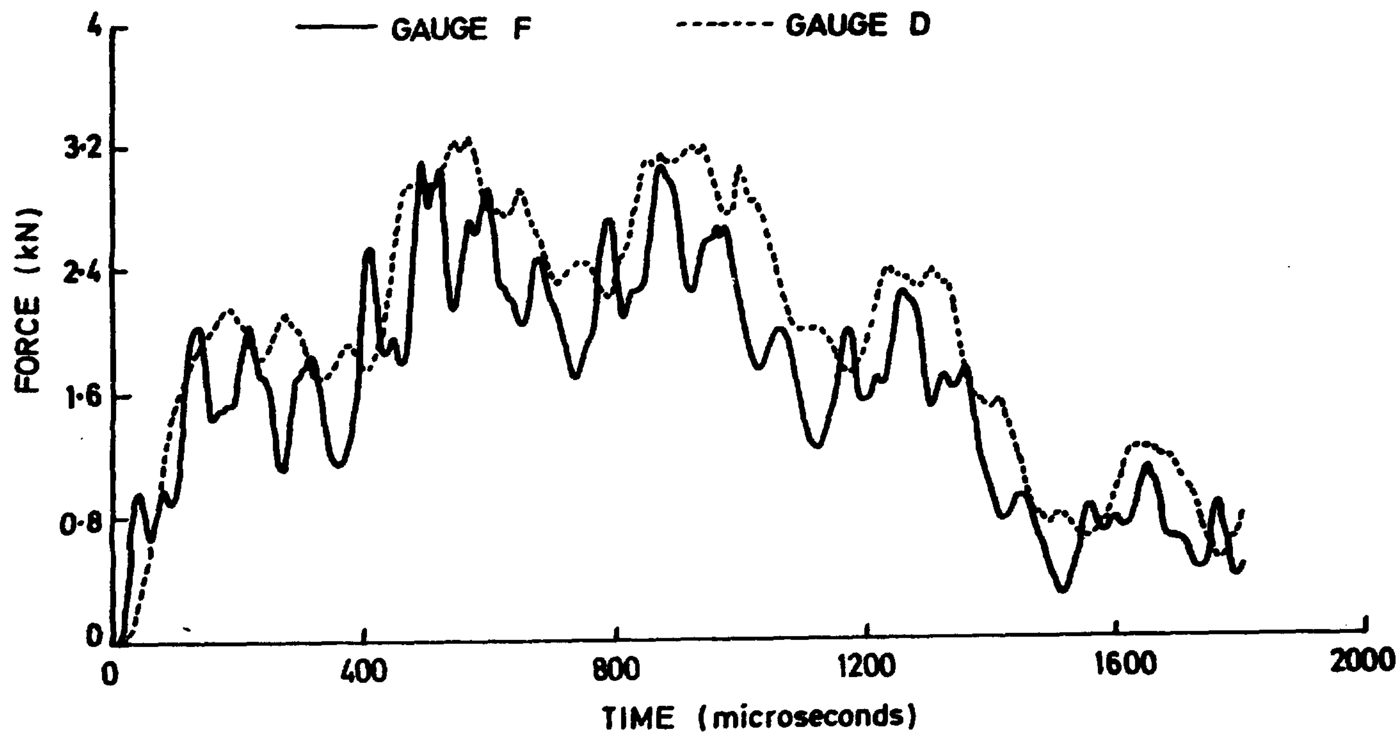

Fig. 3.18 <u>COMPARISON OF SIGNALS FROM BACK SURFACE STRAIN GAUGES D AND F FOR TEST OF Fig. 3.16</u>

Fig. 3.19 LOAD-TIME AND DISPLACEMENT-TIME CURVES FOR IMPACT AT 60psi ON TYPE V HYBRID SPECIMEN

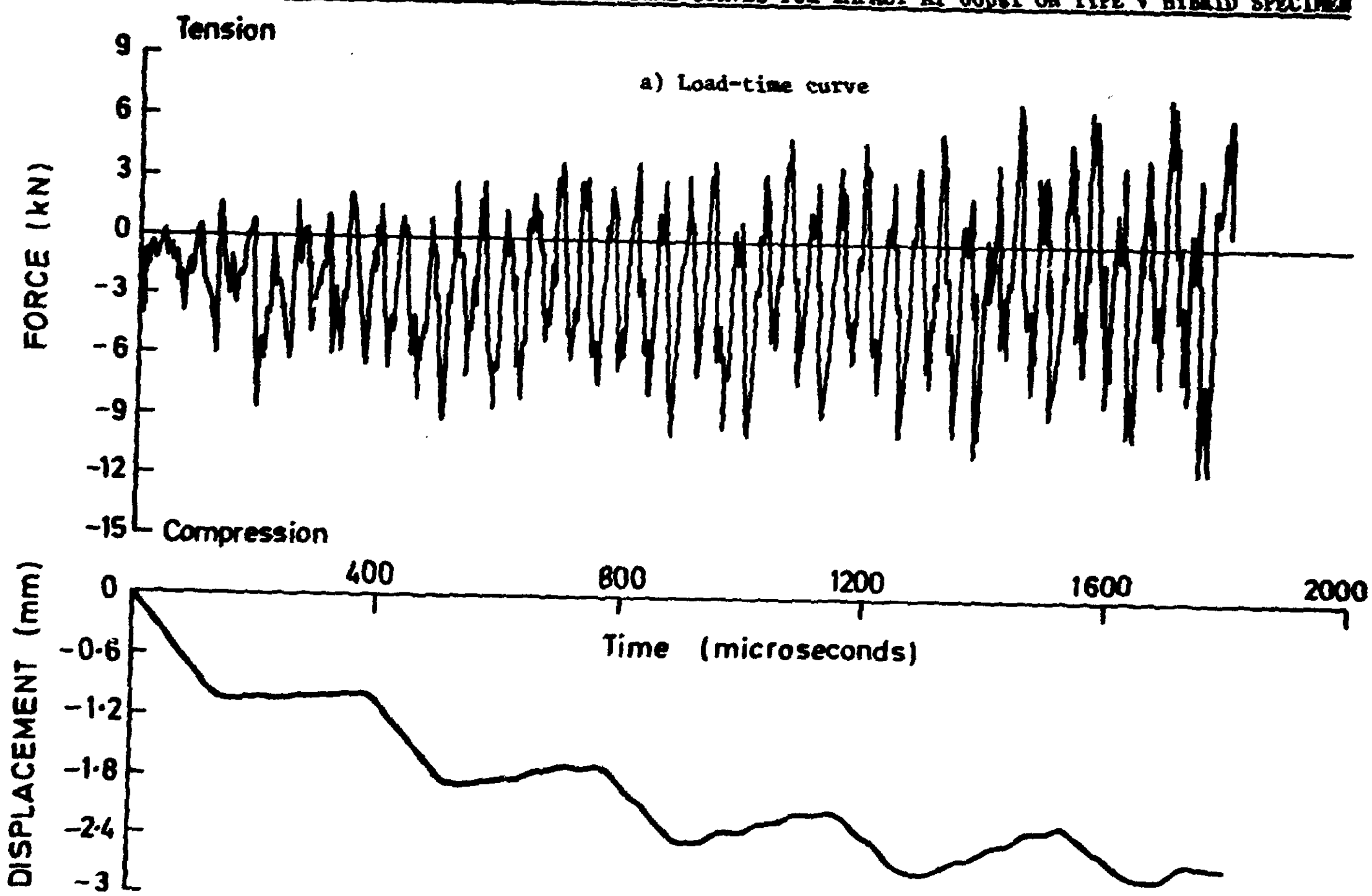

b) Displacement-time curve

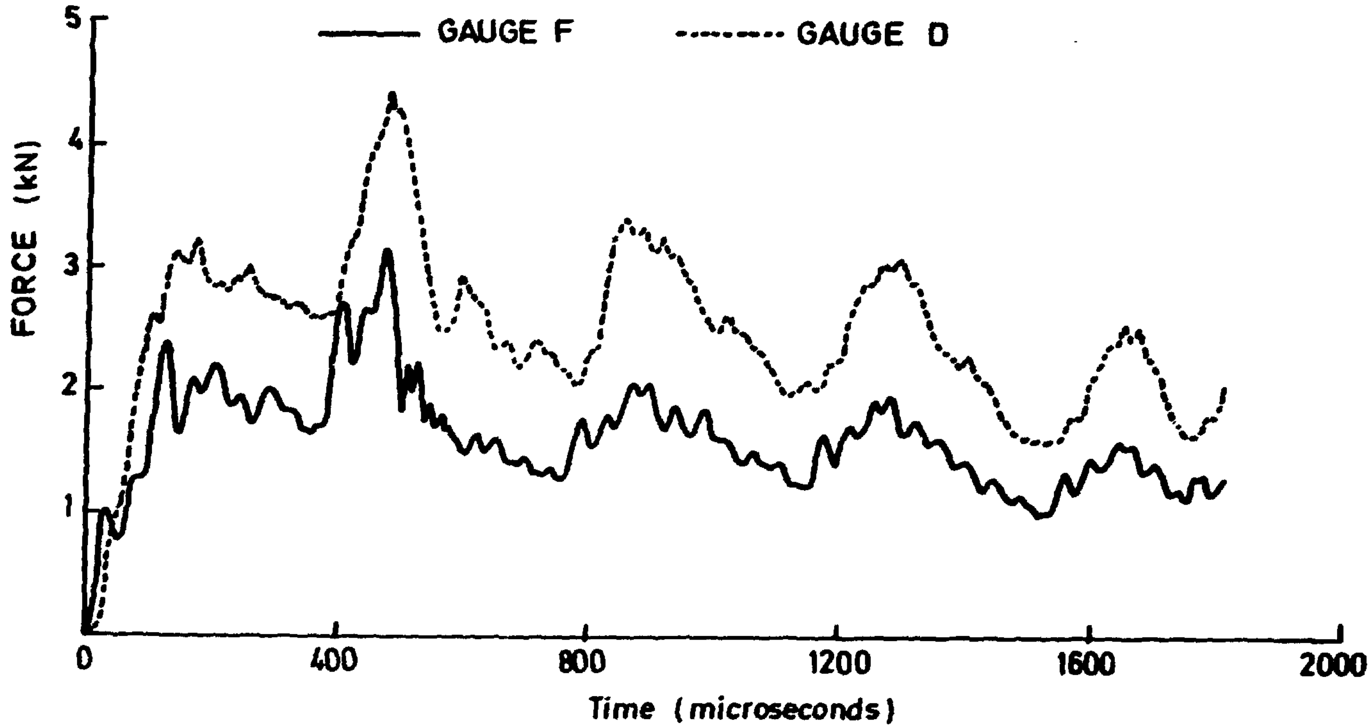

Fig. 3.20 COMPARISON OF SIGNALS FROM BACK SURFACE STRAIN GAUGES D AND F FOR TEST OF Fig. 3.19

agreement between the results from these two gauges was obtained, here gauge D predicts a significantly higher load than gauge F, suggesting that the calibrations of fig. 2.12 have been affected differently by the damage induced at this higher impact pressure and thus casting doubt on the validity of the measured loads.

The behaviour shown in fig. 3.19a is typical of that found in all tests at the higher pressures and at all pressures on specimens of lower strength and stiffness. Further attempts to estimate the applied load, therefore, were abandoned until the modified loading system becomes available. Reliable displacement-time curves, such as that of fig. 3.19b, are available, however, and show significant differences in response for different specimens. Thus, for the type VII hybrid the maximum displacement at 40psi is about 1mm, increasing to about 1.6mm at 60psi (figs. 3.21a and b). In both cases the peak displacement is reached after about 0.8ms and is followed by a significant recovery. For the woven all-glass laminate, however, see figs. 3.22a and b, the displacement is still increasing after 1.6ms, the end of the calculated part of the test, having reached in this time a peak of about 2mm at 30psi and about 4mm at 60psi.

3.2.2 Damage Assessment

Specimens were C-scanned, both before and after testing, to estimate the area of delamination and were then either sectioned on a diametral plane to observe damage by means of the optical microscope or were deplied and the extent of fibre damage determined by measuring the residual ply quasi-static tensile strength. Typical sets of C-scan photographs for the all-carbon laminates after impact at firing pressures of 30, 40 and 60psi, and for the type V and VI hybrid laminates, after impact at firing pressures of 40 and 60psi, are shown in figs. 3.23, 3.24 and 3.25 respectively. The residual ply strengths, normalised with respect to the strength of the undamaged carbon or glass plies, are shown in figs. 3.26, 3.27 and 3.28, respectively, for the same specimens. Open symbols denote glass plies and filled symbols carbon plies. Also included in fig. 3.27 are the results for an untested and deplied specimen from which the average undamaged tensile strengths of the glass and carbon plies, respectively 0.44 and 2.33kN, may be determined and an indication of the experimental scatter in estimating the ply strength, from 0.94 to 1.08, may be obtained.

For the all-carbon laminate, see fig. 3.22, no delamination is observed after impact at 30psi while at both 40 and 60psi a delaminated region of approximately circular shape, centred on the point of impact, may be seen, the diameter increasing from about 15mm at 40psi to about 20mm at 60psi. Although considerable experimental scatter is obtained when determining residual ply strengths for the coarse weave carbon plies, the results presented in fig. 3.26 do indicate very little fibre damage at 30psi and a very marked deterioration in strength both for the first three plies directly under the point of impact and also increasingly from the middle of the specimen to the back surface. At 60psi all 13 plies showed some reduction in strength while at 40psi plies 4 to 8 were not significantly affected, lying within the scatter band for the ply strengths of the 30psi test. Rear surface cracks, visible to the naked eye on the specimen tested at 60psi, see fig. 3.23d, explain the very low residual strength of the back surface plies. No such damage was obvious on the front surface despite the marked reduction in ply strength also observed here.

a) Impact at 40psi

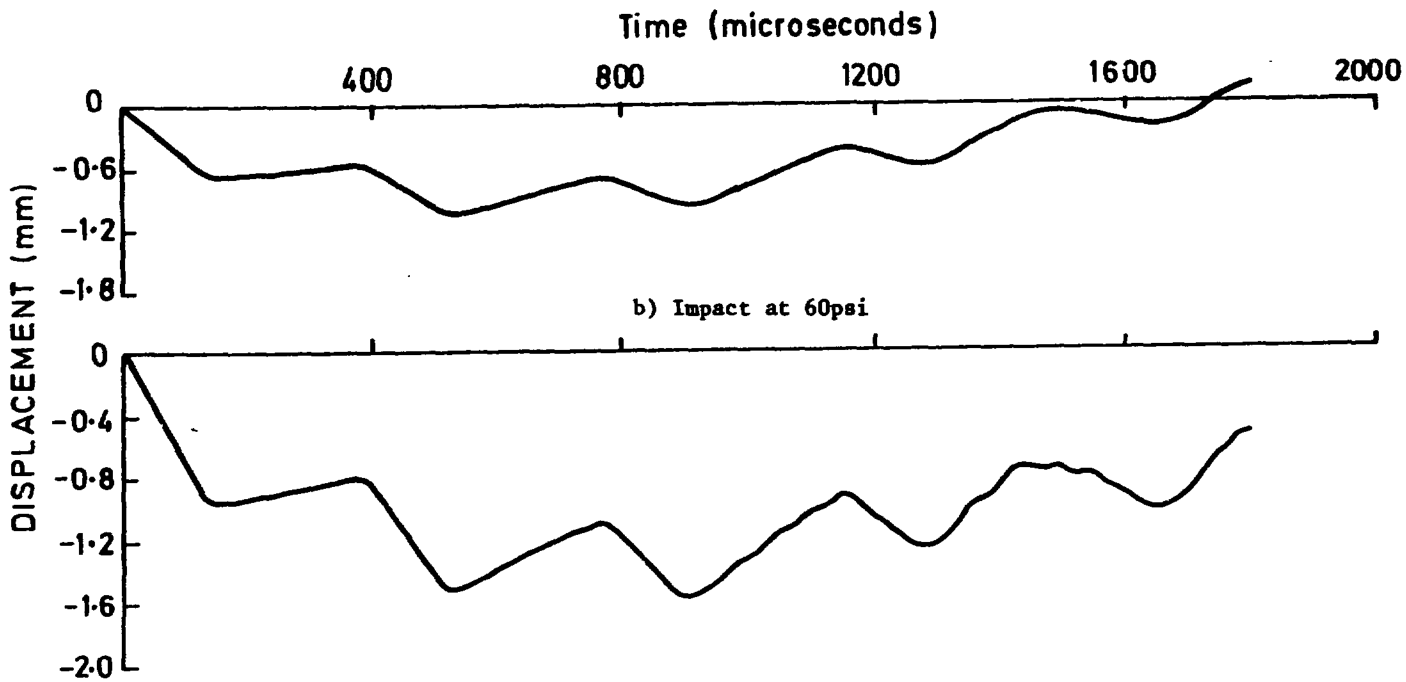

Fig. 3.21 DISPLACEMENT-TIME CURVES FOR IMPACTS ON TYPE VII HYBRID SPECIMENS

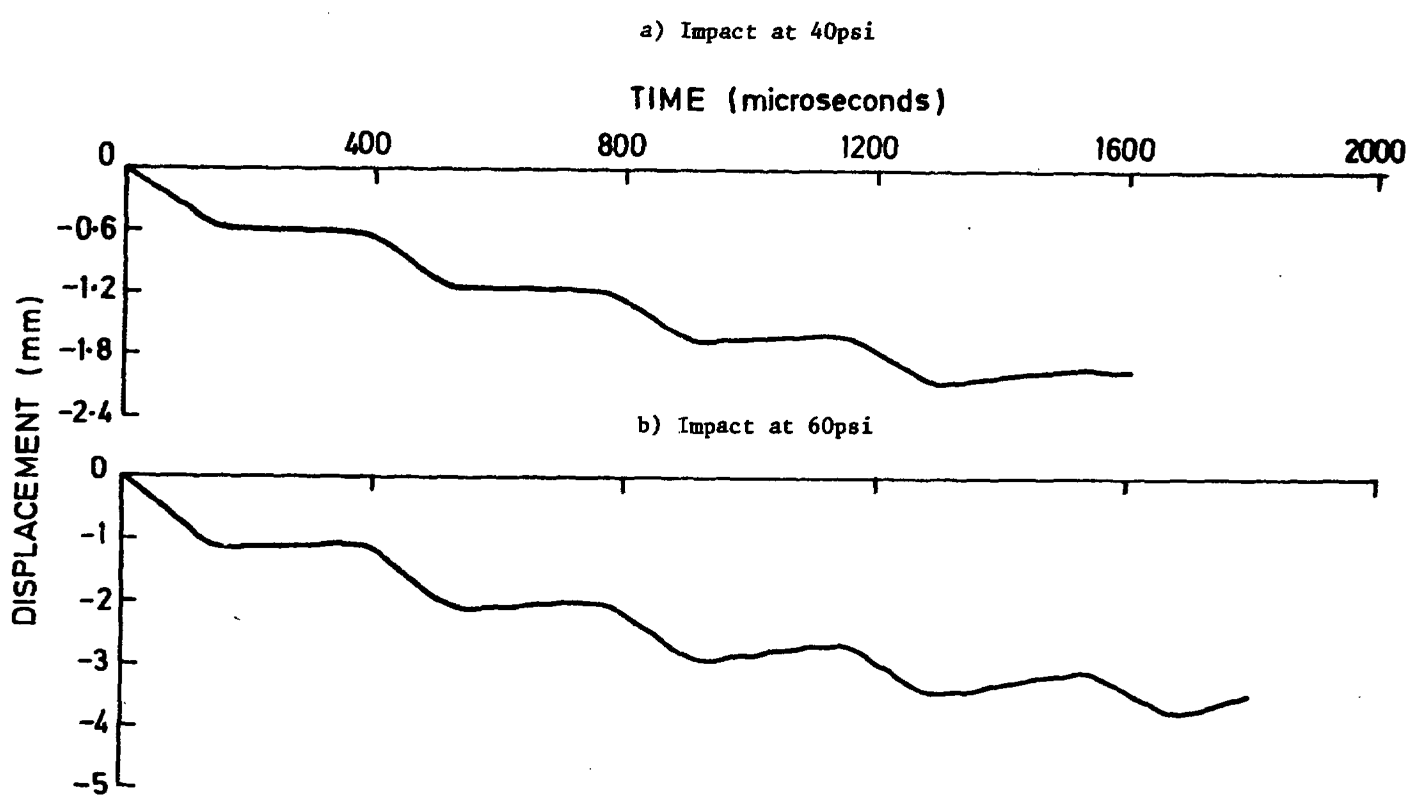

Fig. 3.22 DISPLACEMENT-TIME CURVES FOR IMPACTS ON WOVEN ALL-GLASS SPECIMENS

Fig. 3.23 IMPACT DAMAGE IN ALL-CARBON SPECIMENS

a) C-scan for specimen impacted at 30psi

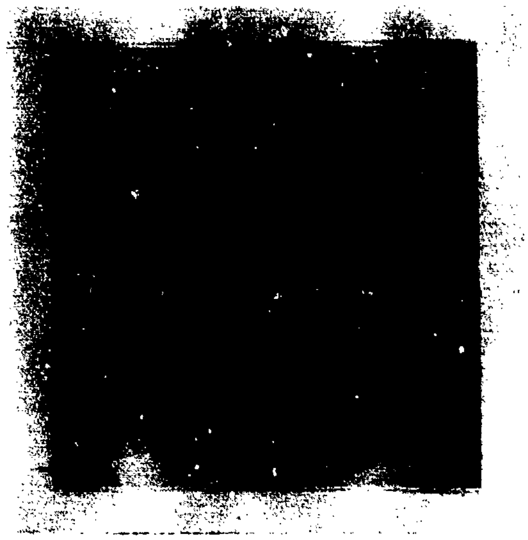

b) C-scan for specimen impacted at 40psi

c) C-scan for specimen impacted at 60psi

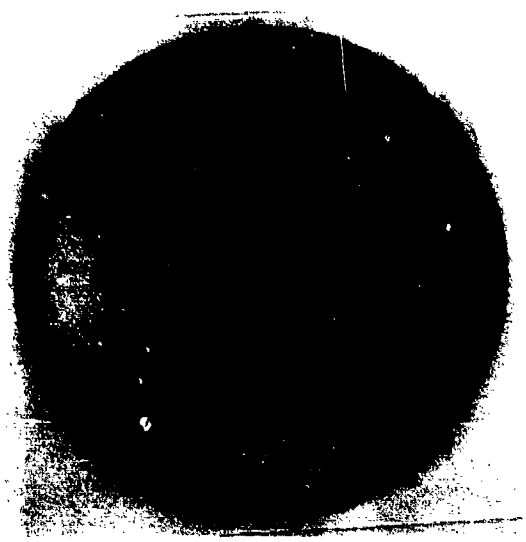

d) Back surface cracks in specimen impacted at 60psi

Fig. 3.24 C-SCANS FOR TYPE V HYBRIDS

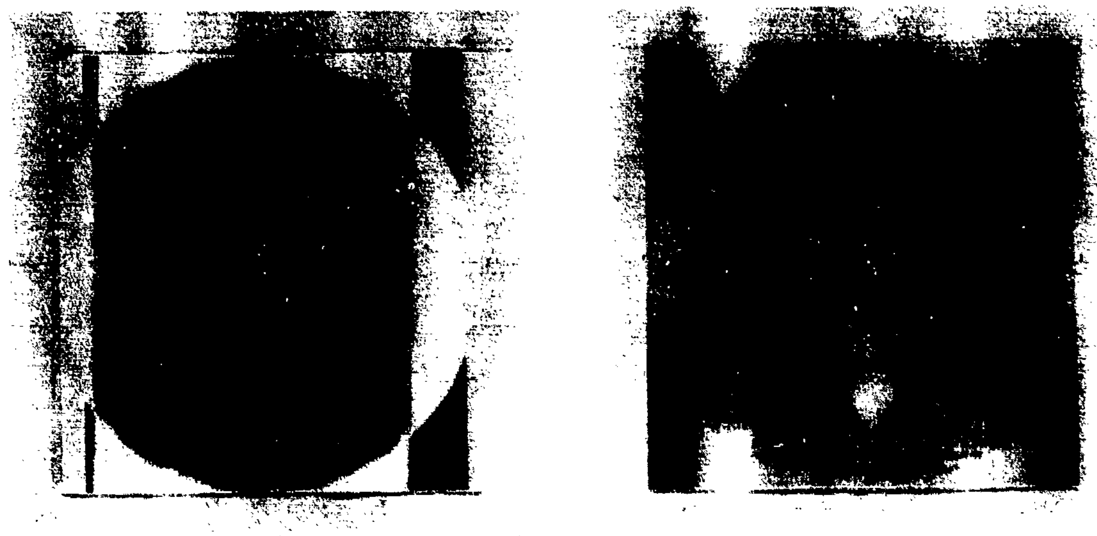

a) Impacted at 40psi

b) Impacted at 60psi

Fig. 3.25 C-SCANS FOR TYPE VI HYBRIDS

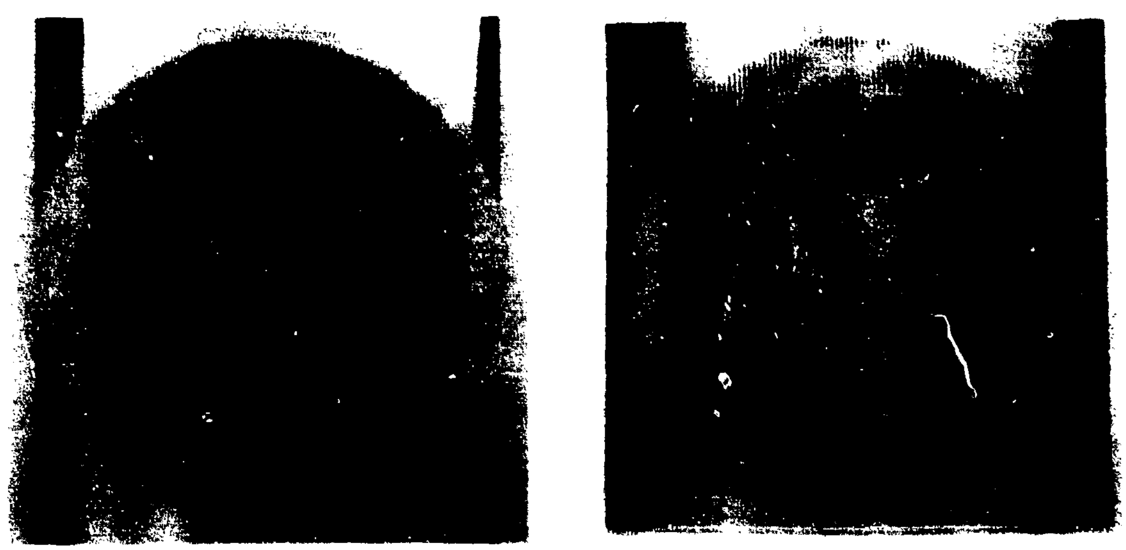

a) Impacted at 40psi

b) Impacted at 60psi

Fig. 3.26 NORMALISED RESIDUAL PLY STRENGTHS FOR ALL-CARBON SPECIMENS

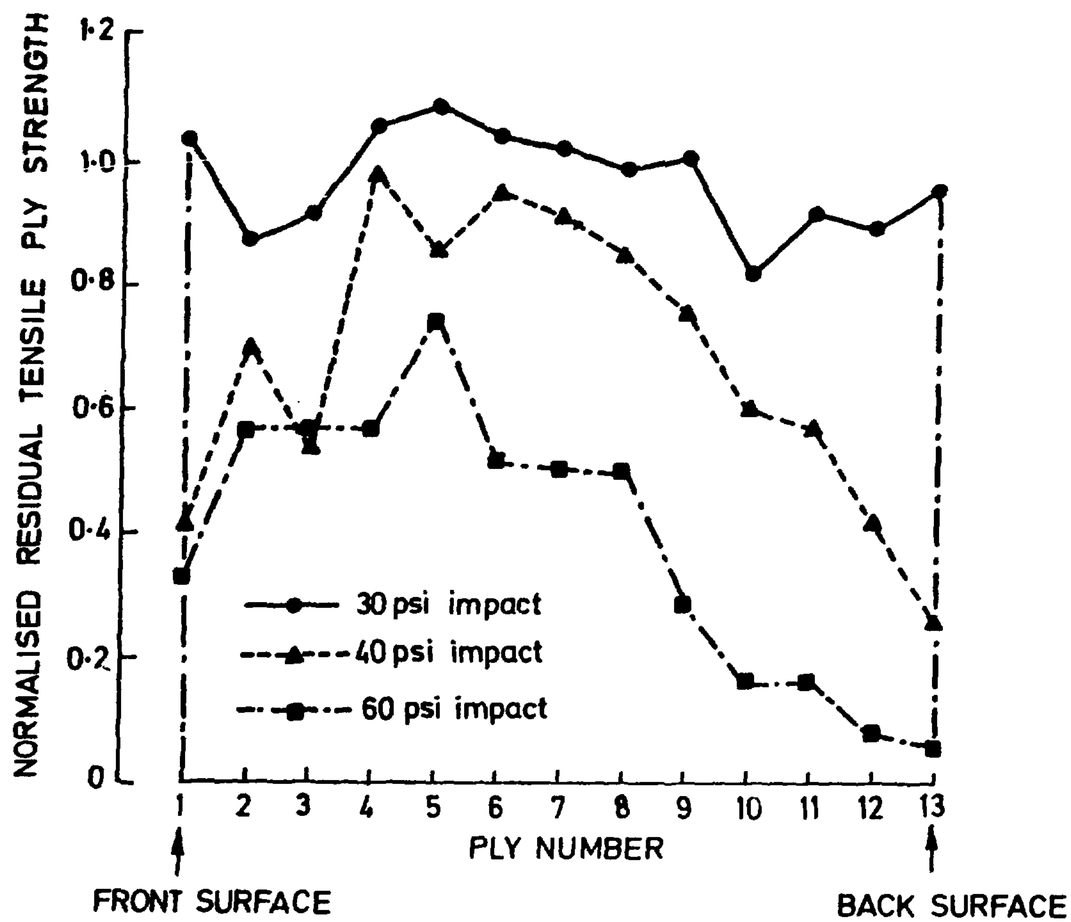

Fig. 3.27 NORMALISED RESIDUAL PLY STRENGTHS FOR TYPE V HYBRID SPECIMENS

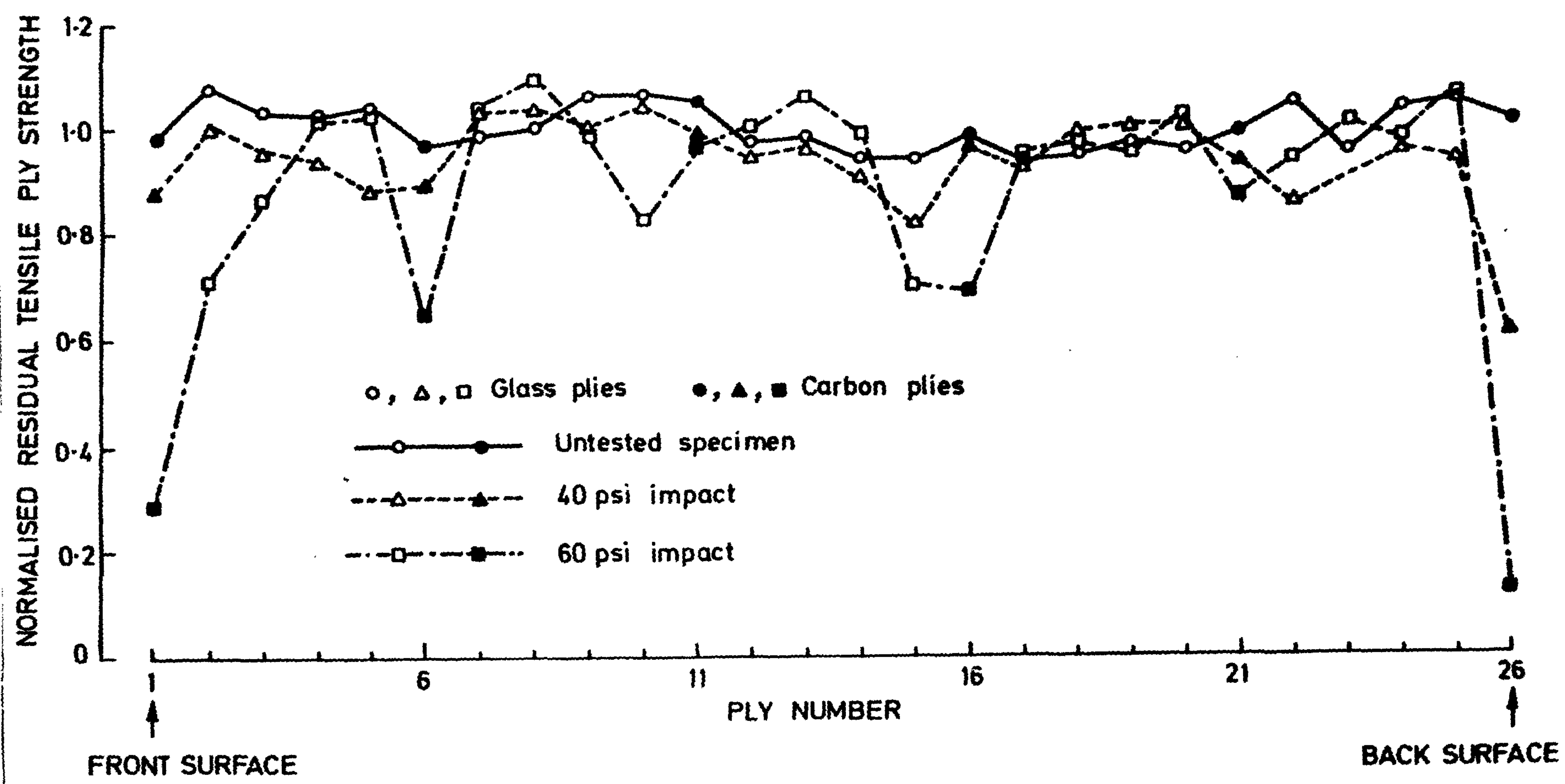

Fig. 3.28 NORMALISED RESIDUAL PLY STRENGTHS FOR TYPE VI HYBRID SPECIMENS

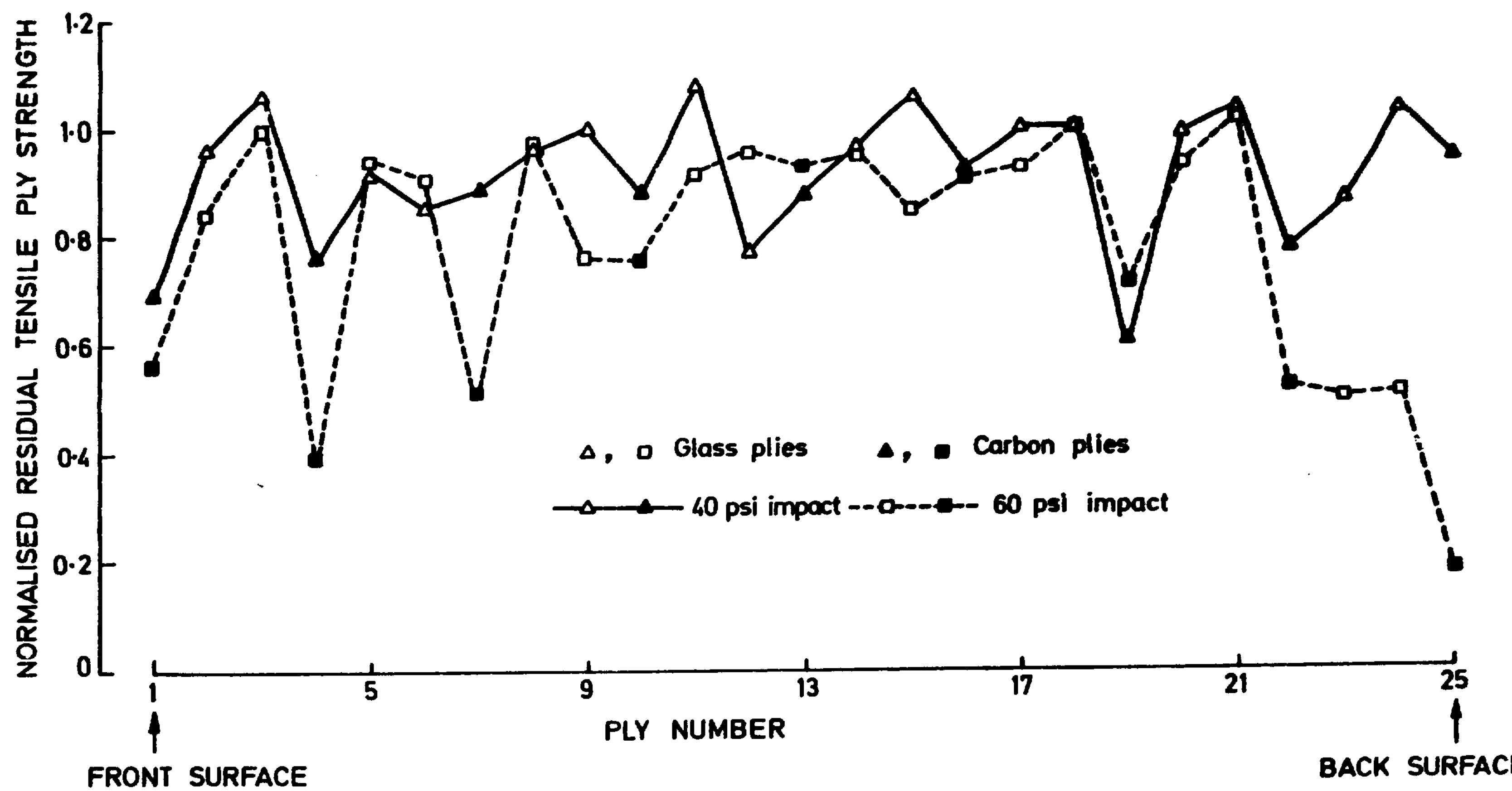

C-scans for the type V and type VI hybrid laminates after testing at both 40 and 60psi are shown in figs. 3.24 and 3.25 respectively. For both hybrids the delamination area at 40psi is approximately circular in shape with a mean diameter of between 5 and 10mm, significantly less than for the all-carbon laminate at the same pressure, fig. 3.23b. Increasing the pressure to 60psi, however, has a very marked effect, raising the mean diameter to between 25 and 30mm, significantly greater than for the all-carbon laminate at this pressure, fig. 3.23c. This change in delamination behaviour is accompanied by a change in the nature of the fibre damage as indicated by the residual ply strength tests. The marked reduction in normalised residual ply strength from the middle of the specimen to the back surface, seen in the all-carbon specimens, fig. 3.26, is not shown by the type V and type VI hybrid lay-ups, figs. 3.27 and 3.28. Significant damage is only observed in these specimens in the plies immediately under the point of impact and, in the tests at 60psi, in the plies very close to the back surface. There is also some evidence, particularly in fig. 3.28 and in tests at 60psi, to suggest greater fibre damage in the carbon reinforced plies than in the neighbouring glass-reinforced plies.

4. PREDICTION OF DYNAMIC MODULI FOR HYBRID LAMINATES

Analytical expressions were developed in previous reports (2,3) from which the tensile elastic moduli of the various hybrid lay-ups could be calculated in terms of the experimentally determined stiffness matrices for the two types of reinforcing ply. These expressions were used to predict the quasi-static tensile elastic moduli for the three carbon/glass hybrid lay-ups from the corresponding quasi-static stiffness matrices for the carbon and the glass reinforcing plies. In the present section an attempt is made to repeat these calculations using the results of impact tests to determine the corresponding stiffness matrices. The hybrid dynamic tensile moduli may then be predicted from the equation

$$E_x = \phi' / (1 + \alpha)(1 + \alpha\mu)(Q_{22})_a^2 \tag{4.1}$$

where

$$\phi' = (1 + \alpha\beta)(1 + \alpha\mu)(Q_{11})_a(Q_{22})_a - (1 + \alpha\lambda)^2(Q_{12})_a^2 \tag{4.2}$$

For a hybrid lay-up consisting of m carbon plies, each of thickness h_a, and (n - m) glass plies, each of thickness h_b, the parameters α, β, λ and μ are given by

$$\alpha = (m/(n-m))(h_b/h_a); \quad \beta = (Q_{11})_b/(Q_{11})_a;$$
$$\lambda = (Q_{12})_b/(Q_{12})_a; \quad \text{and} \quad \mu = (Q_{22})_b/(Q_{22})_a; \tag{4.3}$$

where the elements of the stiffness matrices for the carbon plies and the glass plies are, respectively, $(Q_{11})_a$, $(Q_{12})_a$ and $(Q_{22})_a$ and $(Q_{11})_b$, $(Q_{12})_b$ and $(Q_{22})_b$.

4.1 Determination of the Dynamic Stiffness Matrices for the Carbon and the Glass Plies

The elements of the stiffness matrices, (Q_{ij}), are given by

$$Q_{11} = E_A/(1 - \nu_{AB}\nu_{BA})$$
$$Q_{22} = E_B/(1 - \nu_{AB}\nu_{BA})$$
$$Q_{12} = \nu_{AB}E_B/(1 - \nu_{AB}\nu_{BA}) = \nu_{BA}E_A/(1 - \nu_{AB}\nu_{BA}) \quad \text{and} \tag{4.4}$$
$$Q_{66} = G_{AB}$$

As noted in section 3.1.2, two distinct sets of values were obtained for E_A and E_B, one from the normal waisted design of specimen, the other from the parallel-sided coupons. Poisson's ratio values, however, were only derived from tests on the second of these. Two estimates were made of G , using either equation (3.1) or equation (3.2). Of these the former, but not the latter, is affected by the choice of values for E_A and E_B while both use data obtained in tests on waisted specimens. Table 4.1 summar-

ises the data obtained in these tests and needed to determine the elements of the stiffness matrices.

TABLE 4.1 **Mean Dynamic Elastic Constants for Carbon and Glass Plies**

Material	E_A GPa	E_B GPa	G_{AB} GPa	G_{AB} GPa	ν_{AB}	ν_{BA}	ν^*_{BA}
All-carbon,							
Waisted	48.7	49.0	4.03	4.02			
Parallel	55.9	60.9	3.93		0.061	0.079	0.066
All-glass,							
Waisted	24.0	17.1	3.81	3.55			
Parallel	28.7	23.6	3.55		0.176	0.155	0.145

where G^*_{AB} is determined from equation (3.1), G^{**}_{AB} is determined from equation (3.2) and ν_{BA} is derived from the symmetry hypothesis.

Using this data the stiffness matrices have been calculated for the all-carbon and the all-glass plies in terms of both sets of tensile moduli. Taking the results from the waisted specimens the stiffness matrices are found to be

$$(Q_{ij})_{CFRP} = \begin{bmatrix} 48.9 & 3.00 & 0 \\ 3.00 & 49.2 & 0 \\ 0 & 0 & 4.03 \end{bmatrix} \quad \text{and} \qquad (4.5)$$

$$(Q_{ij})_{GFRP} = \begin{bmatrix} 24.6 & 3.09 & 0 \\ 3.09 & 17.5 & 0 \\ 0 & 0 & 3.81 \end{bmatrix} \qquad (4.6)$$

while using the results from the parallel-sided coupons these become

$$(Q_{ij})_{CFRP} = \begin{bmatrix} 56.1 & 3.70 & 0 \\ 3.70 & 61.1 & 0 \\ 0 & 0 & 3.93 \end{bmatrix} \quad \text{and} \qquad (4.7)$$

$$(Q_{ij})_{GFRP} = \begin{bmatrix} 29.5 & 4.26 & 0 \\ 4.26 & 24.2 & 0 \\ 0 & 0 & 3.55 \end{bmatrix} \qquad (4.8)$$

4.2 Predicted Dynamic Moduli for Hybrid Specimens

The parameter , see equations (4.3), depends only on the hybrid lay-up. Previously determined values (3), again used here, are

Hybrid, type 1 : $\alpha = 1.27$
Hybrid, type 2a: $\alpha = 0.57$
Hybrid, type 2b: $\alpha = 0.28$

Parameters β, λ and μ are also determined from equations (4.3) using the appropriate elements from the various stiffness matrices, either equations (4.5) and (4.6) for the waisted specimen tests, or equations (4.7) and (4.8) for the parallel-sided coupons.

Using data obtained from the waisted specimens we obtain

$$\beta = 0.503; \quad \lambda = 0.356; \quad \mu = 1.03; \tag{4.9}$$

The corresponding values of ϕ' are obtained from equation (4.2) and the hybrid modulus in the warp direction, $E_A = E_x$ estimated from equation (4.1). A modified version of equation (4.1),

$$E_y = \phi'/(1 + \alpha)(1 + \alpha\beta)(Q_{11})_a \tag{4.10}$$

is used to estimate the hybrid modulus, $E_B = E_y$, in the weft direction. Results obtained in this way are listed in Table 4.2 below.

TABLE 4.2 Predicted Dynamic Hybrid Elastic Moduli from Tests on Waisted Specimens

Specimen	ϕ' $(GPa)^2$	E_A (GPa)	E_B (GPa)
Type 1 Hybrid	5667	35.0	31.2
Type 2a Hybrid	3702	39.8	37.5
Type 2b Hybrid	3005	43.4	42.1

Similar calculations using data obtained from tests on parallel sided coupons give alternative values of

$$\beta = 0.526; \quad \lambda = 0.396; \quad \mu = 1.15; \tag{4.11}$$

The corresponding values of ϕ', E_A and E_B are listed in Table 4.3. The variation of the predicted hybrid moduli with the volume fraction of carbon reinforcing plies is shown in fig. 4.1. The predicted values agree closely with the rule of mixtures, i.e. they fall on the straight line joining the mean values measured for the all-carbon and the all-glass specimens. This is not surprising since for the present loading configuration, see equation (33) of the earlier report (2), the laminate theory approach is essentially

TABLE 4.3 Predicted Dynamic Hybrid Elastic Moduli from Tests on Parallel-Sided Coupons

Specimen	ϕ' $(GPa)^2$	E_A (GPa)	E_B (GPa)
Type 1 Hybrid	8510	40.8	40.1
Type 2a Hybrid	5426	46.1	47.4
Type 2b Hybrid	4344	50.0	52.7

Fig. 4.1 LAMINATE THEORY PREDICTIONS OF HYBRID TENSILE MODULI UNDER IMPACT LOADING

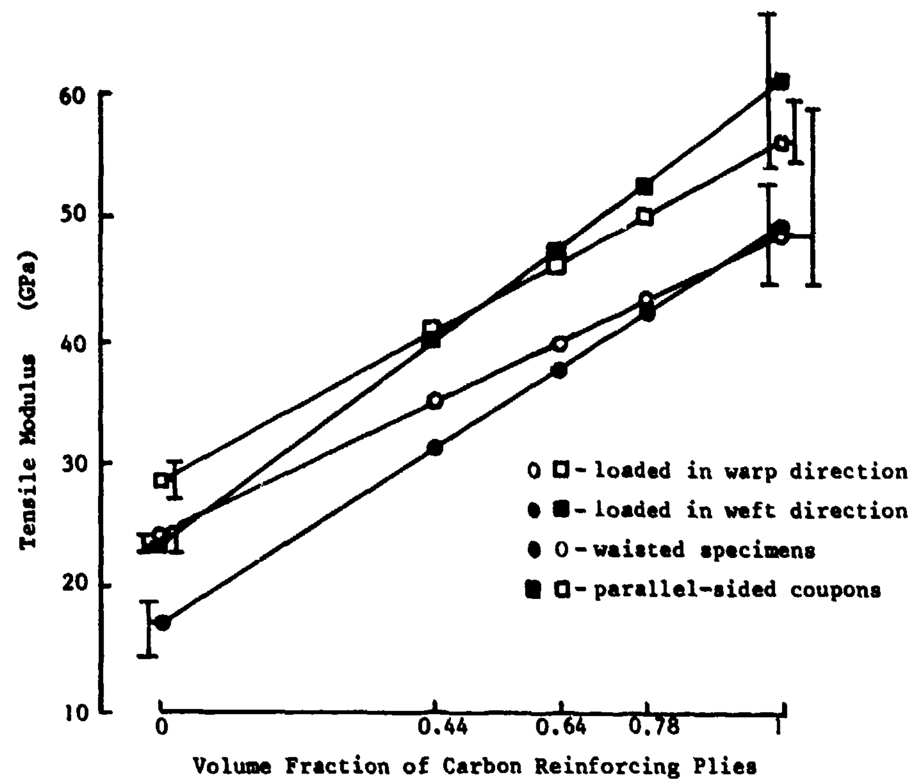

Fig. 4.2 COMPARISON BETWEEN LAMINATE THEORY PREDICTIONS AND EXPERIMENTALLY MEASURED TENSILE MODULI
(Waisted specimens loaded in weft direction)

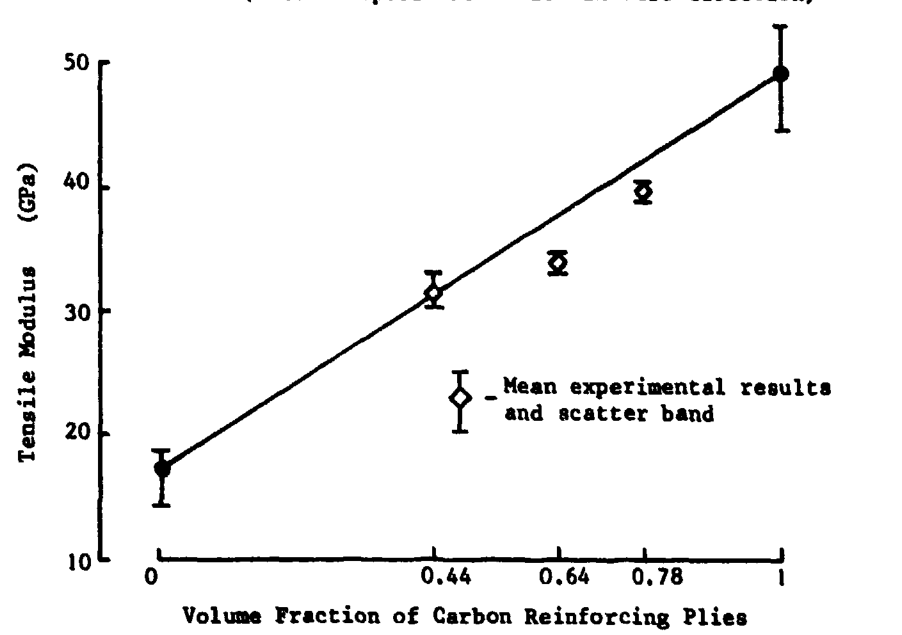

a refined version of the rule of mixtures. The experimental results were obtained on waisted specimens loaded in the weft direction. As shown in fig. 4.2, they fall very close to but just slightly below the corresponding predictions in fig. 4.1. The difference between the experimentally measured and the theoretically measured values is no greater than the experimental scatter in the measured values, about ±5%. The scatter band and the number of tests performed are indicated in figs. 4.1 and 4.2 for the experimentally determined moduli for the all-glass and all-carbon plies and in fig. 4.2 for the experimentally determined hybrid moduli.

5. DISCUSSION

5.1 Predicted Hybrid Tensile Moduli under Impact Loading

It is clear from the results presented in fig. 4.1a that, as in the previous quasi-static calculations (3), the laminate theory predictions of the hybrid dynamic tensile moduli follow extremely closely those determined using the rule of mixtures. Both depend on experimentally measured moduli for the all-carbon and the all-glass reinforcing plies in the warp and weft directions. Scatter bands for these measurements are given in fig. 4.1a and are significantly larger for the coarse-weave all-carbon plies than for the fine-weave all-glass plies.

Two anomalies are apparent in fig. 4.1a. Firstly, as discussed earlier, tensile moduli for the all-carbon and the all-glass plies determined in tests on parallel-sided coupons gave significantly higher values than those determined in tests on the standard design of specimen waisted in the thickness direction. This leads to two different sets of laminate theory predictions for the hybrid tensile moduli in both the warp and the weft directions. In practice the experimentally measured hybrid moduli were obtained in the weft direction on waisted specimens. As shown in fig. 4.1b, they fall just below the corresponding laminate theory prediction, the lowest of the lines in fig. 4.1a. The maximum discrepancy between the laminate theory prediction and the experimental measurement is about 10% and is for the type 2a hybrid. This contrasts with the quasi-static results previously obtained (3) where, for the warp direction, the experimental results had scatter bands which bridged the laminate theory and rule of mixtures predictions. Since the impact tests were performed at an early stage in this investigation, it is planned to repeat the experimental measurements of dynamic tensile modulus, in both warp and weft directions, as a further check on the accuracy of the reported results. The discrepancy between the experimental measurements of modulus on the parallel sided coupons and the waisted specimens, however, appeared in relatively recent tests and is more difficult to understand. Currently a stress analysis, using finite elements, is being undertaken of the various specimen designs and may lead to an explanation of this behaviour although, from the results obtained so far, this does not seem to be very likely.

The second anomaly concerns the behaviour of the all-carbon plies which show, see Table 3.1, a greater stiffness in the weft direction and a greater strength (3) in the warp direction. This effect was observed, but was of insignificant magnitude, in the tests on the waisted specimens. It appears to a more marked extent in the tests on the parallel-sided coupons, although it must be admitted that the scatter band for the warp moduli measurements lie within those for the weft moduli. A similar behaviour is not observed in the all-glass plies so it clearly does not arise merely from the change in specimen design but may also relate to the difference in reinforcement geometry between the coarse-weave of the carbon plies and the fine-weave of the glass plies.

A further difference between the two types of reinforcement is apparent when considering the rate-dependence of the elements of the stiffness matrices. As shown in Table 5.1, all elements of the stiffness matrix for

TABLE 5.1 Effect of Strain Rate on the Elements of Stiffness Matrices for Carbon-Reinforced and Glass-Reinforced Plies
(as determined from measurements on waisted specimens)

			Q_{11}	Q_{12}	Q_{22}	$Q_{66} = G_{AB}$
All-carbon	Quasi-static tests	(GPa)	46.2	6.1	44.1	2.7
	Impact tests	(GPa)	48.9	3.0	49.2	4.0
All-glass	Quasi-static tests	(GPa)	17.0	2.3	14.1	1.6
	Impact tests	(GPa)	24.6	3.1	17.5	3.8

glass-reinforced plies and all elements except Q_{12} of the stiffness matrix for carbon-reinforced plies are found to increase in magnitude with increasing strain rate, the rate-sensitivity being, in general, twice as great for the glass plies as for the carbon plies. The most marked increase is in Q_{66}, i.e the in-plane shear modulus G_{AB}, which is more than doubled for the glass reinforced plies and increases by about 50% for the carbon-reinforced plies. Since the shear modulus is more strongly dependent than the other elastic constants on the properties of the matrix, its marked rate-dependence is not unexpected. A rather smaller increase is apparent in Q_{11} and Q_{22}, between 20 and 40% for the glass-reinforced plies and between 5 and 10% for the carbon-reinforced plies. An anomalous behaviour is shown, however, by the element Q_{12} which increases by about 30% in the glass-reinforced plies but decreases in impact tests on the carbon-reinforced plies to less than half its quasi-static value. It is likely that this difference in behaviour follows from the much coarser weave in the carbon reinforced plies leading to more significant edge effects, there being only 5 carbon tows across the specimen width as compared with 25, in the warp direction, or 17, in the weft direction, across the width of the all-glass specimens.

5.2 Transverse Impact Testing Technique

The original intention had been to develop an improved transverse impact test in which the instrumentation provided would allow an unambiguous determination of the force, velocity and displacement applied to the specimen without the need to assume conditions of quasi-static equilibrium within the specimen. In the event reliable velocity- and displacement-time data have been obtained but problems have been encountered in the accurate measurement of force. These difficulties are greater the higher the impact velocity and the lower the stiffness (or load-carrying capacity) of the specimen and are fundamental to the instrumented Hopkinson input-bar technique used here.

In consequence two improvements to the testing technique are being considered. The simplest is to alter the loading configuration, making the projectile and input bars of the same material and of the same length and cross-sectional area. In the absence of a specimen only one loading wave will be seen in each bar following impact, the unloading wave from the free end completely cancelling the initial loading wave. The resistance of the

specimen will reduce the magnitude of the reflected unloading wave so further reflections will follow but the amplitude of these waves should be less and the rate of decay greater than in the present set-up.

However, if the input bar were not in contact with the specimen at the instant the projectile made contact, the effect of the impact would be to give the input bar a velocity equal to that previously had by the projectile while leaving it in an unstressed state. When it subsequently impacts the specimen the gauge signals from stations I and II will be a direct measure of the load applied to the specimen which could, therefore, be determined much more accurately. It is true that the velocity would now be determined as the difference between two measurements but one of these, the velocity of the input bar before impact with the specimen, is likely to be constant, assuming the input bar is indeed unstressed at this stage. These two improvements to the testing technique are being implemented and the results will be reported on in due course.

5.3 Transverse Impact Test Results

A full discussion of the experimental results is inhibited by the lack of reliable load measurements in most of the tests. Also discussion is made more difficult by the differences between the various laminates from which the specimens were made. These laminates were designed primarily for their suitability in the ongoing tensile impact testing programme. Under a tensile loading configuration the high strain to failure (and the correspondingly high energy absorbed) observed in glass-reinforced plies at impact rates of strain in all-glass specimens is significantly reduced in tests on carbon/glass hybrids where the much lower failure strain in the carbon-reinforced plies limits the amount of damage that the glass plies can sustain. In the transverse impact loading configuration, therefore, different responses might be expected if the outer plies, where the higher strains will be experienced, are predominantly either glass-reinforced or carbon-reinforced. There will, of course, be an interaction between the magnitude of these surface strains and the specimen thickness, a geometrical effect, and stiffness, which will vary with the hybrid lay-up.

While the present results do not allow an unambiguous isolation of these various effects several observations can be made. Thus, considering results for all five hybrid lay-ups, as reported on in (13), a comparison may be made between the behaviour of the type IV and type V hybrids and the all-carbon laminate. All three are of a similar thickness, between 3.6 and 3.8mm, and both hybrids have a single carbon reinforcing ply at both the front and back surfaces. Normalised residual tensile ply strengths similar to those in fig. 3.27, with damage mainly limited to the front and back surface regions, are shown by both hybrids. This compares with the all-carbon laminate which shows a much greater reduction in ply strength throughout the thickness, see fig. 3.26, and rear surface cracks after testing at 60psi, see fig. 3.23d. The initially higher stiffness of the all-carbon laminate probably indicates that it supported a higher impact load at a given firing pressure. Nevertheless, the presence of the glass-reinforced plies has clearly limited the extent of fibre damage. A second difference between the all-carbon laminate and the two hybrids is apparent from the C-scans, figs. 3.23, 3.24 and 3.25. Thus, while at 40psi the de-

lamination area in the hybrids is smaller than in the all-carbon laminate, at 60psi the reverse is the case, suggesting that with increasing impact velocity damage is accommodated in the hybrids by greater delamination and in the all-carbon laminate by increased fibre fracture. Both processes are evident in the micrograph of fig. 5.1. This is for a second type V hybrid specimen, impacted at 40psi and then sectioned on a diametral plane perpendicular to the warp direction. In this test a back surface strain gauge rosette had been fixed at the centre of the specimen. Immediately below this on the outer surface of the specimen was a single carbon reinforced ply followed by four glass-reinforced plies. Fibre fracture is apparent across the weft tow of the outer carbon layer, and is associated with a crack in the matrix initiating at the outer surface below the strain gauge and arresting at the first glass ply it encounters. Delamination is seen between the warp and weft tows of the carbon-reinforced ply, leading to transverse cracks in the warp tow of the outer carbon layer, these cracks also arresting at the neighbouring glass-reinforced ply. The micrograph also shows the relatively large void content due to the hand lay-up technique employed to manufacture these laminates.

A second general observation may be made from the results obtained in tests on the type VI and type VII hybrids. These have a thickness of 4.3 and 4.5mm respectively and also have a single carbon-reinforced ply on each surface. As with the type IV and type V hybrids the delamination area is relatively small at 40psi and considerably increased at 60psi, similar to the behaviour shown in the C-scan of fig. 3.27, suggesting that for these hybrids also increasing delamination was the primary process of damage accommodation at the higher pressures. However, an additional feature of these tests is apparent when their normalised residual ply strengths are considered, see fig. 3.28. These show, in the main, a much greater reduction in the strength of the carbon plies than in that of the glass plies. This effect is particularly marked at 60psi where, for the type VII hybrid, the glass plies remained largely undamaged. If the normalised residual ply strengths are replotted for the tests at 60psi with separate curves for the glass and the carbon plies, see fig. 5.2, the effect is more clearly apparent and is seen also to occur in the type IV and type V hybrids. This is the sort of behaviour which would be expected in view of the ability of glass-reinforced plies to retain their strength to higher strains, particularly under impact loading.

Fig. 5.1 **MICROSECTION THROUGH TYPE V HYBRID SPECIMEN IMPACTED AT 40psi**

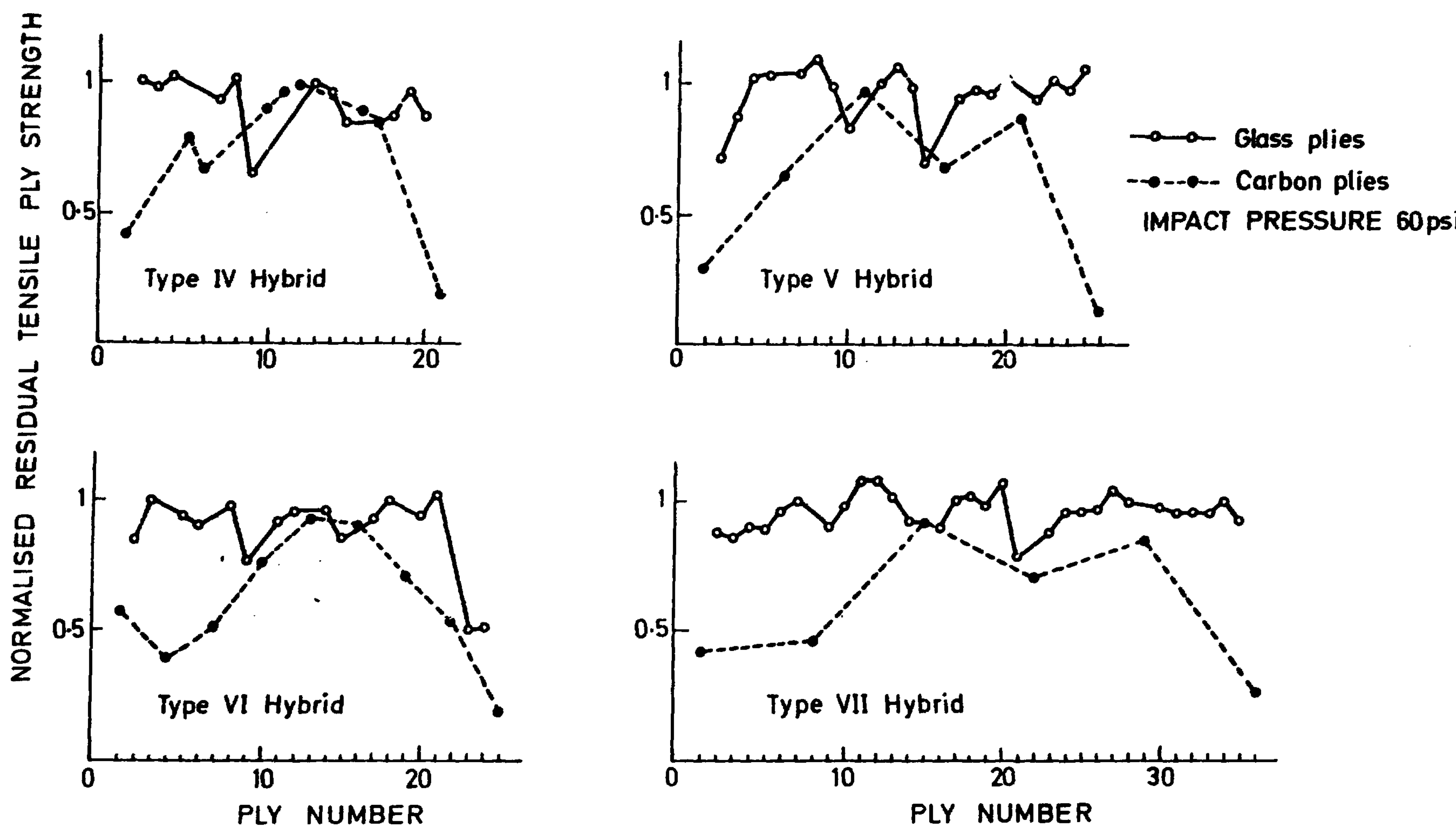

Fig. 5.2 NORMALISED RESIDUAL PLY STRENGTHS OF CARBON AND GLASS PLIES FOR IMPACTS AT 60psi

6. CONCLUSIONS

1. Impact tests have been performed using the standard waisted design of tensile specimen for both the all-glass and the all-carbon reinforced laminates loaded in the warp (A), weft (B) and 45° (C) directions to determine the tensile and in-plane shear moduli and using parallel-sided coupons for the same laminates loaded in the warp and weft directions to determine the two values of Poisson's ratio and to make a second estimate of the tensile moduli. Significantly higher values of tensile moduli were obtained from the tests on the parallel-sided coupons.

2. Dynamic stress-strain curves for all-carbon and all-glass laminates loaded in the C direction have been obtained. Compared with previous results (3) for impact tests on the same laminates loaded in the warp and weft directions, the maximum stress here is reduced by about one half and the corresponding failure strain more than doubled.

3. Using the elastic constants determined in the impact tests on the all-carbon and the all-glass laminates dynamic two-dimensional stiffness matrices have been determined for both types of reinforcing ply using results from both waisted specimens and parallel-sided coupons. In terms of the modified laminate theory developed previously (3), estimates for the hybrid dynamic tensile moduli have been obtained and are found to follow closely the simple 'rule of mixtures' predictions. Experimental values for the hybrid dynamic tensile moduli measured in the weft direction fall slightly below, by up to 10%, the theoretical predictions for the weft direction based on stiffness matrices determined from tests on waisted specimens.

4. An impact testing machine for composite materials has been developed in which a transverse load is applied to the centre of a thin circular laminate and the subsequent deformation is monitored using an instrumented Hopkinson-type input bar. The duration of loading is of the order of 1 to 2 milliseconds, the specimen being effectively in quasi-static equilibrium for most of this time. Except at the lowest impact velocities on the stiffest laminates the Hopkinson-bar measurement of the applied load is unsatisfactory. An alternative technique, based on signals from specimen back surface strain gauges which have been calibrated quasi-statically, gives an improved estimate of the applied load but breaks down when significant damage develops in the specimen.

5. Although the lack of a reliable estimate of the impact loads leads to difficulties in making a detailed comparison between results from specimens with different ply lay-ups and hybrid volume fractions, two general trends were observed.

   a) At increasing impact velocity, damage in the woven all-carbon laminate is primarily by fibre fracture in plies towards the rear surface. The introduction of glass-reinforced plies, however, leads to a change from fibre fracture to delamination as the principal damage accommodation mechanism.

b) After impact at higher velocities the normalised residual tensile strengths determined for the carbon plies were significantly lower than for the glass plies. This agrees with the results of the previous tensile tests where glass-reinforced plies have been shown to retain their strength under impact loading to considerably higher strains than have carbon-reinforced plies.

7. FUTURE WORK

The present report describes work performed during the final six month period of Grant No. AFOSR-85-0218. This grant is to be succeeded by a new programme, under Grant No. AFOSR-86-0031, entitled "Modelling of the Impact Response of Fibre-Reinforced Composites", which will combine a continuation of the experimental work reported on here with attempts to model the experimental results obtained by numerical techniques, making possible a prediction of the impact response.

The next stages in the experimental programme are expected to involve:-

1. A determination of the compressive strengths of the all-glass and the all-carbon laminates at both quasi-static and impact rates of strain and in both warp and weft directions to provide data on which to base estimates of the hybrid tensile strengths at the two strain rates using the laminate theory approach developed previously (2).

2. Using data obtained in both tension and compression on the all-glass and all-carbon plies and at both the quasi-static and the impact rate, to obtain, in terms of the laminate theory approach, predicted tensile strengths for the hybrid laminates and to compare these with the experimentally determined values.

3. A parallel series of tests to those on carbon/glass hybrids described in previous reports (2,3) at impact, intermediate and quasi-static rates on specimens reinforced with plain-weave fabrics of carbon and Kevlar in various hybrid lay-ups and an examination of the failure processes by optical and scanning electron microscopy.

4. In connection with the proposed analytical studies it is likely that there will be a need (i) to obtain estimates of the elastic properties of the all-carbon and the all-glass laminates in the through-thickness direction and (ii) to attempt an experimental determination of the impact failure strengths associated with both interlaminar shear failure between the plies and, possibly, failure normal to the interlaminar plane. These are both quite major studies, particularly the latter where sufficient results are required to make some estimate of the statistical variation involved.

The initial stages of the proposed analytical programme are expected to include:-

5. An evaluation of the stress (and strain) distribution in the standard design of tensile specimen, waisted in the thickness direction, as used in all experimental measurements so far. Initially all-glass and all-carbon reinforced specimens will be studied, using the stiffness matrices for the two types of reinforcing ply already determined experimentally. The analysis will then be extended to hybrid specimens with different lay-up sequences.

6. By dividing the specimen into a number of elemental segments, or "links", to each of which a failure strength is randomly assigned, the first link to fail, and the corresponding applied load, will be determined. Failure will be related to the local tensile stress and

to the randomly assigned strength level based on a statistical distribution of failure strengths related to experimental measurements. Once such a failure has occurred the stress distribution in the neighbouring segments has to be determined in order to assess whether the next stage in the process is a further tensile failure or whether significantly large normal and/or shear stresses are developed leading to deplying or delamination as possible mechanisms for the next step in the failure process.

7. A study of the stress distribution around the specimen/loading-bar interface for various geometries so as to optimise the load transfer between the loading-bar and the specimen and obtain a design of specimen which will allow tensile failures in impact tests on unidirectionally reinforced specimens.

8. ACKNOWLEDGMENTS

This research was sponsored by the Air Force Office of Scientific Research, Air Force Systems Command, USAF, under Grant No. AFOSR-85-0218, and was supported by the Science and Engineering Research Council with the award of a two year Research Assistantship (RKYL).